

**Deformation and Strain Energy Anomalies in
Bistable and Nonlocal Mechanical Metamaterials**

BY

LARRY APPIAH DANSO

B.Sc., Kwame Nkrumah University of Science and Technology, Ghana, 2009

M.S., University of Illinois at Chicago, Chicago, 2016

THESIS

Submitted in partial fulfillment of the requirements
for the degree of Doctor of Philosophy in Civil Engineering
in the Graduate College of the
University of Illinois at Chicago, 2019

Chicago, Illinois

Defense Committee:

Eduard Karpov, Chair and Advisor

Didem Osevin

Craig Foster

Sheng Wei Chi

Matthew Daly

Hamed Hatami-Marbini (Mechanical and Industrial Engineering)

ACKNOWLEDGEMENTS

I would like to first and foremost express my profound gratitude to my thesis advisor Dr. Eduard Karpov, for his rich advice and support throughout my academic journey at the University of Illinois at Chicago and the preparation of this thesis. Completing this thesis would not have been possible without his depth of knowledge, guidance and patience.

I would like to thank my committee members for their invaluable thoughts, comments and recommendations.

I would also thank the National Science Foundation (NSF), The Army Research Lab (ARL) and the Department of Civil and Materials Engineering for funding the research study undertaken in this thesis which was major support to my graduate study.

I would like to thank my family, parents for their encouragement and best wishes throughout my graduate studies.

Finally, I would like to specially thank my wife, Ama, for her cheers and for believing in me throughout the duration of this academic feet.

CONTRIBUTION OF AUTHORS

Chapter 2 is based on a published manuscript (*Danso, L. A.; Karpov, E.G. Cusp Singularity-Based Bistability Criterion for Geometrically Nonlinear Structures. Extreme Mechanics Letters. 2016, 13, 135-140.*) for which I was the first author and provided major contribution to the entire research study and writing of manuscript.

Chapter 3 is based on a published manuscript (*Karpov, E. G.; Danso, L. A.; Klein J.T. Negative Extensibility Metamaterials: Occurrence and Design Space Topology. Physical Review E. 2017, 96(2), [023002].*) for which I was the second author and contributed to the analytical studies and results discussion. Dr. Eduard Kapov was the first author and he also compiled the manuscript.

Chapter 4 is based on a published manuscript (*Karpov, E. G.; Danso, L. A. Strain Energy Spectral Density and Information Content of Materials Deformation. International Journal of Mechanical Sciences. 2018, 148, 676-683.*) for which I was the second author and contributed to the analytical studies and proof of results. Dr. Eduard Kapov was the first author and he also compiled the manuscript.

Chapter 5 is based on a published manuscript (*Danso, L. A.; Karpov, E.G. Reprogramming Static Deformation Patterns in Mechanical Metamaterials. Materials. 2018, 11, 2050.*) for which I was the first author and provided major contribution to the entire research study and writing of manuscript and published manuscript (*Karpov, E. G., Danso, L. A., Klein J.T. Anomalous Strain Energy Transformation Pathways in Mechanical Metamaterials. Proceedings of the Royal Society A. 2019, 2019004.*) for which I was second author and contributed to analytical studies and results discussion.

TABLE OF CONTENTS

<u>CHAPTER</u>	<u>PAGE</u>
1 INTRODUCTION	1
1.1 Mechanical Metamaterials	1
1.2 Thesis Organization	6
2 DESIGN OF BISTABILITY BEHAVIOR IN ELASTIC STRUCTURES	11
2.1 Introduction	11
2.2 Design Using Stability Diagrams	14
2.2.1 Catastrophe Theory	14
2.3 Bistability Analysis in Elastic Structures	17
2.3.1 2D Four Bar Truss Example.....	18
2.3.2 Simple Truss Stability Diagrams.....	19
2.4 Cusp Curve and the Phase Diagram.....	23
2.5 Periodic lattice Models	25
2.5.1 Stability of the 3D Unit cell Tetrahedral Truss	26
2.6 Conclusions	28
3 NEGATIVE EXTENSIBILITY MECHANICAL METAMATERIAL.....	33
3.1 Introduction	33
3.2 Analysis of Truss Model with An Internal Degree of Freedom	37
3.3 Stability Diagrams	38
3.4 Phase Diagrams	41
3.5 Small Strain Approximation Error Analysis.....	46
3.6 Conclusions.....	48
4 A NUMERICAL STRAIN ENERGY ANALYSIS USING SPECTRAL AND INFORMATION CONTENT OF MATERIALS	51
4.1 Introduction	51
4.2 Developing the Strain Energy Spectral Density (SESD).....	52
4.3 Developing the Strain Energy Spectral Entropy (SESE)	55
4.4 Numerical Calculation of Spectral Entropy (SESE)	56
4.5 Communication in Mechanics.....	58

4.6	Illustrative Example: Gauss-Type Load On A Plane Solid.....	59
4.7	Load And Boundary Approximations.....	66
4.8	Numerical Entropy Versus Analytical Entropy.....	67
4.9	Conclusions.....	68
5	NONLOCAL MECHANICAL METAMATERIAL.....	73
5.1	Introduction.....	73
5.2	Transfer Matrix and Polarization Vectors for A 2D Non-Local Lattices.....	76
5.3	Constructing A 2D Problem Raleigh Wave Solution.....	78
5.4	Non-Raleigh Wave Solution: Essential Boundary Condition.....	79
5.5	Non-Raleigh Wave Solution: Natural Boundary Condition.....	81
5.6	Bandgap Design: Raleigh Wave Mode.....	81
5.7	Periodic Lattice with Repeated Zero Eigenvalues λ_1 & $\lambda_2 \rightarrow \mathbf{0}$	84
5.8	Strain Energy Density of Periodic Lattices.....	85
5.9	Illustrative Examples.....	88
5.10	Conclusions.....	102
6	CONCLUSIONS AND FUTURE WORK.....	109
	CITED LITERATURE.....	112
	APPENDIX.....	118
	VITA.....	142

LIST OF TABLES

<u>TABLE</u>	<u>PAGE</u>
Table I Form of the seven elementary catastrophes	15

LIST OF FIGURES

<u>FIGURE</u>	<u>PAGE</u>
Figure 1.1 Different Poisson's ratio measures	2
Figure 1.2 Origami waterbomb base bistability	3
Figure 1.3 Negative compressibility.....	4
Figure 1.4 Pentamode mechanical metamaterial	5
Figure 2.1 Snap-through Action.....	12
Figure 2.2 A 3D topological view of a cusp catastrophe.....	16
Figure 2.3 A four bar plane truss.....	18
Figure 2.4 Four bar truss stability diagrams.....	21
Figure 2.5 Typical system response curves of the four bar truss in Fig.2.3.....	22
Figure 2.6 Cusp curve phase of the equilibrium potential function of the form $f = y^3 - ay^2 + by$	24
Figure 2.7 A composite material composed of a stiff hexagonal periodic lattice structure embedded in a soft continuum matrix.....	25
Figure 2.8 Design example of a periodic space truss using the bistable tetrahedral unit cell.	26
Figure 2.9 Tetrahedral truss unit-cell.	27
Figure 3.1 Different material responses (red) under uniform tensile force (white).....	33
Figure 3.2 Negative extensibility in an elastic bar.	34
Figure 3.3 Elastic bar-spring metastable (states A and B) structure with one (1) internal degree of freedom.....	36
Figure 3.4 A force-strain curve of the potential in (3-7).....	39
Figure 3.5 Stability diagrams obtained from the potential in (3-7).....	41
Figure 3.6 A phase diagram governed by the potential in (3-7).....	44
Figure 3.7 A phase diagram showing regions of the usual system equilibrium behaviors.	46
Figure 3.8 Negative extensibility intensity.....	47
Figure 4.1 Normal stress σx (4-39) transformation in plane solid when a Gauss-type (4-40) load.....	58
Figure 4.2 Strain energy spectral density (solid line) versus the spatial strain energy density (dashed line) for Fig.4.1 problem.	60
Figure 4.3 (top)Illustration of the strain energy inverse transformation relationship for the Gaussian problem in Fig.1	63
Figure 4.4 The modified analytical (4-27,4-46) versus numerical (4-26) spectral entropies as functions of the material coordinate for Fig.1 problem.....	64
Figure 4.5 The modified analytical (4-27,4-46) versus numerical spectral entropies (ANSYS) as functions of the material coordinate for Fig.1 problem.....	66
Figure 5.1 A sample model of a periodic x-braced lattice, and its associate substructure	77
Figure 5.2 Occurrence of zero eigenvalues in the (q,k) -parameter space of Fig.1 lattice.....	82
Figure 5.3 A Phase Diagram of the lattice material of Fig. 5.1.....	83
Figure 5.4 Deformation decay spectrum for an x-braced lattice (Fig.1) at $k = 0.93$	89
Figure 5.5 Deformation configuration (scaled) of 2DoF x-braced lattice ($k = 0.93, q = 4\pi/5, m = 0 \rightarrow 10, n = 0 \rightarrow 4$) given by the analytical solutions (5-43) and (5-44) in (a) and (b) respectively.....	89
Figure 5.6 Deformation configuration (scaled) of 2DoF x-braced lattice ($k = 0.93, q = 1\pi/5, m = 0 \rightarrow 10, n = 0 \rightarrow 4$) given by the analytical solutions (5-45) and (5-46) in (a) and (b) respectively.....	90

Figure 5.7 Deformation configuration (scaled) of the analytical solutions (5-47), (5-48) and (5-49) respectively for half-cyclic domain of an x-braced lattice ($k = 0.93$, $m = 0 \rightarrow 11$, $n = 0 \rightarrow 4$).....	91
Figure 5.8 Deformation configurations (scaled) of different stiffness parameters under a Raleigh mode solution for $q = 8\pi/11$ in a half-cyclic domain of the x-braced lattice ($m = 0 \rightarrow 11$, $n = 0 \rightarrow 4$).]	92
Figure 5.9 Strain Energy along index n in an x-braced lattice with $k = 0.93$	93
Figure 5.10 Relative Strain Energy against Fourier parameter q	94
Figure 5.11 Deformation decay spectrum for $k = 0.4714$ and $k = 1.0834$	95
Figure 5.12 Deformation configurations (scaled) for a half-cyclic domain of the x-braced lattice ($m = 0 \rightarrow 9$, $n = 0 \rightarrow 4$) at $k = 0.4714$ (a), and $k = 1.0834$ (b).....	96
Figure 5.13 Deformation decay spectrums: (a) Continuum (b) x-braced lattice - $k = 0.5$ (c) x-braced lattice - $k = 1.1$ (d) x-braced lattice - $k = 9.0$	99
Figure 5.14 Spectral strain energy distribution contour maps: (a) Continuum (b) x-braced lattice - $k = 0.5$ (c) x-braced lattice - $k = 1.1$ (d) x-braced lattice - $k = 9.0$	100
Figure 5.15 Volumetric strain energy distribution contour maps: (a) Continuum (b) x-braced lattice - $k = 0.5$ (c) x-braced lattice - $k = 1.1$ (d) x-braced lattice - $k = 9.0$	101
Figure 5.16 Strain energy spectral entropy plots.....	102

SUMMARY

The study of mechanical metamaterials has showcased unusual mechanical properties that have never been realized in conventional materials. These unusual properties lead to fascinating characteristics of the structure or material which could serve as a basis for engineering advanced materials. Mechanical metamaterials formulated from periodic lattice structures derive their distinct properties from the geometry of their unit cells or substructures. Negative Poisson's ratio, negative or zero stiffness, vanishing shear modulus and negative compressibility are some of the interesting mechanical metamaterial properties that have been realized. Engineered or architected materials and structures with such unusual properties could demonstrate significant peculiar deformation and strain energy behaviors and if controlled could be critical features in designs of smart materials, advanced space structures, seismic risk mitigation systems and intelligent and autonomous structures. Therefore, this research work presents a detailed study on the anomalous deformation and strain energy behaviors in bistable and nonlocal periodic lattice mechanical metamaterials. The objective was to develop systematic analytical and computational tools for designing and analyzing unusual deformation and strain energy behaviors in these metamaterials.

Bistable systems with internal degrees of freedom have been studied to possess the negative compressibility metamaterial behavior and so contracts opposite to the direction of the applied force. To study this interesting unexpected deformation behavior in elastic structures, a systematic methodology for designing bistable elastic structures using stability diagrams and phase diagrams is presented. These diagrams are developed using knowledge of bifurcation and cusp curves of geometric singularity from the catastrophe theory and become great tools for understanding the stability behaviors in geometrically nonlinear structures. For a single external degree of freedom elastic truss structure with Green's strain approximation only a single cusp singularity exists, and stability behaviors could be monostability when only one stable state exist and bistability when two stable states exist. However, bistability is found to exist in two forms: superelasticity which is the usual transition between two stable states with no residual deformation after load removal and superplasticity when residual deformation exist after load removal and a reversal force is required for full recovery.

The analytical approach discussed in the bistability studies helped to present a detailed discussion of the negative extensibility metamaterial behavior in simple elastic structure made up of bars and springs with two external vertical degrees of freedom and an internal rotational degree freedom. It is shown that even for simple structures possessing negative extensibility, their stability behaviors could be complex possessing two cusp points or a cusp point of beak forming bifurcation curves. These unusual stability diagram characteristics lead to a pinch hysteresis initiating the negative extensibility behavior and a secondary hysteresis. The phase diagram of the structure studied described five stability behaviors as follows: monostability, superelasticity, superplasticity, negative extensibility superelasticity and negative extensibility superplasticity.

The study of nonlocal mechanical materials like the x-braced periodic lattice has demonstrated that when unit-cell structure stiffness properties are well programmed they could lead to the reverse Saint Venant edge metamaterial behavior. This metamaterial behavior is showcased by the reversal in decay rate of Raleigh modes such that lower wave numbers (coarse) decay faster while higher wave numbers (even) decay slower due to the presence of bandgaps in the deformation decay spectrum of the x-braced lattice. A further study of the metamaterial in a 2D nonlocal periodic lattice structure is introduced which includes building solution forms for a Raleigh mode and for arbitrary natural and essential boundary conditions. A bandgap design is also discussed using the concept of phase diagram to limits for attaining deformation blockage. Repeated zero eigenvalues in 2D nonlocal periodic lattice will be shown to possess a unique capacity to polarize any arbitrary polarization vector of the Raleigh mode associated with the wave number and therefore classified as polarizing lattice structures. Since the nonlocal periodic lattice could possess anomalous strain energy behavior due to complexities in its deformation spectrum, the strain energy spectral density and strain energy spectral entropy measures are developed using analogies to the Parseval's theorem and Shannon's entropy and approaches for both continuum material and lattice materials are detailed. The 45^o maximal strain energy rerouting and the channeling of low energy pockets in the 2D periodic nonlocal x-braced lattice material were identified as anomalous strain energy behaviors far from the behavior in an L -periodic continuum material. Complexities in the spectral energy distribution of a nonlocal periodic lattice could lead to its strain energy spectral entropy having a local maximum compared to a monotonic continuum behavior.

1 INTRODUCTION

1.1 Mechanical Metamaterials

Metamaterials is a term that classify modern engineered materials possessing extreme functionalities that are driven by their preconceived unusual properties. Veselago in 1967 [1], proved the concept of metamaterials to exist when he theoretically showed that materials identified to show both negative permeability and negative permittivity could lead to an exotic property known as negative refractive index. Pendry and Smith [2-4] proved the validity of the negative refractive index metamaterial in their experimental studies and that ignited the field of photonic metamaterials showcasing studies on advanced resolution imaging and wave guiding technology [5-9]. The concept of negative refractive index is also seen in wave mechanics when materials are tuned to have both negative bulk modulus and negative mass density and as such are classified under acoustic or phononic metamaterials. These metamaterials allow sound waves to be manipulated to serve interesting applications such as shielding and reflection of seismic waves when bandgaps exist in their dispersion curves [10-13].

The field of mechanical metamaterials is an emerging addition to the strive in the past decades to produce materials with unforeseen properties and functionalities. In the theory of mechanical metamaterials, the success in optics and acoustics, where negative refractive index is achieved by programming the geometry of individual unit-cells, has been a guiding approach. Therefore, when the uniqueness in the geometry of the unit-cells or components of a material provides an opportunity to manipulate mechanical properties such as deformation, stress, stiffness and energy in unforeseen ways than is likely then such a material is termed a mechanical metamaterial. A look at different reviews [14-15] on mechanical metamaterials have shown that these unusual behaviors are a result of adverse material elastic parameters like the Young's modulus, bulk modulus and shear modulus and the Poisson's ratio. Meaning the right unit-cell structure geometry and overall global configuration can lead to unexpected elastic properties with performance which exceeds that of ordinary materials.

The earliest record of a mechanical metamaterial was seen in a paper by Kolpakov in 1985 [16] that showcased an example of an elastic framed network with negative Poisson's ratio and so the network must expand laterally

when a longitudinal tensile force is applied (See Fig. 1.1) due to their bulk to shear modulus ratio approaching zero. Later in 1987, Lakes [17-18] introduced a re-entrant polyform foam structure which possessed this exotic behavior and that has led research into field of mechanical metamaterials termed auxetics. An auxetic behavior is said to be a property of a non-convex microstructure [19] and could see potential applications in aerospace and marine structures due to their shock absorption and low-density properties [20].

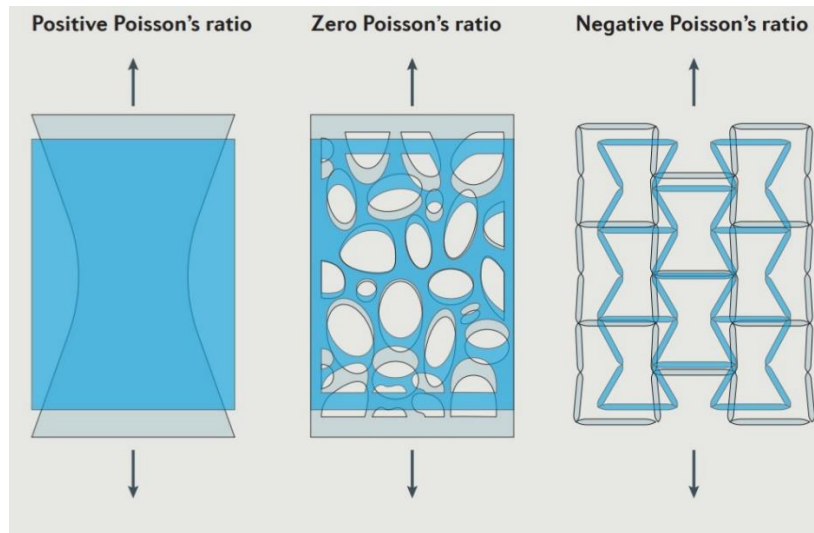


Figure 1.1 Different Poisson's ratio measures: (left) Positive Poisson's ratio exhibited in a rubber sheet when axially applied tensile force causes lateral contraction (deformed state in blue). (middle) Zero Poisson's ratio in a patterned or cellular material such that there is no lateral contraction under tensile axial force even when individual pores contract. (right) Negative Poisson's ratio is seen in an auxetic lattice so that there is lateral expansion under a tensile axial force. [15]

It is well known [21-22] in the field of mechanics that vibration transmission in mechanical components calls for an ideally zero stiffness of a supporting structure. The high dampening efficiency of materials possessing negative stiffness [23-24] has defined like materials as metamaterials. Bistable substructures exhibiting snap-through can characterize designs of these mechanical metamaterials [25]. The topology transformation feature associated with bistable structures can be seen in reprogrammable actuators [26] and reconfigurable origami structures [27-29] with extreme functionalities (See Fig. 1.2). Bistability as a feature of negative stiffness can also lead to some rare metamaterial behavior in engineered structures like negative compressibility [30-33], where a structure contracts under a tensile load in the direction of the load. Structures with multiple degrees of

freedom and an internal degree of freedom could be modelled with this metamaterial ability and they would have the capacity to serve as super dampers for isolation of earthquake and explosion impact.

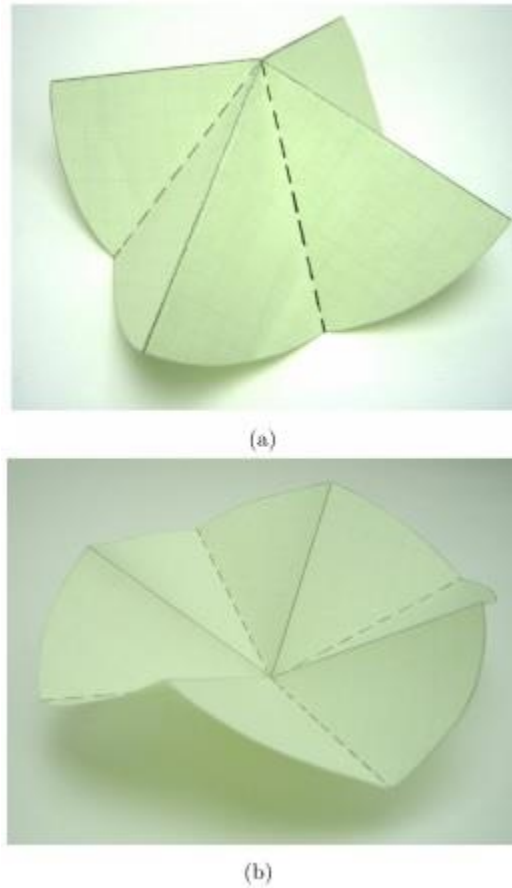


Figure 1.2 Origami waterbomb base bistability: (a) first stable configuration after folding and (b) second stable configuration when vertex is pushed beyond a its base plane. [28]

Taking advantage of such advanced material behaviors the scope and applicability of engineered smart materials, composites and structures could bring worthy innovation in fields like architecture, manufacturing, transportation and medicine. In the ongoing studies on mechanical metamaterials, there is always the need for further discourse to broaden the field of knowledge. If we take for instance negative compressibility (See Fig. 1.3), a bulk property where material contracts under tensile load in the direction of a force, published studies [30-33] have looked at destabilization of stable states of an idealized atomic structure of a material. They analyzed structures having multiple degrees of freedom which included an internal of freedom which showcased an advanced bistability behavior evidenced by a pinched hysteresis leading to negative compressibility.

Therefore, negative compressibility could be harnessed in elastic structures by developing tools that predict efficiently predict multistability responses in these structures. Previous studies [34-38] on multistability have studied structures from dielectric elastomer actuators to three dimensional trusses and have been successful in describing equilibrium state transitions but have been limited in describing a comprehensive design map where the stability of multi-stable systems could be predictive. Developing such a design map means if a negative compressibility behavior is realized in a multi-stable system, we would be confident in predicting such a unique metamaterial property as well. Ability to build units of such peculiar behavior subsequently poses the question of how periodic lattice models could be built to attain a similar collective metamaterial behavior. This achievement would be a notable step at controlling deformation behavior in periodic lattice structures as is seen in acoustic metamaterials where altering bandgap characteristics by tuning individual substructures can lead to sound controlling capabilities like noise control and vibration isolation [10-13].

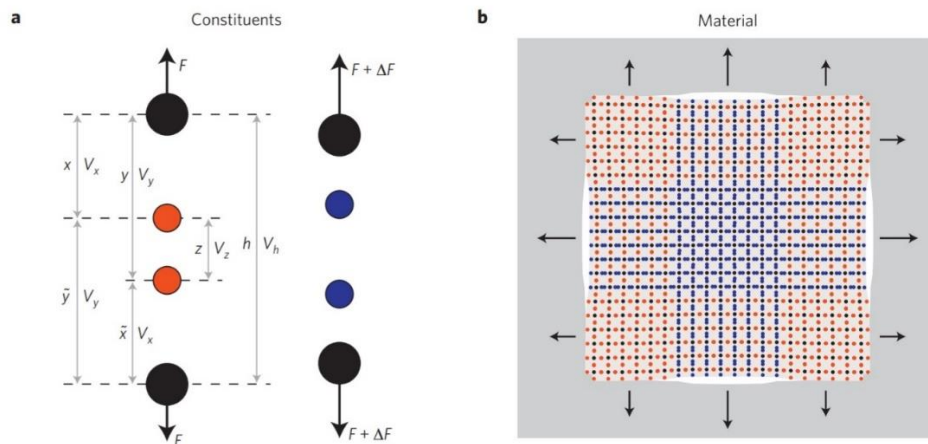


Figure 1.3 Negative compressibility: (a) Four-particle constituent structure showing initial stable state (red) and contracted second stable state (blue) after application of tensile force making it a negative compressible structure. (b) A material made up of the constituent particles in (a) exhibiting negative compressibility metamaterial after applying an isotropic tensile force (see middle of edges). [30]

Deformation in materials is an important area of study in mechanics with the aim of understanding stress and strain distribution to be able to improve resilience and eliminate mechanical failures like crack. Structures with potential for deformation reprogramming would therefore be termed smart possessing hyper functionalities like stress alleviation, deformation recognition etc. Studies on reprogramming mechanical deformation in

periodic lattice network can be seen in the study of pentamode metamaterials [39-41] (See Fig. 1.4), an interesting example where a material can be programmed to block a single mode of deformation. A related field is the study of topological metamaterials, a kind of isostatic lattices which are programmed to have zero-frequency modes when the topological index of its unit-cell structure is tunable [15,42-43]. In another studies [44] on isostatic lattice network, we have seen controlled arbitrary global deformation when unit-cells are periodically actuated.

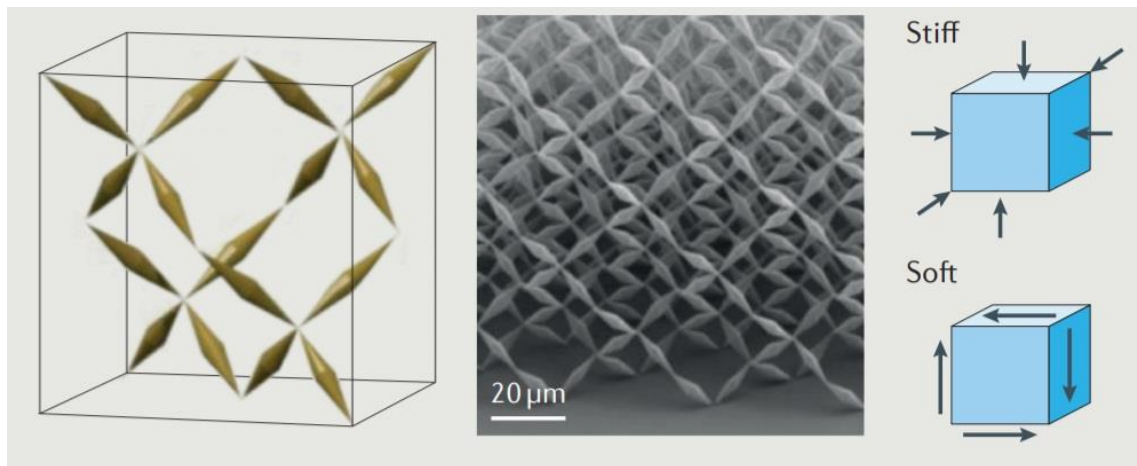


Figure 1.4 Pentamode mechanical metamaterial: (left) hypothetical pentamode lattice and (middle) electron micrograph view of directed ink printed pentamode lattice structure. (right) Pentamode lattice being very stiff under uniform compression and very soft under a shear force due to shear to bulk ratio approaching zero. [15]

Studies recently presented by Karpov [45] on the anomalous behavior of nonlocal x-braced lattices termed as the reverse Saint-Venant edge effect (RSV) is a metamaterial behavior which creates avenue for unique deformation programming functionalities like static deformation blockage and deformation propagation rate reversal in periodic lattices. This is achieved by the existence of exotic features termed bandgaps in materials deformation spectrum analogous to the dispersion curve in acoustic mechanics. The study [45] while constrained to 1D periodic lattices is a state of the art in lattice mechanics which provides an essential understanding for programming applied static deformation patterns lattice structures. Broadening such a knowledge to 2D lattice structures and deepening understanding on how deformation and strain energy transforms in a lattice media could lead to identifying anomalous lattice material behaviors.

1.2 Thesis Organization

The subject of this thesis would be to discuss bistable and nonlocal lattice networks with the potential for metamaterial behaviors like negative extensibility and the reverse Saint-Venant Edge Effect (RSV) respectively, but the overall aim is to identify anomalies in deformation and strain energy behaviors in such structures. Having given an overview of mechanical metamaterials in the ongoing chapter, the rest of the thesis is presented as follows:

The second chapter will be dedicated to the design of bistability behavior in elastic systems and how they could be systematically analyzed in systems with geometrical nonlinearity. The mathematical concept of the catastrophe theory will be introduced as a way of developing stability diagrams and cusp curve phase diagrams that predict bistability behavior and their designability limits.

In the third chapter, we discuss the negative extensibility mechanical metamaterial property as a by-product of bistable systems with multiple degrees of freedom including an internal degree of freedom. The discussion will proceed by developing similar stability diagrams and cusp curve phase diagrams as done in the second chapter to serve as a guide for programming such a rare metamaterial behavior in elastic structural systems and units.

In chapter four, the Parseval's energy theorem as a borrowed concept from signal analysis is presented as a novelty in continuum mechanics. The mechanics analogue of the Parseval's theorem helps to introduce the strain energy spectral density in a continuum media which leads into the discussion of spectral energy transformation against spatial energy transformation in a continuum media. Entropy of mechanical deformation as a parameter to study information, disorder, inhomogeneities introduced by surface loads is also formulated. Such novel theories will be used to develop a numerical strain measurement method, an approach that would be an efficient tool for analyzing anomalies in strain energy in continuum material as well as periodic lattices.

Chapter five starts with a detailed background on static analysis of periodic lattice networks. The method of discrete field analysis as a means of writing a compact governing equilibrium equation is introduced with its comparable operator form that allows for an efficient Discrete Fourier Transform analysis. The transfer matrix and the solution form of the associate substructure of a nonlocal periodic lattice is written as a precursor to

demonstrating the reverse Saint-Venant Edge effect behavior as shown in the study by Karpov. A comprehensive 2D static Raleigh mode solution is presented here and after expanded to solution methods for analyzing arbitrary essential and forced boundary conditions. System design maps for predicting Raleigh mode blockage and the RSV effect in an x-braced lattice and polarizing periodic lattice structures (the scenario of repeated-zero eigenvalues) are also discussed. To end the chapter, the concepts of the Parseval's theorem and entropy in numerical strain energy measurement introduced in Chapter 4 will be used to study anomalous strain energy behavior in 2D x-braced nonlocal lattices by comparing behaviors to continuum strain energy behavior. The last chapter would summarize major conclusions of this thesis and provide suggestions for future work to advance this field of study.

CHAPTER 1 REFERENCES

- [1] Veselago, V.G. The electrodynamics of substances with simultaneously negative values of permittivity and permeability. *Sov. Phys. Uspekhi* **1968**, *10*, 509–514.
- [2] Smith, D.R.; Padilla, W.J.; Vier, D.C.; Nemat-Nasser, S.C.; Schultz, S. Composite medium with simultaneously negative permeability and permittivity. *Phys. Rev. Lett.* **2000**, *84*, 4184–4187.
- [3] Pendry, J.B.; Holden, A.J.; Stewart, W.J.; Youngs, I. Extremely low frequency plasmons in metallic mesostructures. *Phys. Rev. Lett.* **1996**, *76*, 4773–4776.
- [4] Pendry, J.B.; Holden, A.J.; Robbins, D.J.; Stewart, W.J. Magnetism from conductors and enhanced nonlinear phenomena. *IEEE Trans. Microw. Theory Tech.* **1999**, *47*, 2075–2084.
- [5] Pendry, J.B. Negative refraction makes a perfect lens. *Phys. Rev. Lett.* **2000**, *85*, 3966–3969.
- [6] Soukoulis, C.; Wegener, M. Past achievements and future challenges in the development of three-dimensional photonic metamaterials. *Nat. Photonics* **2011**, *5*, 523–530.
- [7] Zhou, J.; Koschny, T.; Kafesaki, M.; Economou, E.N.; Pendry, J.B.; Soukoulis, C.M. Saturation of magnetic response of split-ring resonators at optical frequencies. *Phys. Rev. Lett.* **2005**, *95*, 223902.
- [8] Miyamaru, F.; Saito, Y.; Takeda, M.W.; Hou, B.; Liu, L.; Wen, W.; Sheng, P. Terahertz electric response of fractal metamaterial structures. *Phys. Rev. Lett. B* **2008**, *77*, 045124.
- [9] Guariglia, E. Entropy and Fractal Antennas. *Entropy* **2016**, *18*, 84.
- [10] Cummer, S.A.; Christensen, J.; Alu, A. Controlling sound with acoustic metamaterials. *Nat. Rev. Mater.* **2016**, *1*, 16001.

- [11] Hussein, M.I.; Leamy, M.J.; Ruzzene, M. Dynamics of phononic materials and structures: Historical origins, recent progress, and future outlook. *Appl. Mech. Rev.* **2014**, *66*, 040802.
- [12] Lui, Z.; Zhang, X.; Mao, Y.; Zhu, Y.; Yang, Z.; Chan, C.; Sheng, P. Locally resonant sonic materials. *Science* **2000**, *289*, 1734–1736.
- [13] Wang, Y.Z.; Li, F.M.; Huang, W.-H.; Jiang, X.; Wang, Y.-S.; Kishimoto, K. Wave band gaps in two-dimensional piezoelectric/piezomagnetic phononic crystals. *Int. J. Solids Struct.* **2008**, *45*, 4203–4210.
- [14] Yu, X.L.; Zhou, J.; Liang, H.Y.; Jiang, Z.Y.; Wu, L.L. Mechanical metamaterials associated with stiffness, rigidity and compressibility: A brief review. *Prog. Mater. Sci.* **2018**, *94*, 114–173.
- [15] Bertoldi, K.; Vitelli, V.; Christensen, J.; van Hecke, M. Flexible Mechanical Metamaterials. *Nat. Rev. Mater.* **2017**, *2*(11), p. 17066.
- [16] Kolpakov A.G. On the determination of the averaged moduli of elastic gridworks. *Prikl. Mat. Mekh.* **1985** *59*, 969–977.
- [17] Lakes, R.S. Foam structures with a negative Poisson's ratio. *Science.* **1987**, *235*, 1038–1040.
- [18] Lakes, R.S. Negative Poisson's ratio materials. *Science.* **1987**, *238*, 551.
- [19] Kaminakis, N.T.; Stavroulakis, G.E. Topology optimization for compliant mechanisms, using evolutionary-hybrid algorithms and application to the design of auxetic material. *Composites Part B: Engineering.* **2012**, *43* (6): 2655–2668
- [20] Stavroulakis, G.E. Auxetic behaviour: Appearance and engineering applications. *Physica Status Solidi B.* **2005**, *242* (3): 710–720.
- [21] Molyneux, W. Supports for Vibration Isolation. *Aeronautical Research Council, Great Britain.* **1957**. ARC/CP-322.
- [22] Alabuzhev, P.; Rivin, E.I. Vibration Protection and Measuring Systems with Quasi-zero Stiffness. *CRC Press.* **1989**.
- [23] Dong, L.; Lakes, R. Advanced damper with high stiffness and high hysteresis damping based on negative structural stiffness. *Int. J. Solids Struct.* **2013**, *50*, 2416–2423.
- [24] Spitas, V.; Spitas, C.; Michelis, P. Modeling of the elastic damping response of a carbon nanotube–polymer nanocomposite in the stress–strain domain using an elastic energy release approach based on stick–slip. *Mech. Adv. Mater. Struct.* **2013**, *20*, 791–800.
- [25] Chronopoulos, D.; Antoniadis, I.; Collet, M.; Ichchou, M. Enhancement of wave damping within metamaterials having embedded negative stiffness inclusions. *Wave Motion.* **2015**, *58*, 165–179.
- [26] Chen, T.; Shea, K. An Autonomous Programmable Actuator and Shape Reconfigurable Structures using Bistability and Shape Memory Polymers. *Cornell University Library.* Nov **2017**.
- [27] Waitukaitis, S.; Menaut, R.; Chen, B. G-g; van Hecke, M. Origami multistability: From single vertices to metasheets. *Phys. Rev. Lett.* **2015**, *114*, 055503.

- [28] Hanna, B. H.; Lund, J. M.; Lang, R. J.; Magleby, S. P.; Howell, L. L. Waterbomb base: A symmetric single-vertex bistable origami mechanism. *Smart Mater. Struct.* **2014**, *23*, 094009.
- [29] Silverberg, J. L. et al. Origami structures with a critical transition to bistability arising from hidden degrees of freedom. *Nature Mater.* **2015**, *14*, 389–393.
- [30] Nicolau, Z. G.; Motter, A. E. Mechanical metamaterials with negative compressibility transitions, *Nature Mater.* **2012**, *11*, 608.
- [31] Nicolau, Z. G.; Motter, A. E. Longitudinal inverted compressibility in super-strained metamaterials, *J. Stat. Phys.* **2013**, *151*, 1162.
- [32] Chen, M. L.; Karpov E. G. Bistability and thermal coupling in elastic metamaterials with negative compressibility, *Phys.Rev. E.* **2014**, *90*, 033201.
- [33] Imre, A.R. Metamaterials with negative compressibility – a novel concept with a long history, *Materials Science-Poland.* **2014**, *32*, 126–129
- [34] Cai, J. G.; Xu, Y. X.; Feng, J.; Zhang, J. 2011. Mechanical Behavior of Bistable Struts. *J. Mechanical Engineering Science Proc. IMech.* **2011**, 226 Part C.
- [35] Plante, J.S.; Santer, M. Compliant Bistable Dielectric Elastomer Actuators for Binary Mechatronic Systems. *Proceedings Of IDECT/CIE 2005 ASME Mechanism and Robotics Conference, Long Beach, California, USA*, **2005**, 24-28.
- [36] Kinoshita, T.; Oshaki, M. Synthesis of Bistable Compliant Structures from Truss Mechanisms. *Journal of Computational Science and Technology.* **2009**, *3*(2).
- [37] Hu, N.; Burgueno, R. Buckling-induced smart applications: recent advances and trends. *Smart Materials and Structures.* **2015**, *24*: 063001.
- [38] Shon, S.; Lee, S.; Ha, J.; Cho, C. 2015. Semi- Analytic Solution and Stability of Space Truss Using a Higher-Order Taylor Series. *Materials.* **2015**, *8*, 2400-2414.
- [39] Milton, G. W.; Cherkaev, A. V. Which Elasticity Tensors are Realizable? *Journal of Engineering Materials and Technology.* **1995**, *117* (4): 483.
- [40] Kadic, M.; Bückmann, T.; Stenger, N.; Thiel, M.; Wegener, M. On the practicability of pentamode mechanical metamaterials. *Appl. Phys. Lett.* **2012**, *100*, 191901.
- [41] Fraternali, F.; Amendola, A. 2017 Mechanical modeling of innovative metamaterials alternating pentamode lattices and confinement plates. *J. Mech. Phys. Solids.* **2017**, *99*, 259-271.
- [42] Kane, C. L.; Lubensky, T. C. Topological boundary modes in isostatic lattices. *Nat. Phys.* **2014**, *10*, 39–45.
- [43] Rocklin, D.Z.; Zhou, S.; Sun, K.; Mao, X. Transformable topological mechanical metamaterials. *Nature Comm.* **2015**, *8*, 14201.

[44] Donev, A.; Torquato, S. Energy-efficient actuation in infinite lattice structures. *J. Mech. Phys Solids*. **2003**, *51*(8), 1459-1475.

[45] Karpov, E.G. Structural metamaterials with Saint-Venant edge reversal, *Acta Materialia*. **2017**, *123*, 245-254.

2 DESIGN OF BISTABILITY BEHAVIOR IN ELASTIC STRUCTURES

(This chapter is based on a material previously published as Danso, L. A.; Karpov, E.G. Cusp Singularity-Based Bistability Criterion for Geometrically Nonlinear Structures. Extreme Mechanics Letters. 2016, 13, 135-140.)

2.1 Introduction

Bistability is a property where a mechanical system exhibits two stable states of equilibrium. This mechanical behavior is seen in metastable systems or systems that undergo a snap-through action in their force-displacement curves. This snap-through behavior is comparable to the temperature induced elastic hysteresis showcased by ferroelastic solids and other shape memory alloys (SMA) [1-2].

The large deformations accompanying the snap-through action in elastic structures means assumptions of small deformations and rotations would not be enough to analyze the nonlinear behavior and therefore *geometrical nonlinearity* of the structure should be included in analysis [3]. Geometrical nonlinearity is captured in analysis when the equilibrium of the deformed state of the elastic structure is used to determine the response of the structure under a load.

The equilibrium of the deformed state of conservative elastic structural systems could be described by employing the principle of equilibrium potential energy and for bistable systems have been shown to be of the quartic order [3]. This principle implies by minimizing or maximizing the total potential energy of a conservative system with admissible kinematic deformations the state of equilibrium either stable, unstable or neutral could be determined.

In the case of bistable systems, the force-displacement curve plotted from the equilibrium potential shows two states of stable equilibrium as seen in Fig. 2.1. In a forced-controlled system, at a certain critical force f_C at point O corresponding to a neutral equilibrium state (inflection point) there is a transition from stable state A to stable state B which signifies a snap-through action. This snap-through action exists because at the critical

point O, a small change in force would cause a change in displacement that follows a negative stiffness slope which is an unstable and hence the jump to the adjacent stable state.

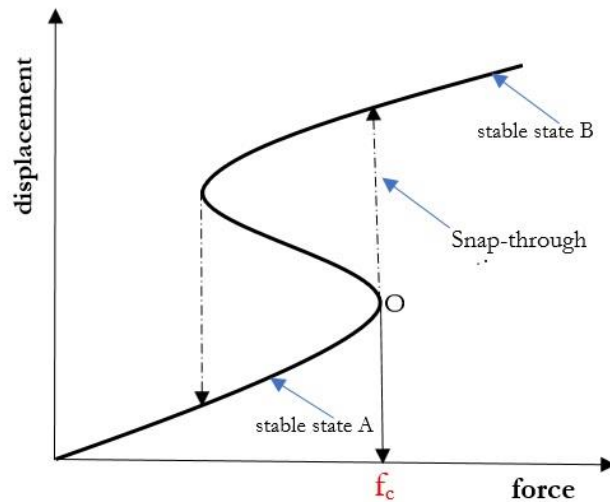


Figure 2.1 Snap-through Action

Due to the high energy storage potential and the multiple stable states of deformation that could be achieved, bistable elastic structures could be beneficial in designing large scale advanced structures as seen in the civil and aerospace industries. Snap-through based reconfigurability has led to significant studies on deployable and shape morphing structures [4-7]. Other authors [8-10], have also studied shell, space truss and frames that have exhibited a snap-through with foreseeable future in smart materials and structures. Mechanical components and electromechanical units as well as small scale MEM devices have comfortably been modelled using truss systems with multi-stability [11-13]. These smart applications have sometimes utilized the snapping effect associated with the buckling instability of these systems [14].

Studies on the Crisfield circular arch truss and other space trusses with repeated truss structures [8-9] have shown multiple snap-through actions which gives confidence for identifying multi-stability behavior in periodic

lattice models. Materials developed from periodic lattice controlled by truss unit-cell structure [15-16] designed with the feature of multiple stable states could see enviable applications in composite materials where stability control is an overarching quality.

Bistable elastic structures are also great candidates for a *negative stiffness* (NS) metamaterial behavior: the case when a structure's deformation direction opposes the direction of the applied force and initiates a negative restoring force or an assisting force (acts in direction of deformation). This NS behavior is achieved only under an unstable state of equilibrium and can only be harnessed under a displacement-controlled regime or when structure or material is embedded in a system with positive stiffness which stabilizes the system [3, 17-19]. Structures designed with NS are functional mechanical metamaterials with vibration isolation and seismic protection properties [20-21].

In previous studies on geometrically nonlinear structures [9, 22-24], numerical methods like the arc-length and intrinsic finite element methods have been used to analyze the stability of trusses and some have exhibited the snap-through behavior. Similarly, the history of optimization of structural response and design which are critical to minimizing design costs by producing high strength and light weight structures have been founded on numerical methods [25-28]. These optimization methods involve a huge computational cost due to the amount of structural analysis even for linear response approximation and therefore geometrical nonlinear analysis is expected to impose undue computational burden [29].

Studies by [29] have suggested a numerical predictive tool like an adaptive neuro-fuzzy inference to be much efficient for optimizing structural response of geometrically nonlinear truss structures. However, the need to provide a universal framework to be able to fully-understand systems with high geometrical nonlinearity as well as those that present multi-stability behavior could mean the use of a full analytical or semi-analytical method [30-33] notwithstanding the success of the available computational methods. The efforts made by these analytical studies in capturing the nonlinear bistable response is commendable, but they do not present a fully analytical path for predictive design.

Hence, the aim of this chapter is to provide a mathematical model for analyzing and controlling the equilibrium stability response in geometrically nonlinear elastic structures and more importantly a systematic framework for predictive design. The approach would be to use a special case of the catastrophe theory [3, 34-39] in geometric singularity studies known as the *cusp* employed to develop optimization tools termed stability diagrams and a phase diagram. A systematic analytical procedure will be illustrated using simple 2D and 3D elastic truss systems.

2.2 Design Using Stability Diagrams

2.2.1 Catastrophe Theory

The catastrophe theory is a theory developed by Rene Thom [34] in the 1960's with great contributions from Zeemann, Arnold and Gilmore [35-37]. It is classified as a branch of the bifurcation theory which studies the changes in qualitative behavior in the topology of dynamical systems. Catastrophe theory by Gilmore is the study of the relationships that could be drawn between qualitative nature of solution space of an equation and the parameters represented in the equation. The ability to develop relationships between parameters underpinning a system's response known as stability diagrams is the importance of the catastrophe theory in the design process. Such parameters are deemed as system parameters describing inherent properties (stiffness, skewness, density) or control parameters when they control the qualitative behavior of the solution space. The variables forming such an equation are termed state variables (deformation, strain) since they account for the state of a system. Catastrophes are characterized by the nonlinear system behavior which is shown by a sudden or large change in qualitative behavior of the state of a system and a jump like that of the snap-through action seen in bistable systems. Rene Thom identified seven elementary catastrophes [34] as given in TABLE I. The topology (See the $f-y$ -plane of Fig. 2.1) of the cusp catastrophe corresponds with the snap-through behavior and therefore elastic structures having a total potential of the quartic form as the cusp generating function would possess the bistability behavior.

2.2.2 Drawing the Stability Diagram

For example, let's assume the first derivative of a generating function to have the form $y^3 - ay^2 + by - f = 0$. This function could be said to have two (2) system parameters (a, b) and one (1) control parameter (f) and referring to TABLE I, has the cusp catastrophe form. Fixing system parameter, a , to a constant value and plotting the three-dimensional space (3D) topology we obtain the plot in Fig. 2.2

Table I Form of the seven elementary catastrophes

Type of Catastrophe	Control/System parameters	State variables	Generating function	First derivative (response)
Fold	a	x	$\frac{1}{3}x^3 - ax$	$x^2 - a = 0$
Cusp	a, b	x	$\frac{1}{4}x^4 - ax - \frac{1}{2}bx^2$	$x^3 - a - bx = 0$
Swallowtail	a, b, c	x	$\frac{1}{5}x^5 - ax - \frac{1}{2}bx^2 - \frac{1}{3}cx^3$	$x^4 - a - bx - cx^2 = 0$
Butterfly	a, b, c, d	x	$\frac{1}{6}x^6 - ax - \frac{1}{2}bx^2 - \frac{1}{3}cx^3 + \frac{1}{4}dx^4$	$x^5 - a - bx - cx^2 - dx^3 = 0$
Hyperbolic umbilic	a, b, c	x, y	$x^3 + y^3 + ax + by + cxy$	$3x^2 + a + cy = 0$ $3y^2 + b + cx = 0$
Elliptic umbilic	a, b, c	x, y	$x^3 - xy^2 + ax + by + cx^2 + cy^2$	$3x^2 - y^2 + a + 2cx = 0$ $-2xy + b + 2cy = 0$
Parabolic umbilic	a, b, c, d	x, y	$xy^2 + y^4 + ax + by + cx^2 + dy^2$	$2xy + a + 2cx = 0$ $x^2 + 4y^3 + b + 2dy = 0$

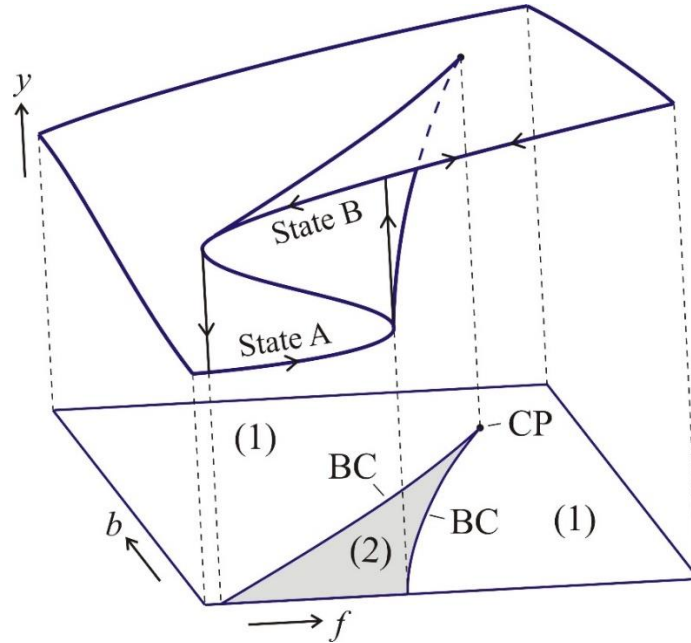


Figure 2.2 A 3D topological view of a cusp catastrophe: The generating function has a first derivative, $y^3 - ay^2 + by - f = 0$. Where system parameter a has been fixed to a constant value. The stability diagram is described by the projection of the topology onto the fb -plane: the locus of all existing (ab -parameterized) bifurcation points (CP – the cusp point; BC – bifurcation curves). (1) – monostability; (2) – bistability (superelasticity/superelasticity).

A projection of this topology unto the (f, y) describes the hysteresis which is typical of a snap-through behavior as shown in Fig. 2.1. Projecting the 3D solution space unto the (f, b) plane, we obtain points when the transitions between two stable equilibriums and what is termed a *stability diagram* [38]. The stability diagram is basically a plot of all bifurcation points (BC) in the system's generating function is governed by the degenerate point condition, $\frac{d^2\Pi}{dv^2} = 0$ and could be defined as the plot of all inflection points in a system when a system is neither stable or unstable. Ability to develop the stability diagram is of great significance since it gives a full view of all types of stability response behaviors in a generating system function and their ranges by varying the control parameter and a system design parameter. On the stability diagram, we see the extent of the bistability (snap-through) with its onset being the cusp point (CP). The cusp point is unique for a stability because it is a

2N-bifurcation point which means tuning two system parameters to achieve bifurcation. On the stability diagram we can also observe bistability to be comprised of two types: superelasticity and superplasticity. Superelasticity being the usual behavior in bistable systems where the system recovers initial state and all deformations during unloading at $f = 0$ and superplasticity is when at $f = 0$, initial state is not fully recovered during unloading. Hence, the need for load reversal for full initial state recovery. All regions besides the bistability behavior are termed monostability regions since they exhibit only one stability state.

2.3 Bistability Analysis in Elastic Structures

Taking advantage of the geometrical nonlinearity characteristic of structures that show multistability, a linearly elastic structure is assumed to undergo small to moderate axial strains less than 0.05 but nodal displacements are large. Buckling instability is eliminated from bar elements of the structure by also assuming a very high Euler load [3, 40]. The total potential energy of the system is first sought and then the first derivative is applied with respect to the available system to obtain the minimum equilibrium potential equation or equations in case of multiple system variables. The derived total potential, Π , has the form:

$$\Pi = U - V \quad (2-1)$$

Where U is the stored strain energy in the bars and V is the potential energy calculated for the applied external load. In an elastic bar or link the stored strain energy could be written in terms of the E - Young's modulus, A - cross-sectional area, L - initial length of bar and l - deformed length as

$$U = \frac{EA(l-L)^2}{2L} \quad (2-2)$$

If the expression k describes the stiffness $\frac{EA}{L}$ in a bar and the Cauchy or engineering strain is defined as $\varepsilon_c = (l - L)/L$, (2-2) can be rewritten as

$$U = \frac{1}{2}kL^2\varepsilon_c^2 \quad (2-3)$$

For purposes of simplification by eliminating square roots when analyzing inclined bars, we replace the Cauchy strain ε_c with the Green's strain ε_G :

$$\varepsilon_G = \frac{l^2 - L^2}{2L^2} \quad (2-4)$$

The relationship between ε_c and ε_G can be obtained as $\varepsilon_G = \varepsilon_c + \frac{1}{2}\varepsilon_c^2$ [41] and for very small to moderate axial strains as mentioned earlier, the offset in value is approximately less than 0.3%. The strain energy in the bars sustains an external potential that is expressed in terms of the applied load F and nodal displacement v as $V = Fv$.

Formulating all the terms for the total potential energy in (1-2) which serves as the generating function in catastrophe theory. The equilibrium minimum potential energy and the degenerate point condition can then be used to find the system response curves and the stability diagrams as shown above. If the equilibrium potential function is a cubic order polynomial with a minimum one system design parameter and a control parameter (See TABLE I), then the cusp or stability diagrams can be generated to predict the behavior of a system response curve whether monostability or bistability (superelasticity/superelasticity).

2.3.1 2D Four Bar Truss Example

In this section, we analyze the four-bar truss in Figure 2.3 which is far from the ideal von Mises trusses whose stability has been studied by several authors [3, 42-43]. The top bars and bottom bars have stiffnesses k_1 and k_2 respectively.

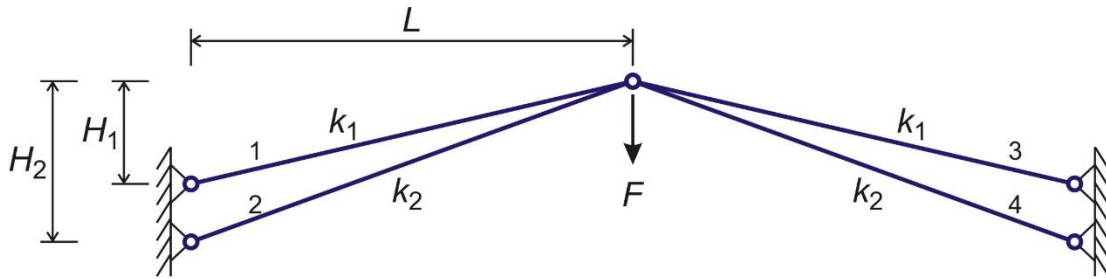


Figure 2.3 A four bar plane truss

The bars 1-4 in Figure 2.3 would there have their Green's strains calculated from (2-4) as

$$\varepsilon_{1,3} = \frac{v^2 - 2H_1v}{2(L^2 + H_1^2)} \quad (2-5)$$

$$\varepsilon_{2,4} = \frac{v^2 - 2H_2v}{2(L^2 + H_2^2)} \quad (2-6)$$

We then derive the stored strain energies in the bars from (2-3) in the equations below.

$$U_{1,3} = \frac{1}{8} \frac{k_1}{(L^2 + H_1^2)} [v^2 - 2H_1v]^2 \quad (2-7)$$

$$U_{2,4} = \frac{1}{8} \frac{k_2}{(L^2 + H_2^2)} [v^2 - 2H_2v]^2 \quad (2-8)$$

Substituting equations (2-5 - 2-8) into Equation (2-1), the total potential equation has the form:

$$\Pi = \frac{k_1}{4(L^2 + H_1^2)} [v^2 - 2H_1v]^2 + \frac{k_2}{4(L^2 + H_2^2)} [v^2 - 2H_2v]^2 - Fv \quad (2-9)$$

Hence, the first derivative $\frac{d\Pi}{dv}$ satisfying the state of equilibrium of the structure is

$$\frac{d\Pi}{dv} = \frac{k_1}{(L^2 + H_1^2)} (v^2 - 2H_1v)(v - H_1) + \frac{k_2}{(L^2 + H_2^2)} (v^2 - 2H_2v)(v - H_2) - F = 0 \quad (2-10)$$

By introducing the dimensionless parameters: g – applied force, γ – stiffness, h – truss height and y – deformation, (2-10) becomes

$$g = (y^3 - 3y^2 + 2y) + \gamma(y^3 - 3hy^2 + 2h^2y) \quad (2-11)$$

$$g = \frac{F(L^2 + H_1^2)}{k_1 H_1^3} \quad \gamma = \frac{k_2(L^2 + H_1^2)}{k_1(L^2 + H_2^2)} \quad h = \frac{H_2}{H_1} \quad y = \frac{v}{H_1} \quad (2-12)$$

We further obtain a much simpler form of Equation (2-11) by expanding, grouping and dividing terms with the coefficient of the highest order term. This gives the final equilibrium equation to be analyzed for stability as

$$f = y^3 - ay^2 + by \quad (2-13a)$$

$$f = \frac{g}{1+\gamma}, \quad a = \frac{3(1+h\gamma)}{1+\gamma}, \quad b = \frac{2(1+h^2)}{1+\gamma} \quad (2-13b)$$

2.3.2 Simple Truss Stability Diagrams

The equilibrium equation in 2-13a now becomes a great tool for understanding the stability behavior inherent in the truss system shown in Fig. 2.3. Using the stability diagrams approach mentioned earlier, it is possible to draw up relationships existing between parameters within the structure's equilibrium function (2-13a). In 2-13a, y is the state variable, f serves as the control parameter and a, b are the system or design parameters. The stability diagram as seen prior comprises bifurcation curves made up of bifurcation points of a system. These bifurcation

points are points of inflection of the system equilibrium function and so these can be plotted directly without the graphical projection of the solution topology used in Fig. 2.2 by applying the degenerate/ inflection point condition $\frac{d^2\Pi}{dv^2} = 0$. Taking derivative of (2-13a) and solving for y we obtain the expression:

$$y = \frac{a \pm \sqrt{a^2 - 3b}}{3} \quad (2-14)$$

Substituting the above equation back into (2-13a) and fixing either a or b we obtain expressions (f, a) and (f, b) which describes the bifurcation curves that plots the stability diagram. For example, by designing the truss structure in Fig. 2.3 to have the following design parameters: $H_1 = 0.05 \text{ m}$, $H_2 = 0.01 \text{ m}$, $L = 0.1 \text{ m}$, $k_1 = 10^5 \text{ N/m}$ and $k_2 = 10^6 \text{ N/m}$, we calculate the design parameters as $a = 0.78$ and $b = 0.16$. So, for the stability plot of f against b we fix a at 0.78 and for the relationship between f and a , b is fixed to a constant value of 0.16 as observed in Fig. 2.4. Therefore, using Fig. 2.4 we can predict that the four-bar truss will undergo a superelastic forward transition at a critical dimensionless load at 0.0098 (131 N) and a superelastic reverse transition at 0.003 (40 N).

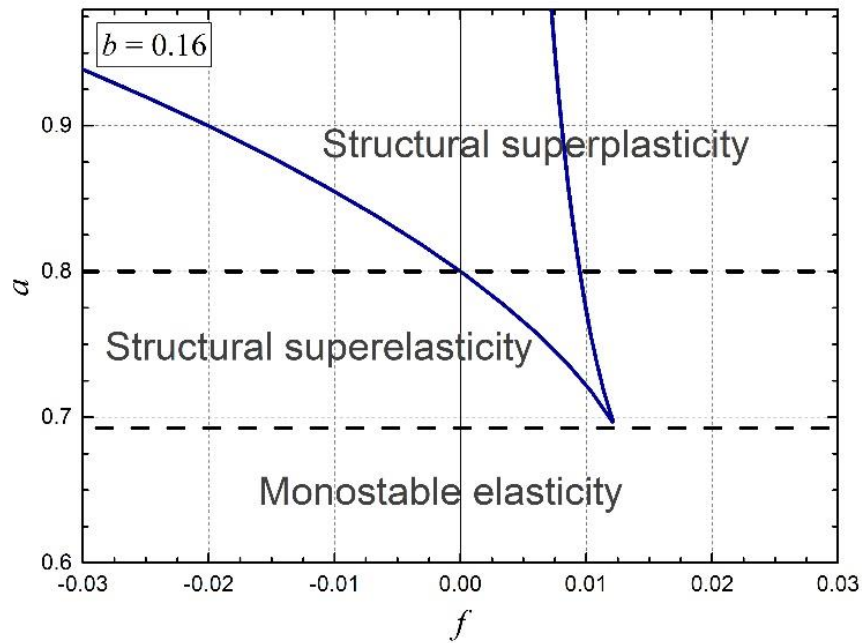
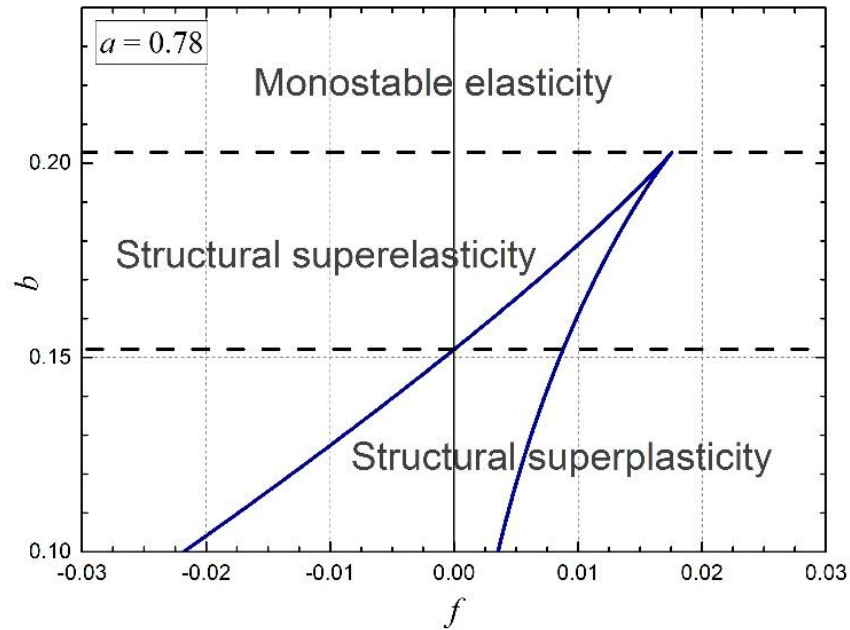


Figure 2.4 Four bar truss stability diagrams: top - (f, b) and bottom - (f, a) by fixing $a = 0.78$ and parameter $b = 0.16$ respectively. The region of structural superelasticity signifies a reversible transition between two stable states of a loading and an unloading regime but the region of superplasticity when bistability exists, however at $f=0$, truss is not at initial undeformed state and to achieve that force reversal must be applied. Monostable elasticity region characterizes a single stability state response of the truss.

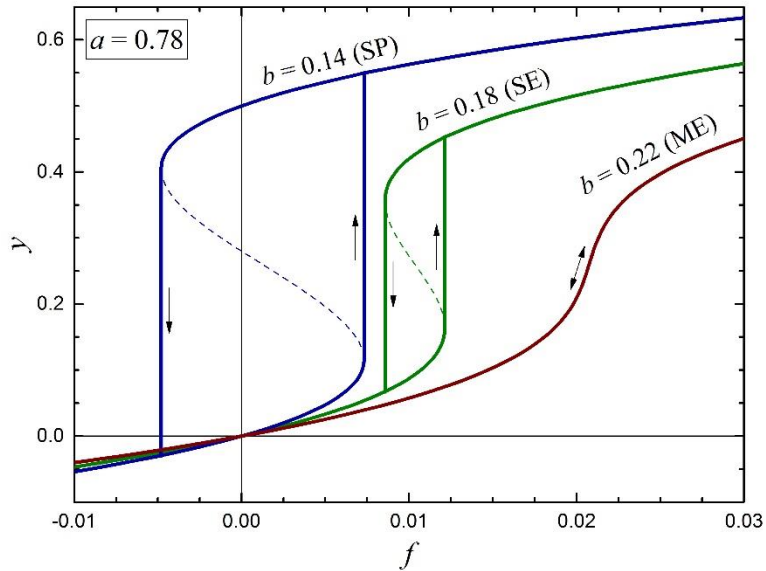


Figure 2.5 Typical system response curves of the truss in Fig.2.3 by fixing the parameter a and varying the parameter b : SE – structural superelasticity, SP – structural superplasticity and ME – monostable elasticity. The unstable equilibrium state of the truss is shown by dash lines. These system equilibrium behaviors are predictable from the stability diagrams in Fig. 2.4.

The force - displacement behavior for the three (3) regions specified on the stability diagrams in Fig. 2.4 can be observed in Fig. 2.5 where the value of a is fixed at 0.78 and we plot the force-displacement response for different values of b . In Fig. 2.5, the hysteretic behavior of the superelastic ($b = 0.18$) and superplastic ($b = 0.14$) regions could be compared to monotonic nonlinear of the monostable elastic region ($b = 0.22$). Since design of the four-bar truss solely depends on the system design parameters a and b , it would be very important to obtain a design map or phase diagram showing the three stability behaviors (superelastic, superplastic, monostable) which depends on only the system or design parameters giving a designer the flexibility and the design tool for predicting the system stability response for a combination of design parameters.

2.4 Cusp Curve and the Phase Diagram

In theory, the plotted bifurcation curves in Fig. 2.4 represent saddle-node bifurcation. However, the point where two bifurcation curves meet, called the cusp point is a point of higher order singularity where bifurcation curves are tangent to each other and is/are unique to a stability diagram. The uniqueness makes it a 2N-bifurcation point which requires tuning two design parameters. The cusp point also serves as the onset of bistability below or above we observe bistability (superelasticity/superplasticity) or monostability as is represented in Fig. 2.4. The ability to plot all the cusp points in a system would demarcate the regions of monostability and bistability in a system. By imposing the conditions of the third derivative $\frac{d^3\Pi}{dv^3} = 0$, second derivative $\frac{d^2\Pi}{dv^2} = 0$ and the first derivative $\frac{d\Pi}{dv}$, we obtain a curve comprising all the cusp points as variation of the design parameters called the *cusp curve* and hence, a clear separation of bistability region from monostability region. Since the bistability region is composed of superelastic and superplastic regions, it is also pertinent for design purposes to plot a curve to show the extent of each of these regions and this is achieved by applying the conditions of the force $f = 0$ and the second derivative $\frac{d^2\Pi}{dv^2} = 0$. These conditions give the onset of superplasticity for the pair of design parameters. For the four-bar truss, functions for the two (2) curves explained above are obtained as

$$b = \frac{a^2}{3} \tag{2-15}$$

$$b = \frac{a^2}{4} \tag{2-16}$$

A phase diagram for designing the four-bar truss (See Fig. 2.3) for the various stability responses using onset of bistability condition in (2-15) and onset of superplasticity condition in (2-16) is shown in Fig. 2.6.

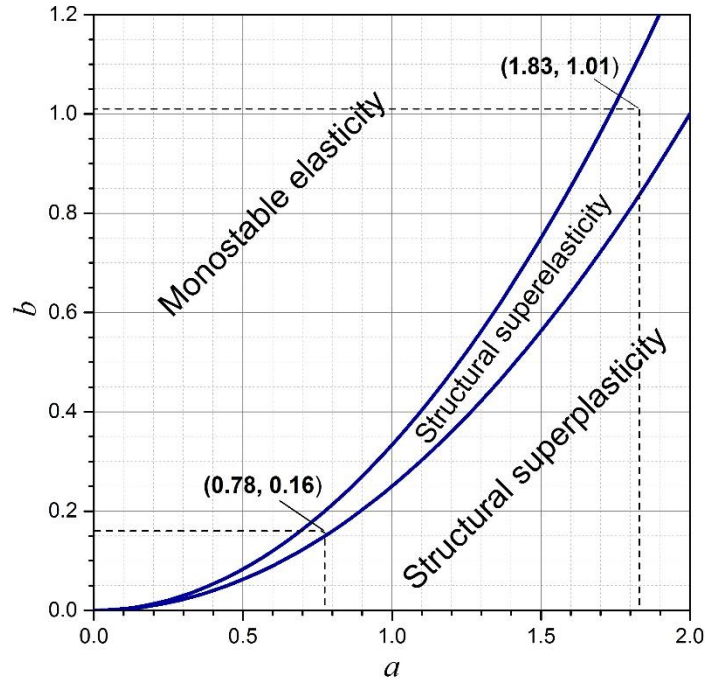


Figure 2.6 Cusp curve phase diagram of elastic structures having equilibrium potential function of the form $f = y^3 - ay^2 + by$. The cusp curve in Eqn. 2-15 represents both the limit of monostability and the onset of bistability while the cusp curve in Eqn. 2-16 represents both the limit of structural superelasticity and the onset of structural superplasticity.

To showcase the predictive power of the cusp curve phase diagram (Fig. 2.6), we plot values for the system design parameters $a = 0.78$ and $b = 0.16$ for the example discussed above on the phase diagram in Fig. 2.6, the system lies within the structural superelasticity and that corresponds with the expected behavior seen in the stability diagrams. Therefore, the desired system equilibrium response is achieved by tuning the design parameters. The narrow band of the of the structural superelasticity region shows the importance of the phase diagram or cusp curve map in bistability studies and without such a phase map the designer might be lost to rareness of such a phenomenon.

2.5 Periodic lattice Models

In Fig. 2.7, a material having a stiff core structure of hexagonal bar elements and a soft surrounding matrix is shown. The unit-cell of this periodic material in Fig. 2.7 is made up of the interactions between the core structure and the soft matrix forming a triangular truss that can be analyzed for bistability. The unique behavior of the unit-cell structure if bistable could lead to a reconfigurable material that could be programmed to resist compliance in certain directions.

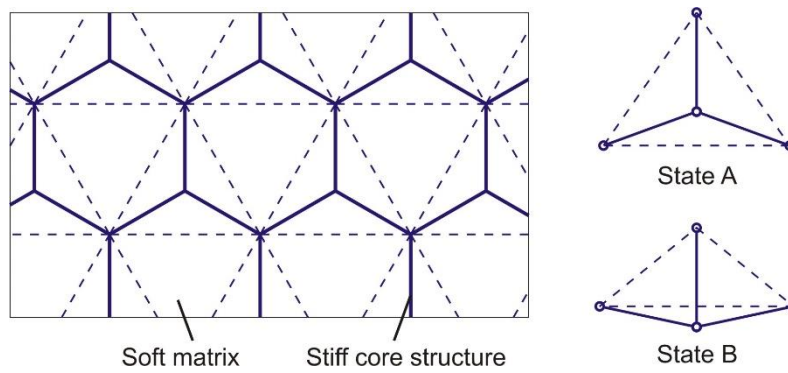


Figure 2.7 A composite material composed of a stiff hexagonal periodic lattice structure embedded in a soft continuum matrix. The existence of elastic interactions between the nodal points of the core and soft continuum forms a hypothetical tetrahedral truss.

The study of bistability in plane periodic lattices is easily extended to 3D lattices and frameworks by analyzing the unit-cell structure. In Fig. 2.8, is a lattice made up of tetrahedron-shaped substructures and for the purpose of studying its states of stability, the unit-cell is idealized with internal bars as shown on the right. Structural applications of such a lattice with bistability could be evident in shell and plate structures or engineered lattices materials fabricated by additive manufacturing.

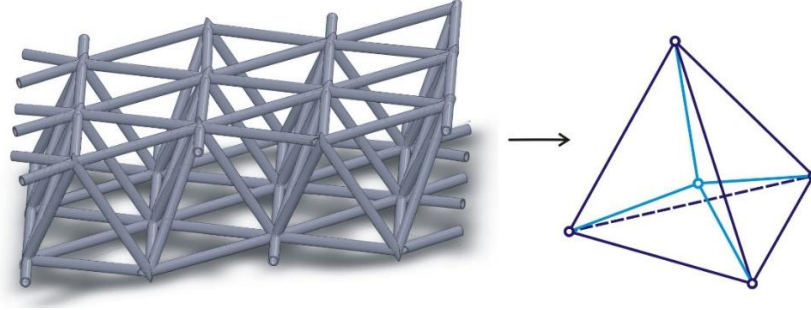


Figure 2.8 Design example of a periodic space truss using the bistable tetrahedral unit cell (internal bars of the individual tetrahedrons are not shown on the left image).

2.5.1 Stability of the 3D Unit cell Tetrahedral Truss

The tetrahedral unit cell will have the stiffness properties as shown in Fig. 2.9. The vertical central bar is assumed to be rigid ($k_4 \gg k_{1-3}$) so it undergoes no deformation and therefore no strain energy is stored. Hence, only nine bars contribute to the stored strain energy. The external load is applied at the apex which could form an analytical generalization for a periodic lattice under a distributed load [44]. Before analysis, we made these assumptions: the base triangle is equilateral, exterior bars have same length and inclined interior bars are equal in length. For a simplified analysis, the top node was constrained vertically while the bottom nodes were constrained to move in the base plane of the tetrahedral. Therefore, the strain energies stored in the bars are

$$\begin{aligned}
 U_1 &= \frac{k_1}{24B^2} (u^2 + 2Bu + v^2 - 2\sqrt{2}Bv)^2 \\
 U_2 &= \frac{k_2}{8(H^2+B^2)} (u^2 + 2Bu + v^2 - 2Hv)^2 \\
 U_3 &= \frac{k_3}{8B^2} (u^2 + 2Bu)^2
 \end{aligned} \tag{2-17}$$

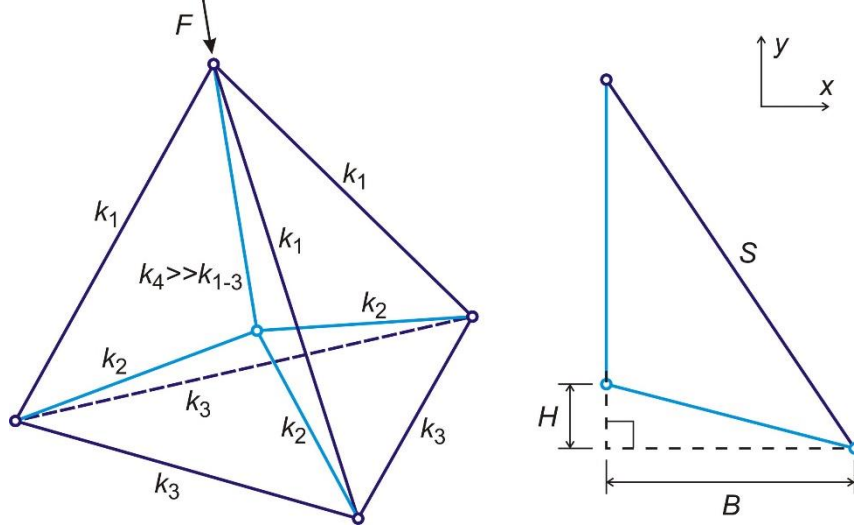


Figure 2.9 Tetrahedral truss unit-cell: (Left) 3D view showing stiffness and interior core structure having a rigid vertical bar. (Right) side view showing base length B and inclined length $S = \sqrt{3}B$.

The total strain energy Π expression is formulated from (2-1) as

$$\Pi = \frac{k_1}{8B^2} (u^2 + 2Bu + v^2 - 2\sqrt{2}Bv)^2 + \frac{3k_2}{8(H^2+B^2)} (u^2 + 2Bu + v^2 - 2Hv)^2 + \frac{9k_3}{8(B^2)} (u^2 + 2Bu)^2 - Fv \quad (2-18)$$

Since there are two (2) state variables u and v , the two equilibrium equations for the total potential energy above are

$$0 = \frac{d\Pi}{dv} = \frac{k_1}{2B^2} (u^2 + 2Bu + v^2 - 2\sqrt{2}Bv)(v - \sqrt{2}B) + \frac{3k_2}{2(H^2+B^2)} (u^2 + 2Bu + v^2 - 2Hv)(v - H) - F \quad (2-19)$$

$$0 = \frac{d\Pi}{du} = \frac{k_1}{2B^2} (u^2 + 2Bu + v^2 - 2\sqrt{2}Bv) + \frac{3k_2}{2(H^2+B^2)} (u^2 + 2Bu + v^2 - 2Hv) + \frac{9k_3}{2(B^2)} (u^2 + 2Bu) \quad (2-20)$$

The equilibrium equations are written in dimensionless forms below.

$$g = (x^2 + 2x + y^2 - 2\sqrt{2}y)(y - \sqrt{2}) + \alpha(x^2 + 2x + y^2 - 2hy)(y - h) \quad (2-21)$$

$$0 = (x^2 + 2x + y^2 - 2\sqrt{2}y) + \alpha(x^2 + 2x + y^2 - 2hy) + \beta(x^2 + 2x) \quad (2-22)$$

$$g = \frac{F}{k_1 B}, \quad \alpha = \frac{3k_2}{k_1(h^2+1)}, \quad \beta = \frac{9k_3}{k_1}, \quad y = \frac{v}{B}, \quad x = \frac{u}{B} \quad (2-23)$$

By rearranging (2-22), we obtain (2-24) and to obtain (2-25) with a single dimensionless state variable y , the results of (2-24) is substituted into (2-21):

$$(x^2 + 2x) = -\gamma(y^2 - 2\sqrt{2}y) - \alpha\gamma(y^2 - 2hy) \quad (2-24)$$

$$\gamma = \frac{1}{\alpha + \beta + 1} \quad (2-25)$$

$$g = [(1 - \gamma)(y^2 - 2\sqrt{2}y) - \alpha\gamma(y^2 - 2hy)](y - \sqrt{2}) + \alpha[(1 - \alpha\gamma)(y^2 - 2hy) - \gamma(y^2 - 2\sqrt{2}y)](y - h) \quad (2-26)$$

Equation (2-26) is simplified to a similar form for the four-bar truss in (2-13) as:

$$f = y^3 - ay^2 + by \quad (2-27)$$

$$f = \frac{g}{1 + \alpha - \gamma - 2\alpha\gamma - \alpha^2\gamma}, \quad a = -\frac{3\sqrt{2}(\gamma + \alpha\gamma - 1) + 3h(\alpha\gamma - \alpha + \alpha^2\gamma)}{1 + \alpha - \gamma - 2\alpha\gamma - \alpha^2\gamma}, \quad b = \frac{4(1 - \gamma) - 4\sqrt{2}\alpha\gamma h + 2h^2(\alpha - \alpha^2\gamma)}{1 + \alpha - \gamma - 2\alpha\gamma - \alpha^2\gamma} \quad (2-28)$$

At this point, the foregoing analysis will follow that of the four-bar truss by reference to stability diagrams (Fig. 2.4) and phase diagram (Fig. 2.6) since the only difference between equations (2-13) and (2-27) are the definitions of the terms (f, a, b, y) .

We specify the following stiffness values for the tetrahedral truss shown in Fig. 2.9: $B = 0.1m$, $H = 0.05m$, $k_1 = 10^4 N/m$, $k_2 = 3 \cdot 10^4 N/m$ and $k_3 = 2 \cdot 10^4 N/m$ and calculate the system parameters $a = 1.83$ and $b = 1.01$. As shown in Fig. 2.5, this pair of system parameters yields a superelastic structural response. The forward and reverse transition critical loads are 0.175 (986 N) and 0.149 (839 N) respectively for the tetrahedral truss and are obtained by plotting new stability diagrams using similar methods shown earlier.

2.6 Conclusions

In this chapter, it was shown how to design bistability behavior in elastic structures by generating stability and phase diagrams. These plots of cusp point singularity representations serve as great tools for predicting bistability behavior which was illustrated using simple 2D and 3D truss systems. Employing the Green's strain

by assuming moderately small strains it has been possible to develop basic forms of the equilibrium governing equation which could be termed canonical equilibrium equations for generalizing solutions to several range of simple truss and periodic lattice systems under an external load application. In this study, we showed the rarity of the superelastic bistability response region in the analyzed trusses using the phase diagram which could be applied to solving the issue of uncertainty when designing complex truss structures for bistability. The approach outlined in this chapter, gives a systematic analytical procedure for the analysis and optimization of the design of elastic truss unit cell that could be used in understanding bistability behavior in periodic lattices.

It reasonable to say that sensitivity of critical control parameters of the uncertainty in the design space could be high in an essentially nonlinear system, depending on its performance mode and the mathematical structure of the potential energy formulation. These aspects require separate studies.

Even though this chapter has studied elastic structures with only external degrees of freedom. The success of this study provides a pathway for analyzing multi-stable elastic structures having multiple degree of freedom including internal degree of freedoms and also provides the recipe for creating a negatively compressible metamaterial [44, 45] which has been shown to exist in structures with this complexity.

CHAPTER 2 REFERENCES

- [1] Massad, J. E.; Smith, R.C. A Domain Wall Model for Hysteresis in Ferroelastic Materials. *J. Intell. Mater. Syst. Struct.* **2003**, *14*(7), 455–471.
- [2] Salje, E. K. H.; Hayward, S.A.; Lee, W.T. Ferroelastic phase transitions: structure and microstructure. *Acta Cryst.* **2005**, *A61*, 3–18.
- [3] Bazant, Z. P.; Cedolin, L. Stability of Structures, *Oxford University Press*, **1991**, 228-231.
- [4] Miura, K.; Variable Geometry Truss Concept. *The Institute of Space and Astronautical Science, Sagamihara, Japan*. **1984**, Report No. 614.
- [5] Gantes, C. J.; Connor, J. J.; Logcher, R. D.; Rosenfeld, Y. Structural analysis and design of deployable structures. *Comput. Struct.* **1989**, *32*(3–4), 661– 669.

- [6] Rhodes, M.; Mikulas, M. M., Jr. Deployable Controllable Geometry Truss Beam. *NASA Technical Memorandum*. **1985**, 86366.
- [7] Noemi F.; Adnan I. 2013. Overview of highly flexible, deployable lattice structures used in architecture and civil engineering undergoing large displacements. *YBL Journal of Built Environment*. **2013**, 1(1): 85–103.
- [8] Crisfield, M. A. Non-Linear Finite Element Analysis of Solids and Structures. *Advanced Topics, John Wiley & Sons, London, UK*. **1997**, Volume 2.
- [9] Hrinda A.G., 2010. Snap-through Instability Patterns in Truss Structures. *NASA Langley Research Centre, AIAA*. **2010**, 2010-2611.
- [10] Schioler, T.; Pellegrino, S. Space Frames with Multiple Stable Configurations. *AIAA Journal*. **2007**, 45(7), 1740–1747.
- [11] Cai, J. G.; Xu, Y. X.; Feng, J.; Zhang J. Mechanical Behavior of Bistable Struts. *J. Mechanical Engineering Science Proc. IMech*. **2011**, Vol. 226 Part C.
- [12] Plante, J.S.; Santer, M. Compliant Bistable Dielectric Elastomer Actuators for Binary Mechatronic Systems. *Proceedings Of IDECT/CIE 2005 ASME Mechanism and Robotics Conference, Long Beach, California, USA*, **2005**, 24-28.
- [13] Kinoshita, T.; Oshaki, M. 2009. Synthesis of Bistable Compliant Structures from Truss Mechanisms. *Journal of Computational Science and Technology*. **2009**, 3(2).
- [14] Hu, N.; Burgueno R. Buckling-induced smart applications: recent advances and trends. *Smart Materials and Structures*. **2015**, 24, 06300.
- [15] Karpov, E. G.; Dorofeev, D. L.; Stephen, N. G. Characteristic Solutions for the Statics of Repetitive Beam-Like Trusses. *International Journal of Mechanical Sciences*. **2002**, 44(7): 1363-1379.
- [16] Karpov, E. G.; Stephen, N. G.; Dorofeev D. L. On Static Analysis of Finite Repetitive Structures by Discrete Fourier Transform. *International Journal of Solids and Structures*. **2002**, 39(16): 4291-4310.
- [17] Lakes, R. S. Extreme damping in compliant composites with a negative stiffness phase. *Philos. Mag. Lett.* **2001**, 81, 95-10
- [18] Wang, Y.-C.; Lakes, R. Stability of negative stiffness viscoelastic systems. *Quart. Appl. Math.* **2006**, 63, 34-55.
- [19] Dong, L.; Lakes, R. Advanced damper with high stiffness and high hysteresis damping based on negative structural stiffness. *Int. J. Solids Struct.* **2013**, 50, 2416–2423.

- [20] Molyneaux, W. Supports for Vibration Isolation. *Aeronautical Research Council, Great Britain*. **1957**, ARC/CP-322.
- [21] Zadpoor, A. A. Mechanical meta-materials. *Mater Horiz*. **2016**, *3*, 371–381
- [22] Wang, S. T.; Blandford, G. E.; Hill, C. D. Nonlinear Analysis of Steel Space Trusses, *International Specialty Conference on Cold Formed Steel Structures*, **1988**, Paper 2
- [23] Blandford, G. E. Progressive failure analysis of inelastic space truss structures. *Computers and Structures*, **1996a**, *58*(5):981–990.
- [24] Blandford, G. E. Large deformation analysis of inelastic space truss structures. *Journal of Structural Engineering ASCE*. **1996b**, *122*(4), 407–415.
- [25] Vanderplaats, G. N. Numerical Optimization Techniques for Engineering Design: With Application. *McGraw-Hill, New York*. **1984**. 2nd Edn.
- [26] Lee, K. S.; Geem, Z. W. A new structural optimization method based on the harmony search algorithm. *Computers & Structures*. **2004**, *82*(9-10), 781-798.
- [27] Hwang, S.F.; He, R.S. Engineering optimization using a real-parameter genetic-algorithm-based hybrid method. *Engineering Optimization*. **2006**, *38*(7), 833-852.
- [28] Perez, R.E.; Behdinan, K. Particle swarm approach for structural design optimization, *Computers & Structures*. **2007**, *85*(19-20), 1579-1588.
- [29] Salajegheh, E.; Salajegheh, J.; Seyedpoor, S.M.; Khatibinia, M. Optimal design of geometrically nonlinear space trusses using adaptive neuro-fuzzy inference system. *Sci. Iran* **2009**, *6*, 403–414.
- [30] Greco, M.; Vicente, E. R. C. Analytical Solutions for Geometrically Non-linear Trusses. *REM: R. Esc. Minas*. **2009**, *62*(2), 205-214.
- [31] Greco, M.; Venturini, W. S. Stability Analysis of Three-dimensional Trusses, *Latin American Journal of Solids and Structures*. **2006**, *3*, 325–344
- [32] Rezaiee-Pajand, M.; Naghavi, A. Accurate solutions for geometric nonlinear analysis of eight trusses. *Mechanics Based Design of Structures and Machines*. **2011**, *39*(1):46–82.
- [33] Shon, S.; Lee, S.; Ha, J.; Cho, C. Semi - Analytic Solution and Stability of Space Truss Using a Higher-Order Taylor Series, *Materials*. **2015**, *8*, 2400-2414.
- [34] Thom, R. Structural Stability and Morphogenesis: An Outline of a General Theory of Models. *Reading, MA: Addison-Wesley*. **1989**.
- [35] Zeeman, E.C. Catastrophe Theory. *Selected Papers 1972–1977*. *Reading, MA: Addison-Wesley*, **1977**.
- [36] Gilmore R. Catastrophe theory for Scientists and Engineers, *Dover*. **1981**.

- [37] Arnold, V. I. Catastrophe Theory, 3rd ed. Berlin: Springer-Verlag. **1992**.
- [38] Strogatz S. H. Nonlinear Dynamics and Chaos. Addison-Wesley Publishing Company. **1994**.
- [39] Yin, J. P.; Marsh, D.; Duffy, J. Catastrophe analysis of planar three-spring systems. ASME Design Engineering Technical Conferences. **1998**, DETC 98/MECH-5919.
- [40] Liagro, S.S.; Valvo, P.S. Large displacement analysis of elastic pyramidal trusses, *International Journal of Solids and Structures*. **2006**, 43(16): 4867–4887
- [41] Ivanco, V. Nonlinear Finite Element Analysis: Script of Lectures. HS Wismar. **2011**.
- [42] Pecknold, D. A.; Ghaboussi, J.; Healey, T. J. Snap-through and Bifurcation in a Simple Structure. *J. Eng. Mech.* **1985**, 111, 909-922.
- [43] Eremeyev, V. A.; Lebedev, P. On the loss stability of von Mises truss with the effect of pseudo-elasticity, *Matemáticas*. **2006**, XIV (2), 111–118
- [44] Loukaides, E.G.; Seffen, K.A. 2015. Multistable grid and honeycomb shells, *International Journal of Solids and Structures*. **2015**, 59, 46-57.
- [45] Nicolaou, Z.G.; Motter, A.E. 2012. Mechanical metamaterials with negative compressibility transitions, *Nature Materials*. **2012**, 11: 608.
- [46] Chen, M. L.; Karpov E.G. Bistability and Thermal Coupling in Elastic Metamaterials with Negative Compressibility. *Physical Review E*. **2014**, 90, 033201.

3 NEGATIVE EXTENSIBILITY MECHANICAL METAMATERIAL

(This chapter is based on a material previously published as Karpov, E. G.; Danso, L. A.; Klein J.T. Negative Extensibility Metamaterials: Occurrence and Design Space Topology. Physical Review E. 2017, 96(2), [023002].)

3.1 Introduction

When a structure contracts or is drawn back on reaching a certain critical load point in the direction of the applied load it is said to have experienced a negative extensibility (Fig. 3.2) analogous to negative compressibility when a material decreases in volume after a decrease in hydrostatic pressure which is totally a different effect compared to the negative Poisson's ratio metamaterial behavior. In comparison, negative compressibility is a bulk material property [1] associated with force applied in all directions of a material (See Fig. 3.1) while negative extensibility is a negative longitudinal or linear compressibility experienced along the direction of the applied force (See Figure 3.2).

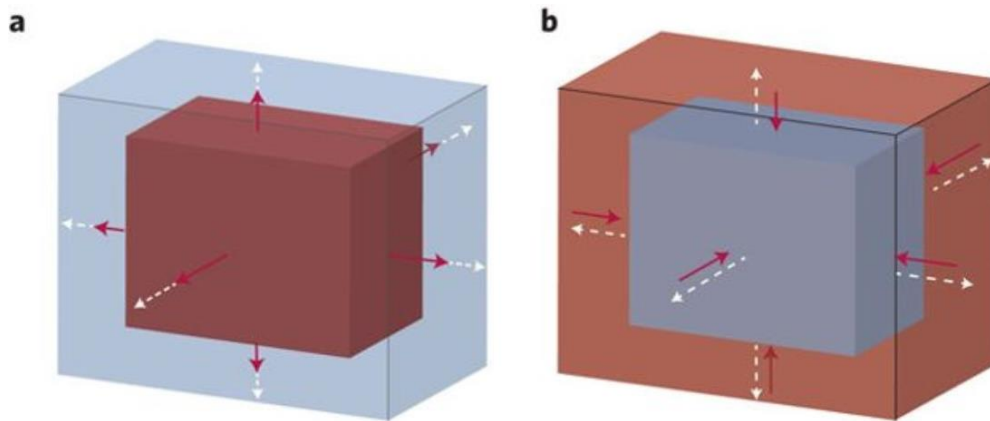


Figure 3.1 Different material responses (red) under uniform tensile force (white): (a) positive compressibility (b) negative compressibility. [1]

As Early as 1999, Baughman [2] presented an exciting study on the possibility of anisotropic systems and materials possessing negative linear or area compressibility due to variation in applied hydrostatic pressure. For example, anisotropy of a truss system based on differing length and material compressibility may allow for

negative linear incompressibility in certain admissible directions and negative area compressibility even though negative volumetric compressibility is not achieved [3-7]. The case of trusses could be compared to the concept of triangular shortening in the study of negative thermal expansion [8-10].

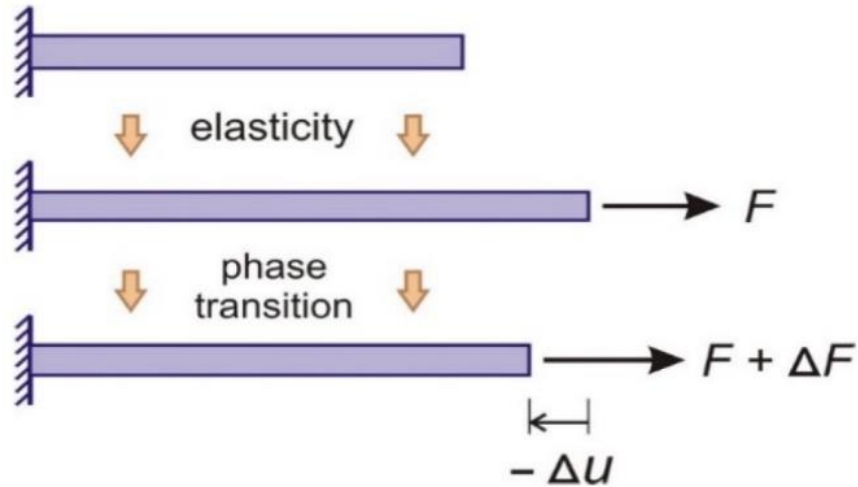


Figure 3.2 Negative extensibility in an elastic bar.

Over decades, studies on negative compressibility was inhibited by the idea of stability being a result of positive compressibility in classical thermodynamics. However, Lakes and Wojcienhowski [11] addressed some of the contradictory works [12-14] of negative compressibility in their profound study titled “Negative compressibility, negative Poisson’s ratio, and stability”. In their study [11], there was an overview of several constraints limiting the study of negative compressibility like assuming systems with no internal degrees of freedom and external fields and specifying positive definiteness as a required condition for stability for free surfaces which is already affirmed in elasticity theory [15]. They however proposed negative compressibility as an instability that is manifested as a phase transformation leading to a qualitative (shape) or quantitative (volume) change in a material’s formation structure.

Henceforth, Nicolau and Motter [16] have been able to showcase this phenomenon of instability based negative compressibility by using an applied force to destabilize a metastable equilibrium of idealized constituents of a

material having both internal and external degrees of freedom. This concept has been subsequently applied by other authors [17-19], where negative compressibility behavior is essentially a by-product of bistability and occurs abruptly mimicking the polyphormic phase transformation. The bistability exhibited by the engineered material is comparable to the behavior studied in Chapter 2 which is essentially a superelastic phase transition that produces a hysteretic response at a critical load.

However, a structural unit or unit cell identified to show a negative extensibility behavior formulates a total potential energy function that possess unique characteristics. Even though this uniqueness is elusive and has no background study, in this study we provide an approach of developing a negative extensibility material by building a periodic lattice composed of bistable unit cells or substructures made up of linearly elastic bars and springs. The design could promise exciting applications in adaptive civil structures, mechanical actuators, explosion impact and earthquake super-dampers [2-3] and can even lead to other metamaterial behaviors like negative Poisson's ratio and negative thermal expansion [1,3,20,21].

In this chapter, we seek to develop a mathematical criterion for understanding in negative extensibility in simple structural units like that outlined for the study of bistability in Chapter 2 that would be beneficial in modelling the behavior in materials even at the atomic scale. The assumption of geometrical nonlinearity as seen in Chapter 2 would be helpful in generating a total potential energy function of a metastable structure with features that may suggest a negative extensibility behavior in a system. For practical applications this metastable structure should be able to damp out the high kinetic energy produced after a phase transition [17]. Since our study on bistability in chapter 2 based on only external degrees of freedom did not showcase any negative extensibility behavior, this chapter shows the need for a complex bistable system which must possess multiple degrees of freedom with at least an internal degree of freedom [16-17].

Therefore, our study of negative extensibility would follow an analytical format similar to that presented in Chapter 2 including a numerical regime for solving the complex nonlinear algebraic solutions. The concept of stability diagrams and phase diagrams are adopted from Chapter 2 to better explain this interesting

phenomenon and show that the behavior could be identified in simple structural systems comprising only elastic bars and springs.

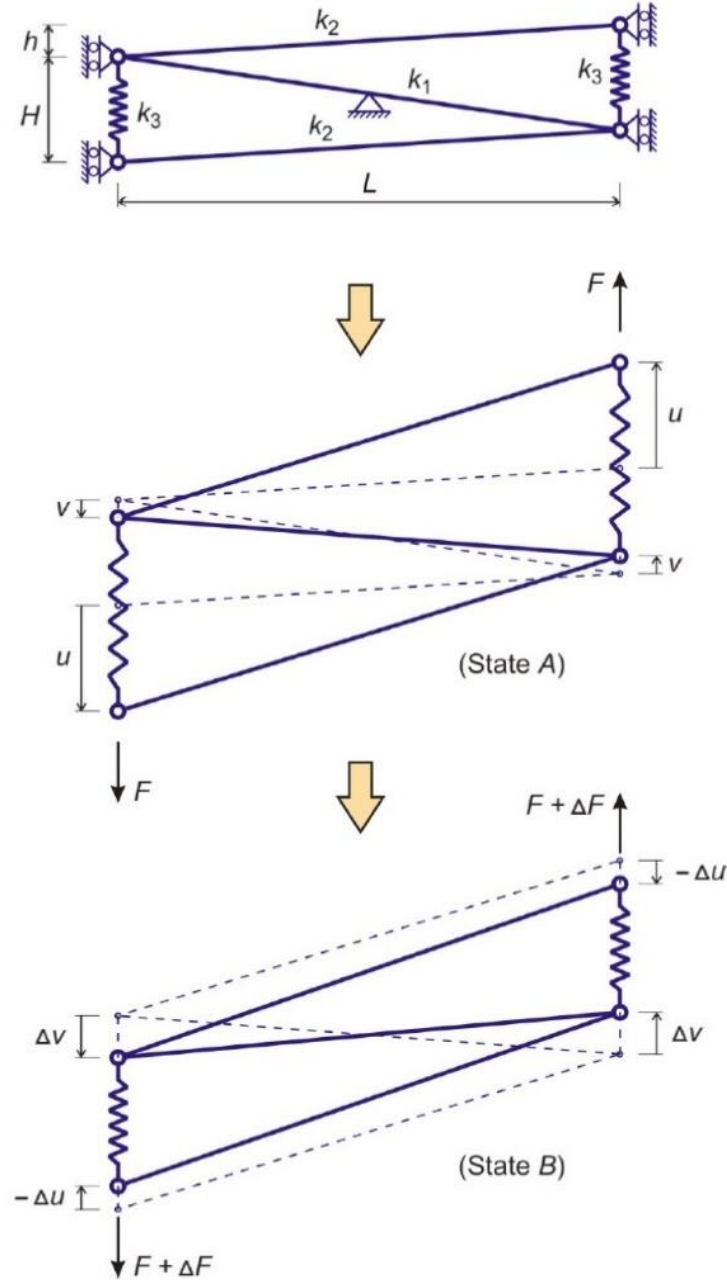


Figure 3.3 Elastic bar-spring metastable (states A and B) structure with one (1) internal degree of freedom due to the rotation of the middle bar and two (2) external degrees of freedom to vertical displacements (u, v) of the springs. Forced - induced structure destabilization creates a large rotation of middle that causes linear contraction termed negative extensibility.

3.2 Analysis of Truss Model with An Internal Degree of Freedom

To study negative extensibility, we identify a simple structural system (Fig. 3.3) composed of only elastic springs and bars. The middle bar k_1 and exterior bars k_2 are assumed to undergo very moderate strains to take advantage of Green's strain which helps to derive a simplified analytical form of the total potential function. The strain in the vertical springs k_3 is calculated using the usual engineering strain. The stored strain energies in these bars and springs are derived in the following equations:

$$\pi_1 = \frac{2k_1}{L^2+(H-h)^2} v^2 (v - H - h)^2 \quad (3-1)$$

$$\pi_2 = \frac{2k_1}{8(L^2+h^2)} (u + v)^2 (u + v + 2h)^2 \quad (3-2)$$

$$\pi_3 = \frac{k_3}{2} (u - v)^2 \quad (3-3)$$

The total potential energy for the entire structure in Fig. 3.3 takes the form

$$\Pi = \pi_1 + 2(\pi_2 + \pi_3 - Fu) \quad (3-4)$$

By introducing dimensionless parameters (U, f, x, y, a, s), we write a simplified form of the total potential energy (3-4) as

$$U = a(x + y)^2(x + y + 2s)^2 + by^2(y - 1 + s)^2 + (x - y)^2 - 2fx \quad (3-5)$$

$$U = \frac{\Pi}{k_3 H^2}, \quad f = \frac{F}{k_3 H}, \quad x = \frac{u}{H}, \quad y = \frac{v}{H}, \quad a = \frac{k_2}{4k_3} \frac{H^2}{L^2+(H-h)^2}, \quad b = \frac{2k_1}{4k_3} \frac{H^2}{L^2+(H-h)^2}, \quad s = \frac{h}{H} \quad (3-6)$$

Where f denotes the force control, (x, y) are the state parameters and (b, s) represent the system design parameters.

At this point, (3-5) can be analyzed for the sought negative extensibility behavior by employing the gradient method of numerical minimization. Setting $a = 0.0665$, $b = 5.21$, $s = 0$, and f ranging from 0.0 to 1.7 with a step size of ± 0.001 and using trial solution $x_0 = y_0 = 0.001$, a large contraction accompanying the state transition ($A \rightarrow B$) is realized as seen on Fig. 3.3 at a critical load $f_c = 1.33$. Further analysis showed that the structure in Fig. 3.3 will produce a negligible negative extensibility effect for the skewness parameter s ranging between -0.5 to 0.5. Therefore, for the discussion to follow we use $s = 0$ ($h = 0$) which typifies a rectangular formed unit-cell structure to gain a better outlook of the negative extensibility behavior in simple structural systems. The new expression in (3-5) after setting $s = 0$ is

$$U = a(x + y)^4 + b(y^2 - y)^2 + (x - y)^2 - 2fx, \quad a = \frac{k_2 H^2}{4k_3 L^2}, \quad b = \frac{2k_1 H^2}{k_3 L^2 + H^2} \quad (3-7)$$

It is obvious from Fig. 3.3 that the negative extensibility behavior in the structural system seen in Fig. 3.2 even though qualitatively similar to negative compressibility of the complex potential of the representative atomic structures formerly studied [16-17], possess a secondary superelastic behavior which will be seen later to be a unique trait of a negative extensibility behavior. Hence the stable state transitions are observed along the path $A \rightarrow B \rightarrow A \rightarrow B \rightarrow A$. In the subsequent sections, with the help of stability diagrams and phase diagrams we will be able to present pictorial views showing entire range of system parameters such that the structure in Fig. 3.2 exhibits this interesting metamaterial behavior.

3.3 Stability Diagrams

A stability diagram is a plot that outlines the extent of stability responses of a system equilibrium potential and provides the critical control parameter required for destabilization or transition to another stable state. The curves in the stability diagrams as seen in Chapter 2 describe points of bifurcation in a system's equilibrium potential and these points describe the equilibrium state of the structure when it is neither stable nor unstable. Such a point can be defined as inflection point and therefore satisfies a second-order derivative condition. A bifurcation point is also a point of destabilization at which a critical value of external load f_c causes a transition (snap-through action) from one equilibrium state to another ($A \rightarrow B$). In the case of a potential with two state variables x, y like in (3-7), two equilibrium potentials corresponding to each state variable are expected as shown below:

$$U'_x = 0: \quad g_1(x, y, f, a, b) = x - y + 2a(x + y)^3 - f = 0 \quad (3-8)$$

$$U'_y = 0: \quad g_2(x, y, f, a, b) = y - x + 2a(x + y)^3 + by(y - 1)(2y - 1) = 0 \quad (3-9)$$

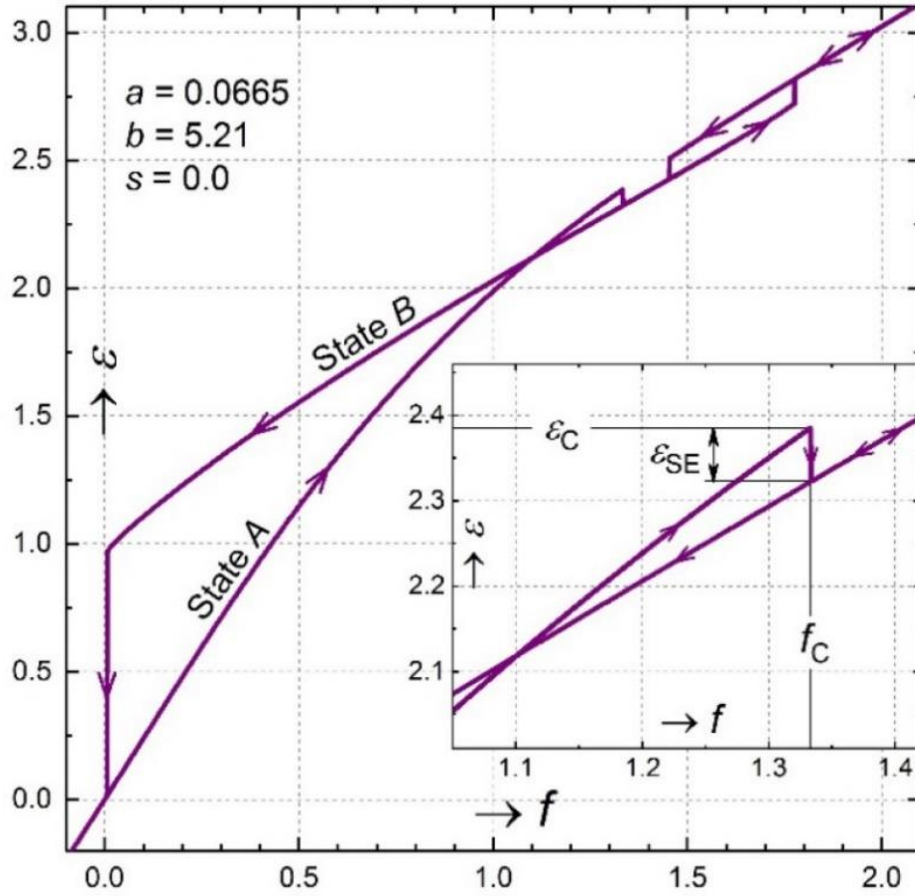


Figure 3.4 A force-strain curve of the potential in (3-7) under a loading and unloading regime exhibiting negative extensibility due a negative superelastic strain, $\varepsilon_{SE} = -2\Delta u/(H + h) = -0.063$ at a critical force $f_c = 1.33$ realized by the pinched hysteresis. The structure experiences two (2) forward transitions and two (2) backward transitions due to secondary hysteresis ($A \rightarrow B \rightarrow A \rightarrow B \rightarrow A$).

Since we have two equilibrium potentials the inflection point condition for bifurcation is met by the determinant of the Hessian matrix of second-order derivatives of these equilibrium potentials,

$$\det H = \begin{vmatrix} U''_{xx} & U''_{xy} \\ U''_{yx} & U''_{yy} \end{vmatrix} = U''_{xx}U''_{yy} - U''_{xy}U''_{yx} = 0$$

$$g_3(x, y, a, b) = 24a(x + y)^2 + b(6y^2 - 6y + 1)(1 + 6a(x + y)^2) = 0 \quad (3-10)$$

Therefore solving Eqns. (3-8 - 3-10), we obtain the values of control and state parameters $\phi(f_C, a, b)$ that describe the bifurcation set. Hence, for finding bifurcation points the following condition must be satisfied:

$$\phi(f_C, a, b): \quad g_1(x, y, f, a, b) = g_2(x, y, a, b) = g_3(x, y, a, b) = 0 \quad (3-11)$$

In comparison to stability diagrams plotted in Chapter 2, stability plots from the locus of points in (3-11) can be complicated and would sometimes require a numerical procedure. In order to obtain the stability plot $\Gamma_b(f, a)$ describing the relationship between the control parameter f and system parameter a with system parameter b fixed, we manipulated (3-11) by algebraic substitution to obtain the following parametric functions:

$$f(a, b) = \frac{b(4-6y+bP_2)}{2P_1} \quad (3-12)$$

$$a(y, b) = -\frac{8b(1-6y+6y^2)P_1^2}{27y^2(2+b-3by+2by^2)^2(1+P_1)^3} \quad (3-13)$$

$$x(y, b) = -\frac{y(12+2b(7-24y+18y^2))+3b^2P_2}{4P_1} \quad (3-14)$$

$$P_1 = 3 + b - 6by + 6by^2, \quad P_2 = 1 - 9y + 26y^2 - 30y^3 + 12y^4 \quad (3-15)$$

Stability diagrams in Fig. 3.5a and Fig. 3.5b are plotted from the parametric curves (3-12 – 3-13) by varying the variable y for fixed values of $b = 3.8$ and $b = 5.21$. In Fig. 3.5b, we see a beak-forming stability plot which means in a stability space, onset of bistability could occur before the cusp point. This feature was not evident in our bistability study which was restricted to a single external degree of freedom. However, developing the other stability diagram $\Gamma_a(f, b)$ for the relationship between f and b for fixed values a was obtained only by implementing a Newton Raphson algorithm for solving (3-11) by running y within the 0.22 to 0.78 and a step size of 0.002. On Fig. 3.5c and Fig. 3.5d, we show stability plots obtained when $a = 0.22$ and $b = 0.78$. These plots are proof of the observed characteristics of a negative extensibility effect in Fig. 3.4, on these plots we see two stable state transitions ($A \rightarrow B \rightarrow A \rightarrow B \rightarrow A$) for both the loading and unloading cycles which exist due to the presence of the two cusp points. They also explain the pinched hysteresis effect accompanying a negative extensibility behavior.

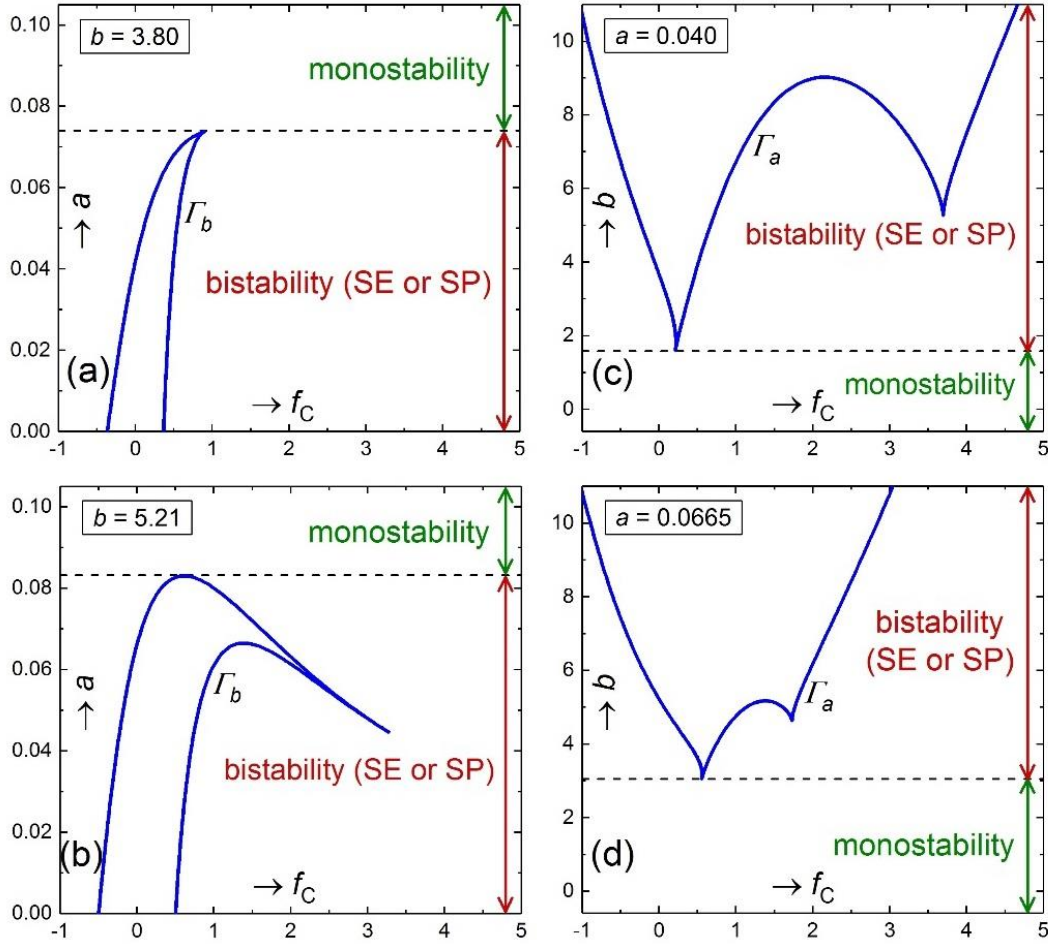


Figure 3.5 Stability diagrams obtained from the potential in (3-7) showing the three (3) typical system equilibrium behaviors seen in Chapter 2 (monostability, superelasticity (SE) and superplasticity (SP)). The double transition bifurcation curves explain the double transition observed in Fig. 3.4 and the beak – shaped bifurcation curve (bottom left) is a unique feature meaning bistability may be achieved before the cusp point.

3.4 Phase Diagrams

The phase diagram presented in the study of bistability was a plot of relationship between the system parameters and mainly a plot of all cusp points in a system based on the third-order derivative condition of the total potential energy $\frac{d^3\pi}{dx^3}$ with respect to the single external degree of freedom x which is the reference direction

of destabilization. For the structure in Fig. 3.3, a critical load causing bistability induces rotation $\frac{\Delta v}{L}$ of the middle

and destabilizes the entire structure. Therefore, the third-order derivative for the structure in Fig.3.3 will be with respect to internal degree of freedom (rotation) which could be satisfied by the nondimensional external degree of freedom y , U'''_{yyy} :

$$U'''_{yyy} = 0: \quad g_4(x, y, a, b) = 24a(x + y) + 12b(12y - 1) = 0 \quad (3-16)$$

Applying (3-16), the condition to solve for all cusp points describing the onset of bistability in the structure in Fig. 3.2, is stated as

$$\Gamma_s(a, b) = 0: \quad g_1(x, y, f, a, b) = g_2(x, y, f, a, b) = g_3(x, y, f, a, b) = g_4(x, y, a, b) = 0 \quad (3-17)$$

The locus of $\Gamma_s(a, b) = 0$ will therefore plot all supercritical pitchfork bifurcations in the structure but contrary to what was realized in the previous section, this curve will not fully represent the onset of bistability as was the case in Chapter 2. Utilizing the Newton Raphson algorithm, we can solve (3-17) for $\Gamma_s(a, b) = 0$ by varying b from 0 to 6.5 using a step size of 0.02. Fig. 3.6 shows a plot solution generated from this procedure. Having noticed from the stability diagrams in Fig. 3.5 that for the structure being analyzed, the locus of $\Gamma_s(a, b) = 0$ does not fully represent the onset of bistability, we will proceed by finding the missing curves that complete the onset of bistability on Fig. 3.5. We can see in Fig. 3.5b two branches of bifurcation curves forming a beak shape and by choosing a system design parameter a below the upper branch, bistability might exist since we transition two destabilization points. Onset of this assumed bistability Γ_N is plotted as in Fig. 3.6 by searching for points associated with the local maximum of the upper branch. By plotting force-displacement relationships (f, x) and (f, y) for regions (1), (2) and (3) above and below Γ_N on Fig. 3.6, we see in (1) the usual monotonic which defines regions above the upper branch in Fig. 3.4 but for (2) and (3) we notice two stable states exist (f, x) but with no transition points or hysteric behavior to depict bistability in the equilibrium structure. This means the second stable state is unreachable by the loading conditions in Fig. 3.3. On the (f, y) plot, we see a nucleation of the stable state B with the unstable state forming a loop which widens and moves closer to state A as we decrease the parameter a moving from (2) to (3). On the (f, y) plot for point (4) in Fig. 3.6, we finally see a coalescence of the loop with stable state A and a channel making the stable state B reachable. It's (f, x) plot

shows the expected pinched hysteresis for the transition from state A to state B. The onset of the coalescence corresponds with the local maximum of the lower branch of such a stability diagram in Fig. 3.5b and those points are plotted in Fig. 3.6 as curve Γ_O . At vertical position 4 of the system parameter b , the curve Γ_O connects with the curve Γ_S and forms a continuous curve for the onset of bistability. The other section of Γ_S plotted as a dashed line below the curve Γ_O explains the change in behavior in Fig. 3.5b from a two stable state transitions ($A \rightarrow B \rightarrow A \rightarrow B \rightarrow A$) for both loading and unloading cycles seen for the negative extensibility effect to a single stable state transition ($A \rightarrow B \rightarrow A$) for the usual bistability when we decrease the system parameter a below the cusp point.

Like in Chapter 2, it will be beneficial to demarcate the region of structural superplasticity in Fig. 3.6 and again show the region of negative extensibility which is understood to be below the Γ_O but would be limited to the point of a cusp as seen in Fig. 3.5b. The onset of structural superplasticity Γ_E corresponding with the behavior when structure does not resume initial state at $f = 0$ is plotted using the same condition in Chapter 2 that during an unloading cycle when a point of destabilization is reached the critical force must be zero ($f_c = 0$):

$$\Gamma_E(a, b) = 0: \quad g_1(x, y, 0, a, b) = g_2(x, y, a, b) = g_3(x, y, a, b) = 0 \quad (3-18)$$

The curve $\Gamma_E(a, b) = 0$ in Fig. 3.7 prescribes the onset of structural superplasticity which was obtained by using a Newton Raphson algorithm to solve (3-18) by varying b from 0 to 5.21 and utilizing a step size of 0.01. Having noticed in Fig. 3.5 that the usual bistability is possible after a double transition negative extensibility effect, the onset of negative extensibility Γ_M can be highlighted on Fig. 3.7 using the condition that there can be destabilization and subsequent transition from stable state A to stable state B while the overall height of the structure does not change. Modifying (3-11) we obtain this condition:

$$\Gamma_M(a, b) = 0: \quad g_1(x_A, y_A, f, a, b) = g_2(x_A, y_A, a, b) = g_3(x_A, y_A, a, b) = 0 \quad \wedge$$

$$g_1(x_B = x_A, y_B, f, a, b) = g_2(x_B = x_A, y_B, a, b) = 0 \quad (3-19)$$

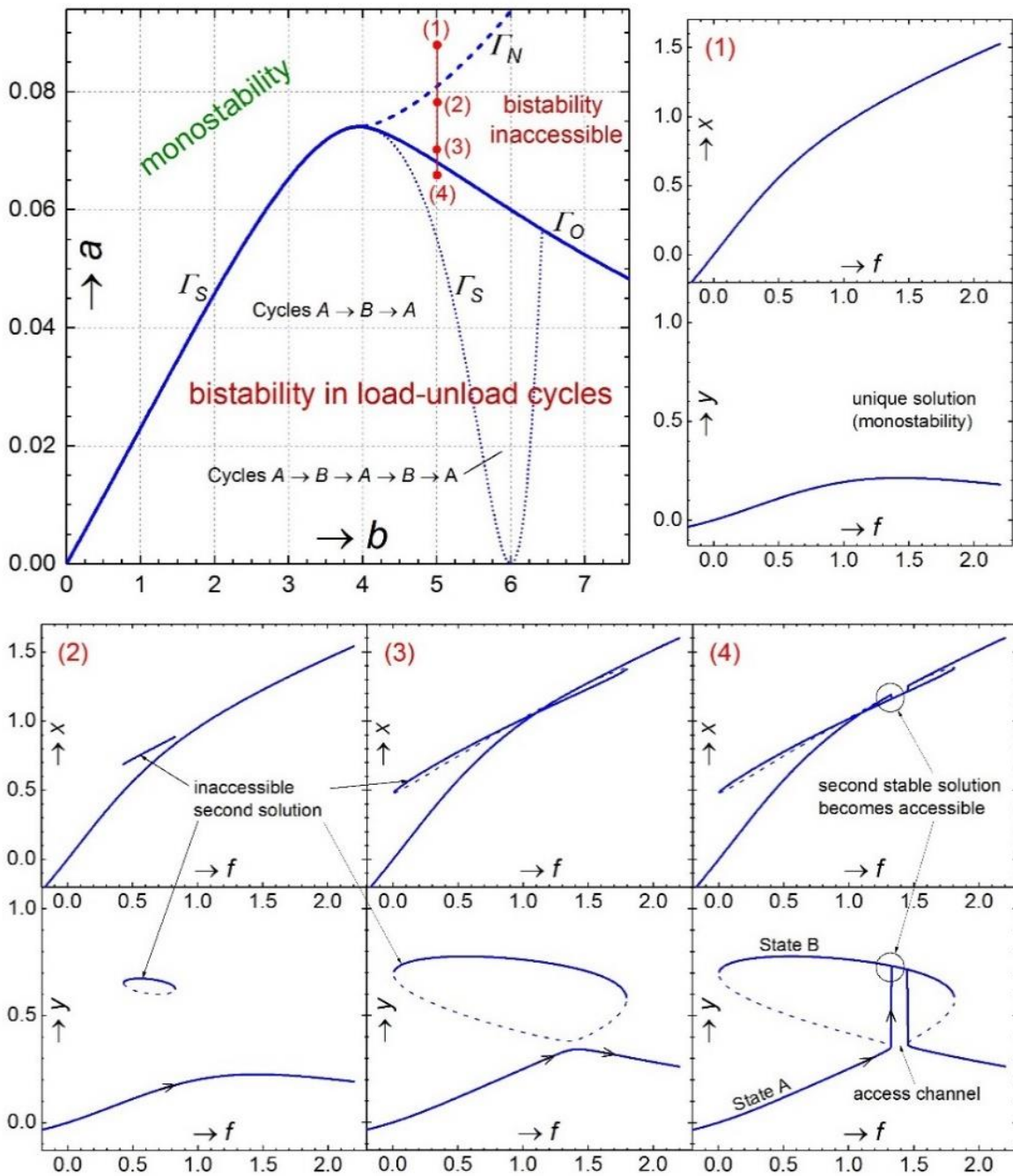


Figure 3.6 A phase diagram governed by the potential in (3-7) showing mechanically admissible regions of bistability (refer to beak shaped bifurcation curves-bottom left in Fig. 3.5) using lines of demarcation (Γ_S – locus of cusp points, Γ_N – locus of nucleation points, Γ_O – locus of coalescence points): (1) structure exhibits monostability (2) bistability cannot be achieved since second stable is inaccessible (3) first stable state approaches second stable state (4) first state coalesces with second stable state and bistability is observed with a pinched hysteresis.

The locus of $\Gamma_M(a, b) = 0$ plotted in Fig. 3.7 was found by employing a Newton Raphson algorithm to solve for x_A, y_A, y_B a, f while varying b from 4.5 to 7.5 and utilizing a step size of 0.01. The shown regions of negative extensibility superelasticity (NESE) and negative extensibility superplasticity (NESP) on Fig. 3.7 separated by the onset of superplasticity boundary Γ_E are regions of negative extensibility with superelastic behavior and negative extensibility of the superplastic type respectively. The phase diagram in Fig. 3.7 can be said to be a full representation of all the structural stability behaviors of the structure in Fig. 3.3.

The band of the negative extensibility region can be further divided to show how the metamaterial behavior varies across the band and most importantly the region for maximal effect. We thereby introduce the negative extensibility relative intensity factor I_{NESE} :

$$I_{NESE} = \frac{\varepsilon_{SE}}{\varepsilon_C} \quad (3-20)$$

While the terms ε_C and ε_{SE} as shown in Fig. 3.4 represent the critical elastic strain and negative superelastic strain respectively. Using the factor I_{NESE} , we can plot contours showing the intensity of the negative extensibility effect from the onset of negative extensibility boundary Γ_M to the onset of nucleation Γ_O . The condition for plotting boundary Γ_M when $I_{NESE} = 0$ is modified with the factor I_{NESE} to account for the contraction resulting in change in height of the structure above this boundary (Fig. 3.3) in the following:

$$x_B = x_A(1 + I_{NESE}) \quad (3-21)$$

The points of the contour lines shown on Fig. 3.8 associated with the relative intensity of the negative extensibility effect I_{NESE} are then found by applying a similar Newton Raphson algorithm. On Fig. 3.8 it is obvious now that the highest intensity should be achieved using system design parameters (a, b) to the left of the vicinity where the boundary Γ_E coincides with the boundary Γ_O .

3.5 Small Strain Approximation Error Analysis

Since in our study of bistability in Chapter 2 and in the current study of negative extensibility, the Green's strain was a nice approximation for small strains in bars and resulted in a much compact total potential function with reduced number of system design parameters.

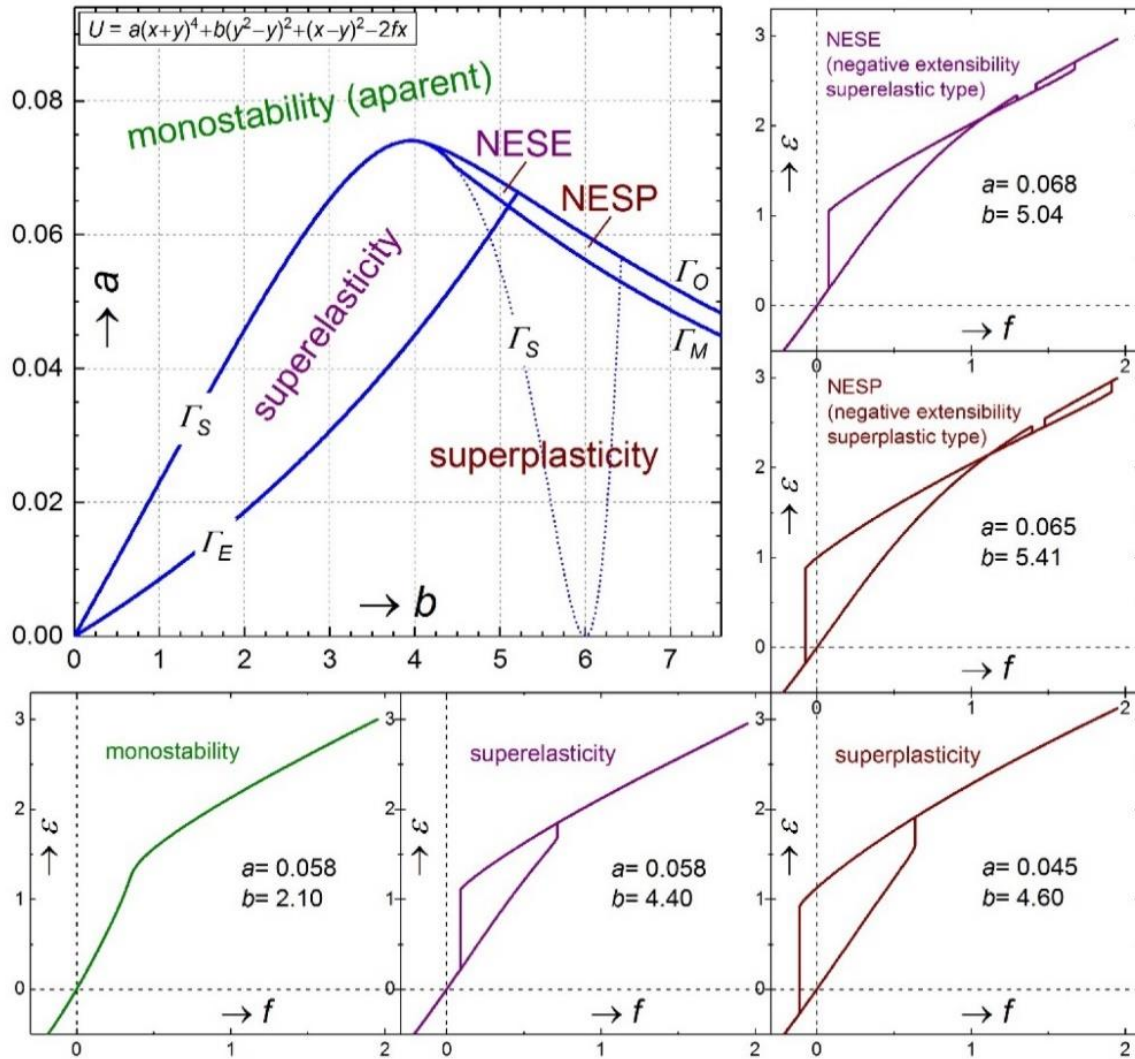


Figure 3.7 A phase diagram showing regions of the usual system equilibrium behaviors (monostability, superelasticity, superplasticity and the negative extensibility metamaterial behaviors (superelastic (NESE) or superplastic (NESP)) demarcated by the boundaries Γ_M – locus of the onset of negative extensibility points and $\Gamma_E, \Gamma_S, \Gamma_O$.

In this section, our aim is to account for the error introduced by this approximation by analyzing the same structure in Fig. 3.3 using the usual engineering strain. In doing so the total potential energy in (3-7) takes the form,

$$\Pi = \pi_1 + 2(\pi_2 + \pi_3 - Fu) \quad (3-22)$$

$$\pi_1 = \frac{k_1}{2}(\sqrt{L^2 + (H - 2v)^2} - \sqrt{L^2 + H^2})^2 \quad \pi_2 = \frac{k_2}{2}(\sqrt{L^2 + (u - v)^2} - L)^2 \quad \pi_3 = \frac{k_3}{2}(u - v)^2$$

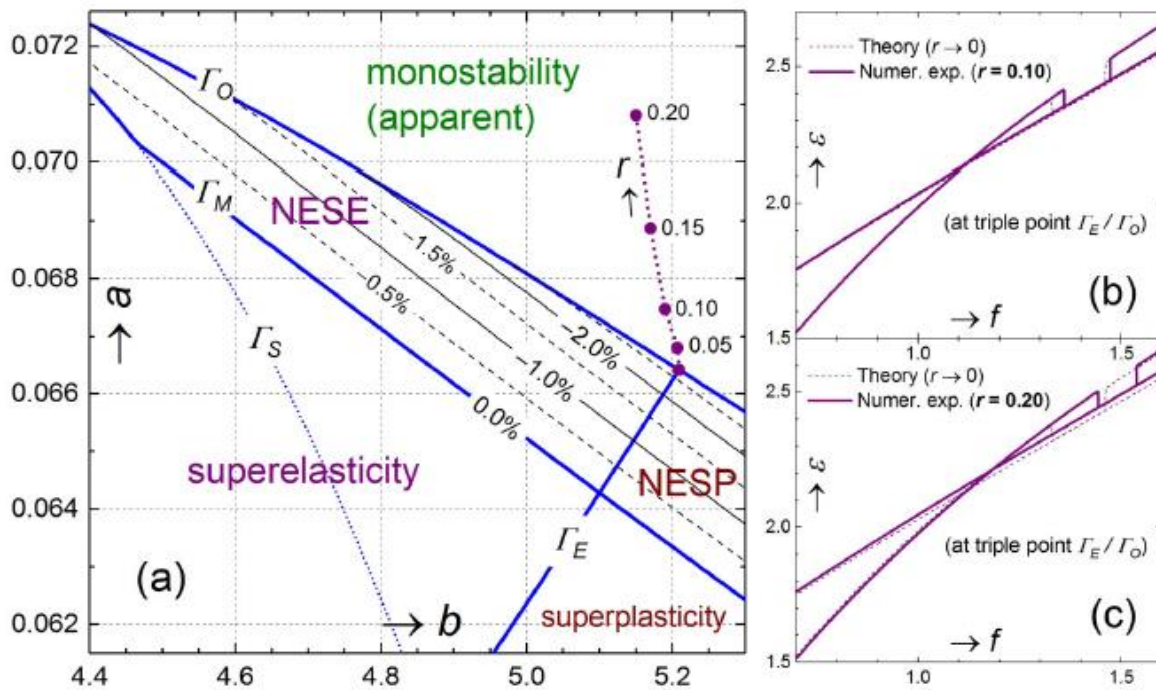


Figure 3.8 Negative extensibility intensity (a) A zoom into the negative extensibility region seen on the phase diagram in Fig. 3.7 and marked by contour lines delineated by the negative extensibility intensity factor (I_{NESE}). The maximal negative extensibility effect is expected around the intersection of the loci Γ_E and Γ_O where I_{NESE} is 2.64%. The point of intersection of Γ_E and Γ_O also corresponds with that of a similar phase diagram governed by (3-22) when the aspect ratio $r \rightarrow 0$ and therefore by increasing r , drifts in position of the intersection Γ_E and Γ_O are plotted. (b) and (c) Show how increase r shifts the force-strain plot governed by 3-7 or 3-22 when $r \rightarrow 0$.

However, it will be realized that the dimensionless form of (3-22) will include a new system design parameter, the aspect ratio of the structure, $r = \frac{H}{L}$, in addition to the rest of the parameters in (3-4) and therefore changes complexity of the potential. Now a 3D phase diagram will be required in terms of three system design parameters. Plotting a plane cross-section of such a 3D phase diagram similar to Fig. 3.7 for different values of the aspect ratio r was sufficient for our analysis. Fig. 3.8 shows that when $r \rightarrow 0$, the approximation of small strain suffices and the point where boundary Γ_E coincides with the boundary Γ_O is exactly as in Fig. 3.7. Increasing the value r results in a shift of this point as shown in Fig. 3.8 and the effect of high negative extensibility effect was assured up to 0.30. On Fig. 3.8, we also show how this shift produces a significant shift in the locations of the critical forces f_C on the force-strain plot.

3.6 Conclusions

In this study we were able to study the effect of multiple degrees of freedom including an internal degree of freedom on bistability behavior in simple structural systems. The stability diagrams of the studied structure in Fig. 3.3 depicted a double cusp and a beak forming stability plot which explained the double transition seen in a negative extensibility behavior. We have been able to show a comprehensive phase diagram (design space) of the various stability states in a simple structure with the potential for negative extensibility but the complexities in the observed stability diagrams obligated a significant amount of numerical procedure. However, it is worthy to note that even though this interesting metamaterial corresponds to a narrow band in the phase diagram (design space) it is achievable in simple structural systems like that analyzed in this study. Analysis of the identified negative extensibility structure using the small strain approximation was justified for very small aspect ratios and therefore the Green's stain would be a good basis for preliminary studies of the negative extensibility effect. A model of the structural system in Fig. 3.3 with design parameters within the vicinity of the high relative negative extensibility effect contours can serve as seismic super dampers and vibration isolators.

Having identified this metamaterial behavior in a simple structure that can form a unit-cell of a periodic structure, it would be interesting in the future to study how the negative extensibility behavior affects the overall

response of a periodic structure and our hope is to observe properties like switch in wave propagation speed and topology reconfiguration.

CHAPTER 3 REFERENCES

- [1] Grima, J. N.; Caruana-Gauci, R. 2012 Mechanical metamaterials: materials that push back. *Nat. Mater.* **2012**, *11*, 565–6
- [2] Baughman, R. H.; Stafstrom, S.; Cui, C.; Dantas, S. O. Materials with negative compressibilities in one or more dimensions. *Science* **1998**, *279*(5356), 1522–4.
- [3] Grima, J.N.; Attard, D.; Gatt, R. Truss-type systems exhibiting negative compressibility. *Phys. Status Solidi B.* **2008**, *245*, 2405–2414.
- [4] Grima, J.N.; Caruana-Gauci, R.; Wojciechowski, K.W.; Evans, K.E. Smart hexagonal truss systems exhibiting negative compressibility through constrained angle stretching. *Smart Mater. Struct.* **2013**, *22*, 084015.
- [5] Cairns, A. B.; Catafesta, J.; Levelut, C.; Rouquette, J.; van der Lee, A.; Peters, L.; Thompson, A. L.; Dmitriev, V.; Haines, J.; Goodwin, A. L. Giant negative linear compressibility in zinc dicyanoaurate. *Nat. Mater.* **2013**, *12*, 212–6
- [6] Weng, C. N.; Wang, K. T.; Chen, T. Design of microstructures and structures with negative linear compressibility in certain directions. *Adv. Mater. Res.* **2008**, *33*(37), 807–14
- [7] Barnes, D. L.; Miller, W.; Evans, K. E.; Marmier, A. S. H. Modelling negative linear compressibility in tetragonal beam structures. *Mech. Mater.* **2012**, *46*, 123–8
- [8] Grima, J. N.; Farrugia, P. S.; Gatt, R.; Zammit, V. A system with adjustable positive or negative thermal expansion. *Proc. R. Soc. A.* **2007**, *463*, 1585–1596.
- [9] Xu, H.; Pasini, D. Structurally efficient three-dimensional metamaterials with controllable thermal expansion. *Sci Rep*, **2016**, *6*, 34924–1~8.
- [10] Ai, L.; Gao, X.L. Metamaterials with negative Poisson’s ratio and non-positive thermal expansion. *Compos. Struct.* **2017**, *162*, 70–84.
- [11] Lakes, R.; Wojciechowski, K. W. Negative compressibility, negative Poisson’s ratio, and stability. *Phys. Stat. Sol. B.* **2008**, *245*, 545-551.
- [12] Munster, A. Statistical Thermodynamics. *1st Engl. ed. (Springer-Verlag, Berlin)*. **1969**, Vol. 1, sect. 4.2, pp. 212, 217, 218, 226; sect. 4.5, p. 261.
- [13] Kubo, R.; Thermodynamics. (*North-Holland Publ. Company, Amsterdam*). **1968**, pp. 140–147.
- [14] Wallace, D. C. Thermodynamics of crystals. (*John Wiley & Sons, New York*). **1972**.

- [15] Timoshenko, S. P.; Goodier, J. N. *Theory of Elasticity. 3rd ed. (McGraw-Hill). 1970*
- [16] Nicolaou, Z. G.; Motter, A. E. Mechanical Metamaterials with Negative Compressibility Transitions. *Nature Materials*. **2012**, *11*, 608-613.
- [17] Nicolaou, Z. G.; Motter, A. E. Longitudinal Inverted Compressibility in Super-strained Metamaterials. *J. Stat. Phys.* **2013**, *151*, 1162–1174.
- [18] Chen, M. L.; Karpov, E. G. Bistability and thermal coupling in elastic metamaterials with negative compressibility. *Physical Review E*. **2014**, *90*, 033201.
- [19] Imre, A. R. Metamaterials with negative compressibility – a novel concept with a long history. *Materials Science-Poland*. **2014**, *32*, 126–129.
- [20] Dudek, K. K.; Attard, D.; Caruana-Gauci, R.; Wojciechowski, K.W.; Grima, J.N. Unimode metamaterials exhibiting negative linear compressibility and negative thermal expansion. *Smart Mater. Struct.* **2016**, *25*, 025009.
- [21] Grima, J. N.; Caruana-Gauci, R.; Attard, D.; Gatt, R. Three-dimensional cellular structures with negative Poisson's ratio and negative compressibility properties. *Proc R Soc A: Mathe, Phys Eng Sci*. **2012**, *468*, 3121–38.

4 A NUMERICAL STRAIN ENERGY ANALYSIS USING SPECTRAL AND INFORMATION CONTENT OF MATERIALS

(This chapter is on a material previously published as Karpov, E. G.; Danso, L. A. Strain Energy Spectral Density and Information Content of Materials Deformation. International Journal of Mechanical Sciences. 2018, 148, 676-683.)

4.1 Introduction

Strain and stress analysis is fundamental in the study of continuum mechanics and therefore earlier methods such as image correlation or photoelasticity have been the choice when the capacity of mathematical or numerical methods have been limited in terms of geometry and boundary conditions [1-2]. An optical monitoring technique like photoelasticity has been useful in applications of detecting critical stresses, qualitative and quantitative measures of distribution of stress and strains around inclusions, discontinuities, farer regions of large domains and in materials with irregular geometry [3-5]. In solid mechanics, lattice-structures have been used over the decades to approximate continuum behavior of materials. Early as 1941, Hrennikoff [6] showed that a plane stress problem was solvable using a lattice framework methodology and proved the method to be efficient compared to the existing mathematical and photoelasticity approaches. The approach has since developed discrete mechanics models [7-9] to answer some important solid mechanics questions in the field of fracture and failure analysis. However, inspired by the successful outcomes of signal characterization methods in signal analysis and information theory, we believe similar methods could be used to understand the spectral characteristics of static deformation and can lead to a comprehensive numerical tool comparable to previously mentioned methods that would define the stress and strain behavior of a continuum body. More importantly the method will provide a cost-effective solution for detecting stress and strain anomalies critical to the integrity of a continuum material.

The two concepts critical to the proposed procedure is the Parseval's theorem and Shannon's entropy. The Parseval's theorem [10-12] found in digital signal analysis stating that the amount of energy contained in both time and frequency domains must be the same will be employed to develop a strain energy spectral density

(SESD) measure which will be a Fourier domain form of the elastic strain energy density in a material or structure. Hence, the SESD becomes an important parameter that produces a spectrum of how mechanically induced stresses are transformed in a material and shows the contribution of the inherent Fourier wave numbers which provides opportunity for energy distribution modification. The SESD will also serve as a variable to calculate a variation of the Shannon's entropy, the strain energy spectral entropy (SESE) which will be defined as a measure of the amount of information obtained from mechanical deformation of the analyzed system. Entropy was proposed by Clausius in the 18th century as a thermodynamics measure of system chaos or disorganization but was later developed by Shannon [13-16] as a qualitative measure of the amount of information. It is therefore considered as a measure for efficiently storing and communicating information. Spectral entropy analysis in mechanics proposes similar benefits as a measure of the smoothness of the SESD spectrum and as a tool for predicting defects in a system's strain energy distribution.

The numerical methods presented in this chapter could be extended to discrete mechanics to monitor and manipulate stress and strain behavior of mechanical metamaterial like the negative Poisson's ratio, reverse Saint Venant edge effect (RSV), basic symmetry breaking, negative elastic modulus [17-26]. For example, the RSV effect in nonlocal lattices by Karpov [24] have shown lattices with unusual spectral features which have potential for anomalous strain distribution behavior.

The formulation of SESD and the spectral entropy will be developed studying a gaussian pressure load acting against a plane solid and for a general solid mechanics problem solution a discrete numerical method is discussed. Illustrative examples will demonstrate how mechanical deformation evolution in space describes information about surface loads in an elastic continuum.

4.2 Developing the Strain Energy Spectral Density (SESD)

The strain energy spectral density (SESD) as mentioned earlier can be formulated as a mechanics analogue of the Parseval's theorem [10-12] in signal processing (see Appendix 4-A.1). This implies writing a Fourier domain form of the spatial domain strain energy density formulation from mechanics. For a plane stress problem, the strain energy density in solid mechanics takes the quadratic form:

$$W(x, y) = \frac{1}{2} \boldsymbol{\varepsilon}^*(x, y) \mathbf{E} \boldsymbol{\varepsilon}(x, y) \quad (4-1)$$

$$\boldsymbol{\varepsilon}(x, y) = \begin{Bmatrix} \varepsilon_x(x, y) \\ \varepsilon_y(x, y) \\ \gamma_{xy}(x, y) \end{Bmatrix} \quad (4-2)$$

where \mathbf{E} is the stress-strain matrix or constitutive matrix (See in Appendix 4-A.15) and $\boldsymbol{\varepsilon}$ and $\boldsymbol{\varepsilon}^*$ are vector column matrices of the strains and its conjugate transpose respectively. Taking an integral of (4-1) over the y spatial coordinate gives

$$\Pi(x) = \int_{-\infty}^{\infty} W(x, y) dy \quad (4-3)$$

The strains vector in (4-2) can be expressed as the inverse Fourier transform (4-A.3) of its Fourier image (4-A.2) as

$$\boldsymbol{\varepsilon}(x, y) = \int_{-\infty}^{\infty} \tilde{\boldsymbol{\varepsilon}}(x, q) e^{-iqy} dq \quad (4-4)$$

and substituted into (4-3) above

$$\Pi(x) = \frac{1}{8\pi^2} \int_{-\infty}^{\infty} \left(\int_{-\infty}^{\infty} \tilde{\boldsymbol{\varepsilon}}^*(x, q') e^{iq'y} dq' \right) \mathbf{E} \left(\int_{-\infty}^{\infty} \tilde{\boldsymbol{\varepsilon}}(x, q) e^{-iqy} dq \right) dy \quad (4-5)$$

Equation (4-5) above can be reconstructed to satisfy integration rules as

$$\begin{aligned} \Pi(x) &= \frac{1}{8\pi^2} \int_{-\infty}^{\infty} \int_{-\infty}^{\infty} \left(\int_{-\infty}^{\infty} e^{iq'y} e^{-iqy} dy \right) \tilde{\boldsymbol{\varepsilon}}^*(x, q') \mathbf{E} \tilde{\boldsymbol{\varepsilon}}(x, q) dq dq' \\ &= \frac{1}{4\pi} \int_{-\infty}^{\infty} \int_{-\infty}^{\infty} \delta(q - q') \tilde{\boldsymbol{\varepsilon}}^*(x, q') \mathbf{E} \tilde{\boldsymbol{\varepsilon}}(x, q) dq dq' \end{aligned} \quad (4-6)$$

Where δ represents the Dirac's delta function (4-A.8 – 4-A.9) and hence the elimination of the integral over the Fourier domain variable q' . So (4-6) when rewritten becomes

$$\Pi(x) = \frac{1}{2\pi} \int_{-\infty}^{\infty} \left(\frac{1}{2} \tilde{\boldsymbol{\varepsilon}}^*(x, q) \mathbf{E} \tilde{\boldsymbol{\varepsilon}}(x, q) \right) dq \quad (4-7)$$

The equation in (4-7) therefore expresses the Fourier domain form of the space integral of the spatial strain energy density expression in (4-3). Therefore, we have been successful in obtaining a mechanics analogue of the Parseval's theorem which can be stated as

$$\int_{-\infty}^{\infty} W(x, y) dy = \frac{1}{2\pi} \int_{-\infty}^{\infty} \tilde{W}(x, q) dq \quad (4-8)$$

$$W(x, y) = \frac{1}{2} \boldsymbol{\varepsilon}^*(x, y) \mathbf{E} \boldsymbol{\varepsilon}(x, y) \quad (4-9)$$

$$\tilde{W}(x, q) = \frac{1}{2} \tilde{\boldsymbol{\varepsilon}}^*(x, q) \mathbf{E} \tilde{\boldsymbol{\varepsilon}}(x, q) \quad (4-10)$$

Here, $W(x, y)$ is the spatial or volumetric strain energy density and $\tilde{W}(x, q)$ is the strain energy spectral density (SESD). The expression (4-8) also states that an integral over strain components vector in quadratic form is quantitatively equal to the integral over the Fourier transform of the strain component vector in quadratic form. The quantity $\tilde{W}(x, q)$ calculated for a deformed body would give the amount of strain energy contained in the wave number interval from q to $q + dq$. The evolution of $\tilde{W}(x, q)$ in space is described by its dependence on the spatial coordinate x .

It is possible also to develop the strain energy spectral density for a three-dimensional (3D) space problem like (4-3) by applying integrals corresponding to the number of the required dimensionality or number of Fourier variables. Following, the procedure above the strain energy spectral density quantities $\tilde{W}(x, y, q)$, $\tilde{W}(x, q_1, q_2)$ and $\tilde{W}(q_1, q_2, q_3)$ under a single, double and triple integral are found (See Appendix A.10-12). However, we restrict the ongoing study to strain energy spectral density $\tilde{W}(x, q)$ of a single Fourier variable in 2D space (4-10) which is the most interesting when studying how material respond to surface loads. Thus, the quantity $\tilde{W}(x, q)$ will give a comprehensive view of how spectral component q affects material's response having seen how deformation in a material is dependent on spectral composition of a surface load. This study will help study further metamaterials behaviors such as the reverse Saint Venant's Edge effect and deformation blockage. The $\tilde{W}(x, q)$ formulation as stated earlier will be an important quantity for deriving the spectral entropy of deformation measure which is illustrated in the next section.

4.3 Developing the Strain Energy Spectral Entropy (SESE)

The strain energy spectral entropy measure is written following Shannon's differential entropy [11,12] definition as

$$S(x) = - \int_{-\infty}^{\infty} \tilde{w}(x, q) \ln \tilde{w}(x, q) dq \quad (4-11)$$

$$w(x, y) = \frac{W(x, y)}{\Pi(x)} \quad (4-12)$$

$$\tilde{w}(x, q) = \frac{1}{2\pi} \frac{\tilde{W}(x, q)}{\Pi(x)} \quad (4-13)$$

$$\int_{-\infty}^{\infty} w(x, y) dy = \int_{-\infty}^{\infty} \tilde{w}(x, q) dq = 1 \quad (4-14)$$

Where $w(x, y)$ and $\tilde{w}(x, q)$ represents the normalized strain energy density and normalized strain energy spectral density respectively. $S(x)$ in our study would be a measure of the smoothness of the strain energy along the spatial coordinate x within a plane solid due to surface loads. Therefore, the study of entropy proposed in mechanics becomes a great tool for fracture and failure assessment in mechanical systems and components.

Similar to how entropy in information theory is high for surprises or uncertainties in stored information, the strain energy spectral entropy (SESD) would be high in regions with stress concentration, cracks, physical inhomogeneities and close to localized surface loads. To illustrate this spectral entropy measure in (4-11), a Fourier transform of Gaussian function is considered:

$$\tilde{w}_G(q) = \frac{1}{2\pi} \int_{-\infty}^{\infty} e^{-\frac{a^2 y^2}{2}} e^{-iqy} dy = \frac{1}{a\sqrt{2\pi}} e^{-\frac{q^2}{2a^2}} \quad (4-15)$$

It is worth noting that $\tilde{w}_G(q)$ is similarly a Gaussian function but with an inverse width a which means that a narrow function in spatial domain would be equivalent to a wide function in Fourier domain. Using (4-15), a differential spectral entropy of the stated Gaussian function has the form:

$$S_G = - \int_{-\infty}^{\infty} \tilde{w}_G(q) \ln \tilde{w}_G(q) dq = \ln(a\sqrt{2\pi e}) \quad (4-16)$$

From (4-16), the width of the Gaussian function a can be varied from 0 to ∞ corresponding to a differential spectral entropy range of $-\infty$ to ∞ .

It is important to note that the normalized strain energy spectral entropy $\tilde{w}(x, q)$ expression in (4-13) would have a unit of length since the y spatial coordinate was not nondimensionalized. Making y dimensionless with a factor such as $\frac{1}{\Lambda}$ introduces a shift in the strain energy spectral entropy (4-11) by $\ln \Lambda$ which should be expected according to (4-14). Hence the range of an absolute strain energy spectral entropy (SESE) would be dependent on the measure of the factor Λ applied.

4.4 Numerical Calculation of Spectral Entropy (SESE)

The Shannon's differential entropy employed in (4-11) and demonstrated in (4-16) may only serve as a theoretical measure with no practical significance with regards to the present study of strain energy transformation in a plane solid in which a usual material assumes a constant decay between two boundary surfaces. The intention of this section is to outline a numerical procedure that results in a spectral entropy measure that has a limited range being positive from boundary to boundary and characterizing the decay in entropy as the strain energy spectral density (SESD) evolves in the continuum material.

The numerical procedure adopted would require discretizing the y spatial coordinate into discrete points (x, y_m) , $m = 0, \pm 1, \dots, \pm M/2$ with equal spacing along a substantially large length of the plane solid. The strain energy components in (4-2) are calculated using the generated points and then their corresponding spectral components obtained by applying the Discrete Fourier Transform (DFT). For example, the DFT for the strain component in the x coordinate direction ε_x gives:

$$\tilde{\varepsilon}_x(x, q_\mu) = \sum_{m=-M/2}^{M/2-1} \varepsilon_x(x, y_m) e^{-i2\pi\mu y_m/L}, \quad q_\mu = \frac{2\pi\mu}{L}, \quad \mu = 0, \pm 1, \dots, \pm M/2 \quad (4-17)$$

The quadratic form of spectral strain vectors in (4-10) is written as

$$\tilde{W}(x, q_\mu) = \frac{1}{2} \tilde{\varepsilon}^*(x, q_\mu) \mathbf{E} \tilde{\varepsilon}(x, q_\mu) \quad (4-18)$$

Also considering the differential entropy (4-11) for a small discrete interval would give

$$S(x) = - \int_{q_\mu}^{q_\mu + \Delta q} \tilde{w}(x, q) \ln \tilde{w}(x, q) dq \approx \Delta q \cdot \tilde{w}(x, q) \ln \tilde{w}(x, q) \quad (4-19)$$

$$\tilde{w}(x, q_\mu) = \frac{\tilde{W}(x, q_\mu)}{\sum \tilde{W}(x, q_\mu)} \quad (4-20)$$

$$\Delta q = q_{\mu+1} - q_{\mu} = \frac{2\pi}{L} \quad (4-21)$$

From the expression in (4-19), the numerical version of the differential spectral entropy measure (4-11) for an L - periodic domain is written below:

$$S(x) \approx -\sum_{\mu=-M/2}^{M/2-1} p_{\mu}(x) \ln \frac{p_{\mu}(x)}{\Delta q}, \quad (4-22)$$

$$p_{\mu}(x) = \Delta q \cdot \tilde{w}(x, q_{\mu}) \quad (4-23)$$

Employing the property $\sum p_{\mu}(x) = 1$, a correlation can be made between a discrete spectral entropy measure $H(x)$ and the continuous spectral entropy $S(x)$:

$$S(x) \approx H(x) + \ln \frac{2\pi}{L} \quad (4-24)$$

$$H(x) = -\sum_{\mu=-M/2}^{M/2-1} p_{\mu}(x) \ln p_{\mu}(x) \quad (4-25)$$

Considering a bell shaped or normal distribution function of discrete points, each discrete point would be unique such that $p_{\mu} = 1/M$ and so $H = \ln M$. Also, assuming a Kronecker delta function (4-A.19) distribution where $p_{\mu} = \delta_{\mu 0}$ then the entropy $H = 0$ and therefore $H(x)$ is said to lie within the closed interval $[0, \ln M]$. Even though the bounds of $H(x)$ can be useful for practical purpose, it becomes more appealing when it is normalized as below:

$$h(x) = \frac{1}{\ln M} H(x) = -\frac{1}{\ln M} \sum_{\mu=-M/2}^{M/2-1} p_{\mu}(x) \ln p_{\mu}(x) \quad (4-26)$$

The above expression $h(x)$ would be a meaningful bounded strain energy spectral entropy of continuum material and its values would satisfy the interval $[0,1]$. From (4-26), it is obvious that a continuum body loaded at one surface with a high concentrated stress such as a Gaussian or a point load would have spectral entropy $h \rightarrow 1$ and as it propagates through the material to the other surface $h \rightarrow 0$. It also important to note from (4-23) that $p_{\mu}(x)$ is dimensionless quantity and so our discrete spectral entropy measure h is an absolute measure

invariant to the scaling of the strain energy spectral as it is in the case of the differential strain energy spectral in entropy in (4-11). To correlate the performance of the discrete entropy measure of a numerical procedure, a calculated differential entropy measure $S(x)$ can be modified by normalization to serve as the control variable in the following expression:

$$s(x) = \frac{1}{\ln M} \left(S(x) - \ln \frac{2\pi}{L} \right) \approx h(x) \quad (4-27)$$

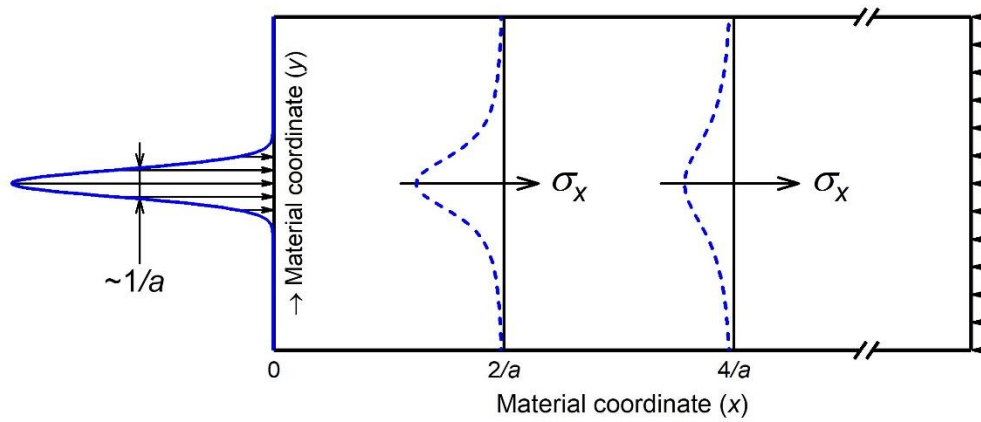


Figure 4.1 Normal stress σ_x (4-39) transformation in a plane solid when a Gauss-type (4-40) load component is applied at boundary ($x = 0$).

4.5 Communication in Mechanics

The spectral entropy expression developed in (4-25) is analogous to the entropy measure attributed to Shannon's work of information theory in communication [13-16]. The mathematical inference of the spectral entropy can be explained as a mean measure of information per an observed event in an assumed random process such that p_μ represents all probable outcomes. The entropy measure following its usage in data and signal processing, is basically the amount of information that can be stored or efficiently communicated and to some degree a measure of information compression [15].

The spectral entropy in (4-25) therefore generates a value of how the strain energy spectral densities (SESD) at a position x account for information about surface loads. This is a process of the strain energy spectral densities

(SESD) capturing the spectral components strain energy contribution due to the surface loads and then calculating the probability p_μ of these SESD's for the entire range of q_μ . So, the expression in (4-25) applied to p_μ denotes the amount of quality information about deformation from surface loads that can be stored or communicated. In signal processing, entropy has been useful in distinguishing a speech from a background noise. The background noise will produce a very high entropy due to presence of several Fourier harmonics with relatively equal probabilities compared to a speech with a signal that is more organized and uniform with the least possible number of Fourier harmonics prevailing [27]. The spectrum of the noise could be defined as a system in chaos or disorder which underlines the earlier definition of entropy in thermodynamics [16].

In mechanics, the spectral entropy will be great tool to measure the amount of information that mechanical forces can introduce into a system. So, on the static deformation inside a continuum material due to surface loads such as a Gaussian, the Saint Venant principle of deformation will be affirmed by (4-25, 4-26) with a high spectral entropy at the initial boundary which decays till it vanishes at the farthest boundary. At the farthest boundary, the deformation is almost uniform such that its strain energy spectral distribution at that point can be represented with a Kronecker delta function and therefore, the zero spectral entropy. The potential use of entropy in mechanics is forecasted for deformation pattern recognition, inverse solution methods in mechanics and stress alleviation in mechanical systems.

4.6 Illustrative Example: Gauss-Type Load On A Plane Solid

In this section, a plane solid body under a plane stress assumption is studied with the aim of deriving formulations for its the strain energy spectral density (4-10,4-13) and spectral entropy (4-11) when acted upon by a Gaussian load at $x = 0$ as shown in Fig. 1. The governing homogenous Navier's equations [28] for this problem over $x > 0$ are

$$\begin{aligned} 2u''_{xx}(x, y) + (1 + \nu)v''_{xy}(x, y) + (1 - \nu)u''_{yy}(x, y) &= 0 \\ (1 - \nu)v''_{xx}(x, y) + (1 + \nu)u''_{xy}(x, y) + 2v''_{yy}(x, y) &= 0 \end{aligned} \quad (4-28)$$

A fundamental solution satisfying the above differential equations in (4-25) can be stated as a decaying static Raleigh wave [24] of the form,

$$C(q)e^{-\eta x}e^{iqy} \quad (4-29)$$

The general displacement solution for a material that decays at a rate η can be written as a superposition of the fundamental solution in (4-29):

$$\begin{aligned} u(x, y) &= \frac{1}{2\pi} \int_{-\infty}^{\infty} C_1(q)e^{-\eta x}e^{iqy} dq \\ v(x, y) &= \frac{1}{2\pi} \int_{-\infty}^{\infty} C_2(q)e^{-\eta x}e^{iqy} dq \end{aligned} \quad (4-30)$$

The equations in (4-28) are satisfied under the following conditions,

$$C_2 = -i \operatorname{sgn}(q)C_1 \quad \eta = |q| \quad (4-31)$$

Where $\operatorname{sgn}(q)$ is the signum function (4-A.13) and using (4-31), the equations in (4-30) are modified as

$$\begin{aligned} u(x, y) &= \frac{1}{2\pi} \int_{-\infty}^{\infty} C(q)e^{-|q|x}e^{iqy} dq \\ v(x, y) &= -\frac{i}{2\pi} \int_{-\infty}^{\infty} \operatorname{sgn}(q)C(q)e^{-|q|x}e^{iqy} dq \end{aligned} \quad (4-32)$$

$C(q)$ is a complex-valued function that is characteristic of the boundary conditions $u(0, y)$ and $v(0, y)$ and equation (4-32) is in complex form whose real and imaginary components are all possible solutions to the governing differential equations in (4-28).

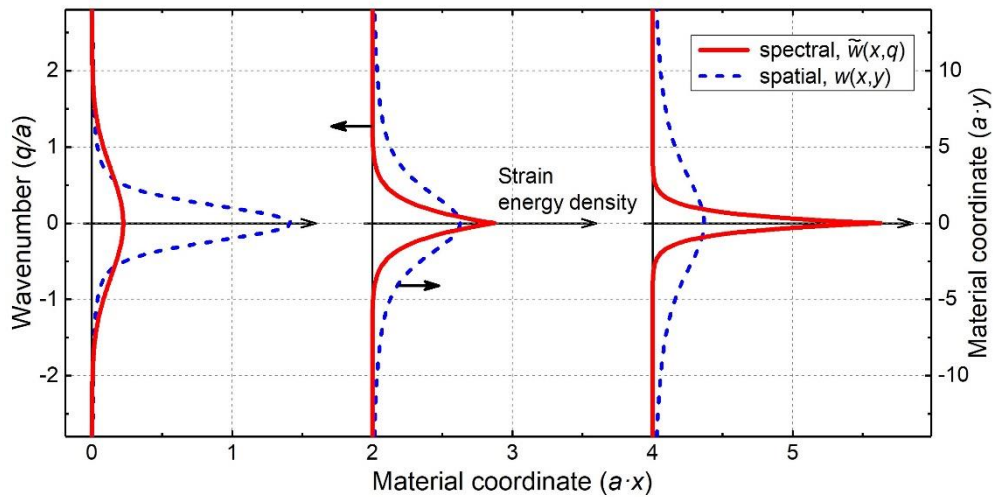


Figure 4.2 Strain energy spectral density (solid line) versus the spatial strain energy density (dashed line) for Fig.4.1 problem. Inverse transformation relationship of widening (spatial, (4-44)) and narrowing (spectral, (4-45)) is observed.

Employing the Fourier inverse definition (4-A.3), the Fourier transforms of the displacement solution in (4-32) are

$$\begin{aligned}\tilde{u}(x, q) &= C(q)e^{-|q|x} \\ \tilde{v}(x, q) &= -i \operatorname{sgn}(q)C(q)e^{-|q|x}\end{aligned}\quad (4-33)$$

The above equations must also satisfy Fourier images (4-A.4) of the governing Navier's equations in (4-28),

$$\begin{aligned}2\tilde{u}''_{xx}(x, q) + iq(1 + \nu)\tilde{v}'_x(x, q) - q^2(1 - \nu)\tilde{u}(x, q) &= 0 \\ (1 - \nu)\tilde{v}''_{xx}(x, q) + iq(1 + \nu)\tilde{u}'_x(x, q) - 2q^2\tilde{v}(x, q) &= 0\end{aligned}\quad (4-34)$$

For the Gaussian load acting on the plane solid, $C(q)$ is assumed to be of the form,

$$C(q) = \frac{1}{a|q|} e^{-\frac{q^2}{2a^2}} \quad (4-35)$$

Since a signum function has the property $|q| = q \operatorname{sgn}(q)$, the Fourier transform solution in (4-33) can be written for the acting Gaussian load as

$$\begin{aligned}\tilde{u}(x, q) &= \frac{1}{a|q|} e^{-x|q| - \frac{q^2}{2a^2}} \\ \tilde{v}(x, q) &= -\frac{i}{a q} e^{-x|q| - \frac{q^2}{2a^2}}\end{aligned}\quad (4-36)$$

Here a is a parameter representing deformation *spectral width*. The Fourier transforms of the strain components (4-2) are subsequently obtained from (4-36) according to (4-A.4) below,

$$\begin{aligned}\tilde{\varepsilon}_x(x, q) = -\tilde{\varepsilon}_y(x, q) &= -\frac{1}{a} e^{-x|q| - \frac{q^2}{2a^2}} \\ \tilde{\gamma}_{xy}(x, q) &= \frac{2i \operatorname{sgn}(q)}{a} e^{-x|q| - \frac{q^2}{2a^2}}\end{aligned}\quad (4-37)$$

Applying the inverse Fourier transform (4-A.3) we obtain the exact strain components (4-2),

$$\begin{aligned}\varepsilon_x(x, y) = -\varepsilon_y(x, y) &= -\frac{1}{\sqrt{8\pi}} (\beta + \beta^*) \\ \gamma_{xy}(x, y) &= \frac{i}{\sqrt{2\pi}} (\beta - \beta^*) \\ \beta = \beta(x, y) &= e^{\frac{a^2(x+iy)^2}{2}} \operatorname{erfc} \frac{a(x+iy)}{\sqrt{2}}\end{aligned}\quad (4-38)$$

Where erfc represents the complimentary error function (4-A.14). Having got the strain components, the stress components are calculated from $\sigma = \mathbf{E}\varepsilon$ and they are invariant with respect to either a plane stress or plane strain assumption (4-A.15):

$$\begin{aligned}\sigma_x(x, y) &= -\sigma_y(x, y) = \frac{E}{1+\nu} \varepsilon_x(x, y) \\ \tau_{xy}(x, y) &= \frac{E}{2+2\nu} \gamma_{xy}(x, y)\end{aligned}\quad (4-39)$$

For application purposes, the Gauss-type load function can be denoted by the horizontal component of the traction force $\mathbf{t} = -\boldsymbol{\sigma}\mathbf{n}$, given a unit normal $\begin{Bmatrix} 1 \\ 0 \end{Bmatrix}$. The Gaussian at $x = 0$ is

$$T_x(y) = -\sigma_x(0, y) = \frac{E}{\sqrt{2\pi}(1+\nu)} e^{-\frac{a^2 y^2}{2}} \quad (4-40)$$

It is interesting to note that the width of the Gaussian is $1/a$ (Fig. 4.1), which is inverse of the spectral width seen in (4-36).

The strain components in (4-38) helps to precisely formulate the strain energy density (4-9) and strain energy spectral density (4-10) for the Gaussian as

$$W(x, y) = \frac{1}{2} \boldsymbol{\varepsilon}^*(x, y) \mathbf{E} \boldsymbol{\varepsilon}(x, y) = \frac{E e^{a^2(x^2-y^2)}}{2\pi(1+\nu)} \operatorname{erfc} \frac{a(x+iy)}{\sqrt{2}} \operatorname{erfc} \frac{a(x-iy)}{\sqrt{2}} \quad (4-41)$$

$$\tilde{W}(x, q) = \frac{1}{2} \tilde{\boldsymbol{\varepsilon}}^*(x, q) \mathbf{E} \tilde{\boldsymbol{\varepsilon}}(x, q) = \frac{2E}{a^2(1+\nu)} e^{-2x|q| - \frac{q^2}{a^2}} \quad (4-42)$$

Taking spatial and Fourier integrals of the energy densities (4-41 – 4-42) as in (4-8), the Parseval's theorem is proven:

$$\Pi(x) = \int_{-\infty}^{\infty} W(x, y) dy = \frac{1}{2\pi} \int_{-\infty}^{\infty} \tilde{W}(x, q) dq = \frac{E e^{a^2 x^2}}{a\sqrt{\pi}(1+\nu)} \operatorname{erfc} ax \quad (4-43)$$

The energy densities in (4-41 – 4-42) can then be normalized to get

$$w(x, y) = \frac{W(x, y)}{\Pi(x)} = \frac{a e^{-a^2 y^2} \operatorname{erfc} \frac{a(x+iy)}{\sqrt{2}} \operatorname{erfc} \frac{a(x-iy)}{\sqrt{2}}}{\sqrt{4\pi} \operatorname{erfc} ax} \quad (4-44)$$

$$\tilde{w}(x, q) = \frac{1}{2\pi} \frac{\tilde{W}(x, q)}{\Pi(x)} = \frac{e^{-\frac{q^2}{a^2} - 2x|q| - a^2 x^2}}{a\sqrt{\pi} \operatorname{erfc} ax} \quad (4-45)$$

In Fig. 4.2, we show profiles of the normalized densities (4-44 – 4-45) inside the plane solid material at different positions of the spatial coordinate x scaled by a . The *inverse property* that exists between the spatial and spectral variables is also seen in the transformation of the energy densities inside the material. The narrowing of the

strain energy spectral density as material dimension ax increases resembles a *low-pass filter* functionality where at each coordinate position ax certain high frequencies or Fourier harmonics are cut-off until at a point in the material that only the Fourier Harmonic $q \approx 0$ exists in the energy spectrum and deformation is said to be uniform.

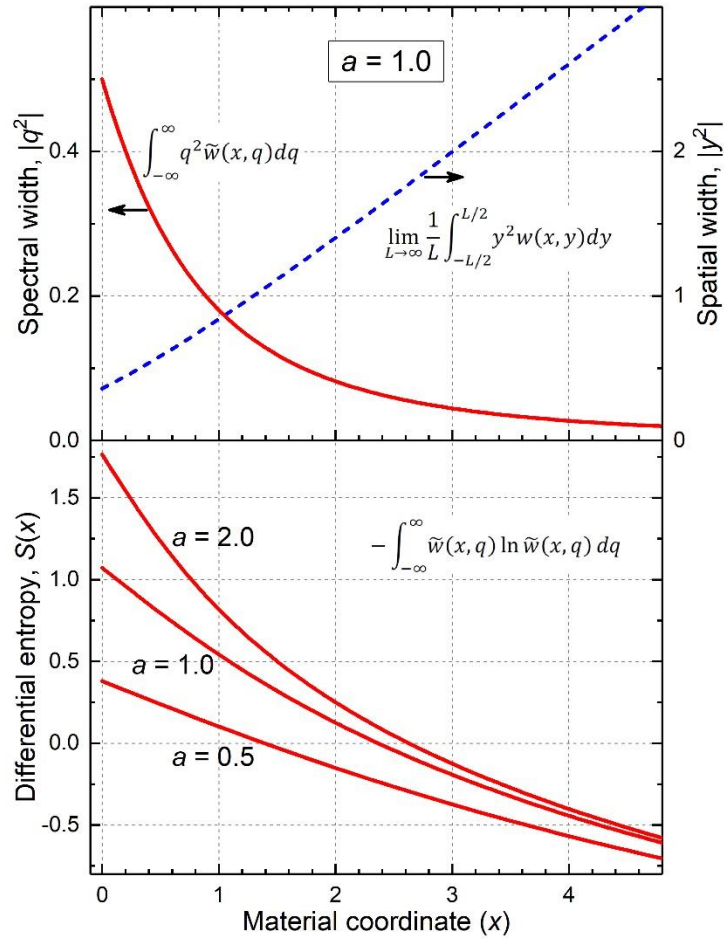


Figure 4.3 (top) Illustration of the strain energy inverse transformation relationship for the Gaussian problem in Fig.1 having spectral width, $a = 1$ and (bottom) differential spectral entropy (4-46) curves as a function of the spectral width.

Next, the differential entropy expression (4-11) is obtained analytically for the Gaussian from (4-44 – 4-45) as follows:

$$S(x) = - \int_{-\infty}^{\infty} \tilde{w}(x, q) \ln \tilde{w}(x, q) dq = \frac{ax e^{-a^2x^2}}{\sqrt{\pi} \operatorname{erfc} ax} + \ln(a\sqrt{\pi e} \operatorname{erfc} ax) \quad (4-46)$$

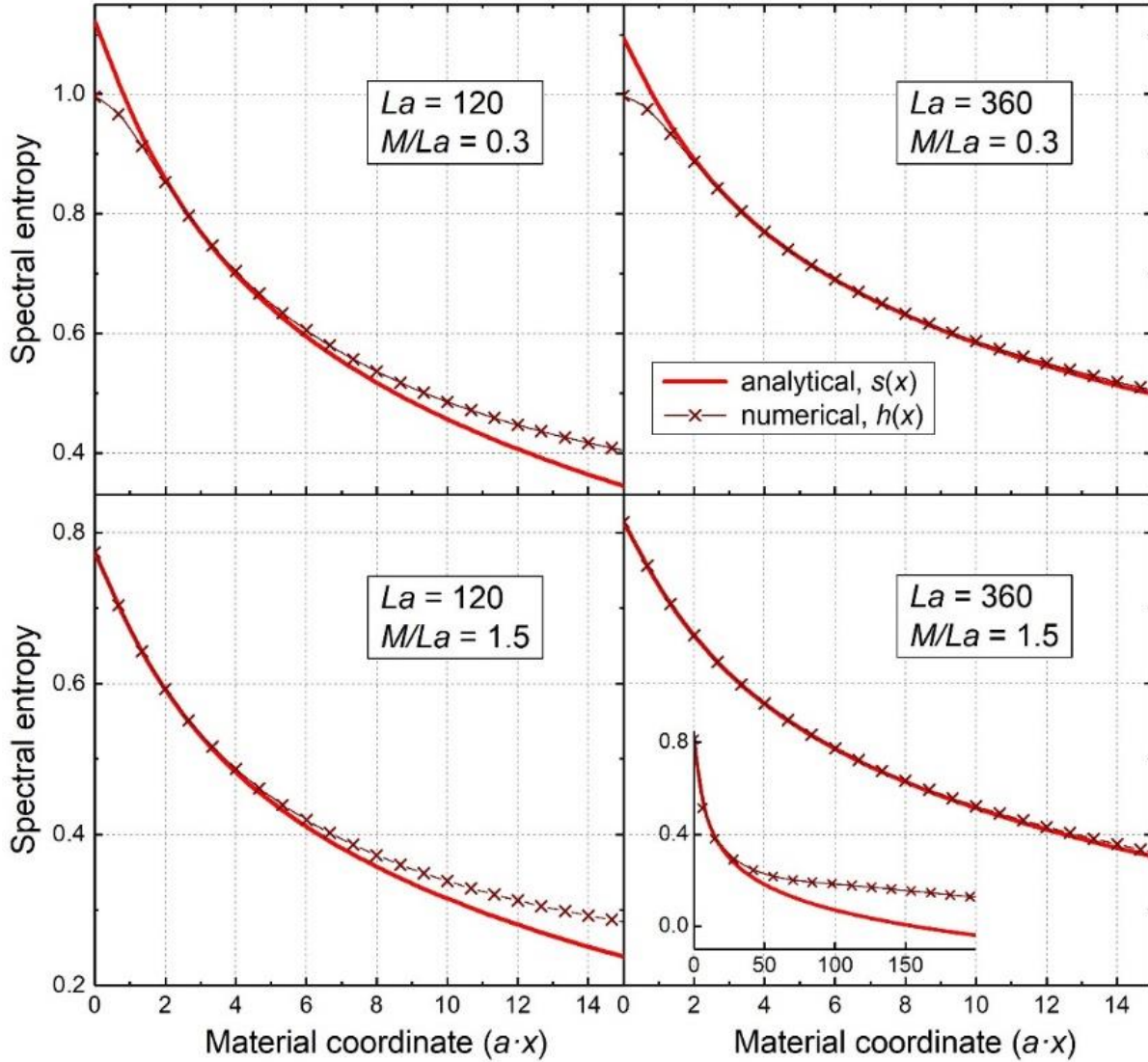


Figure 4.4 The modified analytical (4-27,4-46) versus numerical (4-26) spectral entropies as functions of the material coordinate for Fig.1 problem. When La and $M/La \rightarrow \infty$ there is better matching (bottom right).

The plot in Fig. 4.3 describes how $S(x)$ decays within the material as a function of the material coordinate x which is the result of the normal distribution like form (Fig. 4.2) of the strain energy spectral density at the boundary where the Gaussian is applied and at this point probably all Fourier harmonics contribute. Increasing

the material coordinate x , the differential entropy decreases due to narrowing of the strain energy spectral density reducing the number of probable Fourier harmonics. Fig. 4.3 also shows a characteristic feature related to a Gaussian where we observe a logarithmic increase in the spectral entropy $S(x)$ as the *spectral width* a increases like that seen in (4-16). In equation (4-16), $S_G = \ln(a\sqrt{2\pi e})$ represents spectral entropy for a 1D space which can be compared with the boundary value of the spectral entropy in (4-46), $S(0) = \ln a\sqrt{\pi e}$.

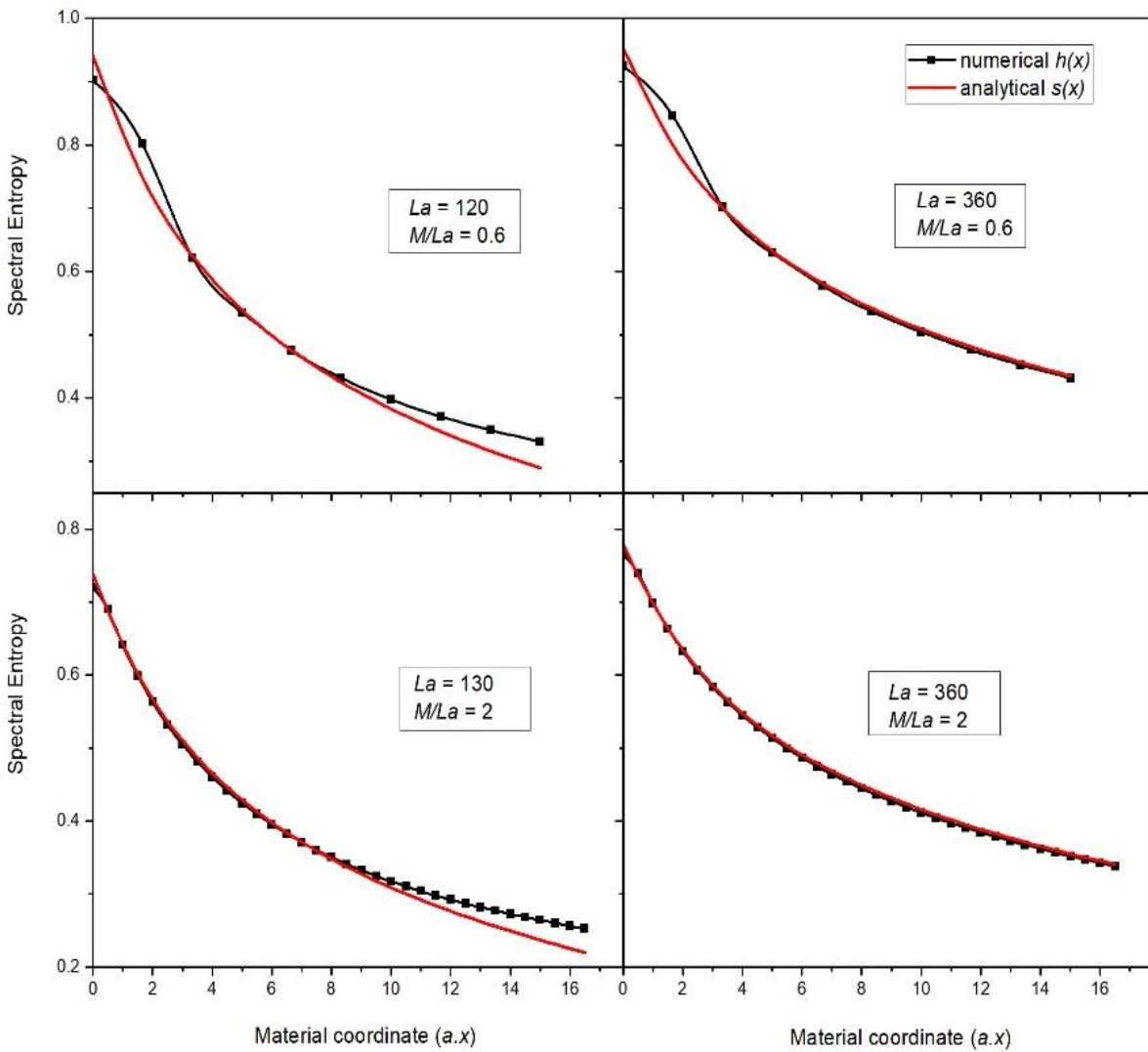


Figure 4.5 The modified analytical (4-27,4-46) versus numerical spectral entropies (ANSYS) as functions of the material coordinate for Fig.1 problem. When La and $M/La \rightarrow \infty$ there is better matching (bottom right)

4.7 Load And Boundary Approximations

The load approximation is to consider the scenario when the *spectral width* a is very large enough i.e. $a \rightarrow \infty$ such that $x \gg \frac{1}{a}$. To satisfy this condition the limits of the normalized energy densities and spectral entropy expressions (4-44 – 4-46) are performed:

$$w_0(x, y) = \lim_{a \rightarrow \infty} w(x, y) = \frac{x}{\pi(x^2 + y^2)} \quad (4-47)$$

$$\tilde{w}_0(x, q) = \lim_{a \rightarrow \infty} \tilde{w}(x, q) = xe^{-2|q|x} \quad (4-48)$$

$$S_0(x) = \lim_{a \rightarrow \infty} S(x) = 1 - \ln x \quad (4-49)$$

By taking a limit of the strain energy approximation in (4-47), we obtain a Dirac delta function:

$$\lim_{x \rightarrow 0} w_0(x, y) = \frac{1}{\pi} \lim_{x \rightarrow 0} \frac{x}{x^2 + y^2} = \delta(y) \quad (4-50)$$

Therefore, the load approximation can also represent a point load approximation where the load is highly localized in the vicinity of $y = 0$. It is interesting to also consider the case when several point loads are periodically arranged on the surface boundary along a length of L . This L -periodic forced boundary problem can be solved by decomposing the displacement field in (4-28) using Fourier series to get

$$w_L(x, y) = \frac{(e^{4\pi x/L} - 1)/L}{1 + e^{4\pi x/L} - 2e^{4\pi x/L} \cos 2\pi x/L} \quad (4-51)$$

$$\tilde{w}_L(x, \mu) = \frac{(2 - \delta_{\mu 0})xe^{-4\pi|\mu|x/L}}{2 \coth 2\pi x/L - 1} \quad (4-52)$$

$$S_L(x) = -\frac{4 \ln 2}{3 + e^{4\pi x/L}} + \ln(2 \coth 2\pi x/L - 1) + \frac{8\pi x/L}{1 - \cosh 4\pi x/L + 2 \sinh 4\pi x/L} \quad (4-53)$$

Where μ is defined as in (4-17). In the case when the y coordinate is restricted to the domain $\{-L/2, L/2\}$, the above equations still apply by having a single point load fixed at the position $y = 0$ at the surface where

$x = 0$. Taking limit of such a domain condition when $L \rightarrow \infty$, results in the energy densities and spectral entropy expressions (4-47 - 4-49) for a point load limit case acting on an infinite boundary:

$$\lim_{L \rightarrow \infty} w_L(x, y) = w_0(x, y) \quad (4-54)$$

$$\lim_{L \rightarrow \infty} L \cdot \tilde{w}_L(x, qL/2\pi) = 2\pi \tilde{w}_0(x, q) \quad (4-55)$$

$$\lim_{L \rightarrow \infty} \left(S_L(x) + \ln \frac{2\pi}{L} \right) = S_0(x) \quad (4-56)$$

4.8 Numerical Entropy Versus Analytical Entropy

Having developed a numerical procedure for calculating differential entropy (4-26) which is applicable when deformations or strains in a plane solid body are available from a finite element analysis program and the strain field solution is not readily know. It is worthwhile to compare this practical entropy solution (4-26) for a Gaussian acting on an infinite boundary to the exact analytical differential entropy expression obtained in (4-46). First, the plane solid will be discretized where there will be a set of points (x, y_m) , $y_m = mL/M$, $m = 0, \pm 1, \dots, \pm M/2$ defined in the plane of the material. The points in the x coordinate direction is arbitrarily spaced for 24 points which could be varied to fit need. The strain components $\epsilon(x, y_m)$ (4-2) would then be obtained by a FEA procedure but here they are calculated from their analytical expressions in (4-38). Using the strain components calculated, the discrete spectral strain components $\tilde{\epsilon}_x(x, q_\mu)$ and spectral strain energy density $\tilde{W}(x, q_\mu)$ in (4-17) and (4-18) are obtained respectively. Finally, the factored discrete spectral strain component set $p_\mu(x)$ (23) is used to calculate the normalized strain energy spectral entropy $h(x)$ in (4-26). This numerical entropy value can then be compared with the modified analytical entropy value $s(x)$ in (27) (See Fig. 4-4). The numerical procedure detailed above can be performed easily using any commercial FEA program and results from such is shown in Fig. 4.5.

In Fig. 4.4 and Fig. 4.5, we make four plots comparing the numerically calculated entropy measure $h(x)$ of the Gaussian to its analytical entropy measure $s(x)$ based on two parametric values M/La and La : ratio of Gaussian load width $1/a$ and the finite element or mesh size L/M and the ratio of the length L to the load

width $1/a$ respectively. The parameter M/La defines an infinite surface boundary with respect to the load width $1/a$ and so when $\frac{M}{La} \rightarrow \infty$, the $s(x)$ values serves as a good benchmark for $h(x)$ at the onset of the deformation or near the surface boundary because the mesh size discretize the load width capturing any small feature at the surface. On the contrary for $\frac{M}{La} \rightarrow 0$, the numerical entropy measure will fail to capture the uniqueness of the Gaussian at the surface since the mesh size is greater than load width and therefore $h(x) \approx 1$ is produced at the surface accounting for equal presence of each Fourier mode contained in the load. This unit value entropy error is eliminated by refining the mesh of the finite element solution or numerical procedure. The parameter La rather defines an infinite boundary according to the plane solid length. For the case when $La \rightarrow \infty$, the high amount of discretization in the plane solid material eliminates the effect of finite boundaries in a numerical procedure and results in accurate comparison of $h(x)$ and $s(x)$ further along the material coordinate axis ax as shown in Fig. 4.4. The practical importance of numerical entropy measure is realized when entropy is calculated at the point of uniform deformation in a material when $h(x) \rightarrow 0$ but $s(x)$ assumes negative values. In continuum mechanics, the numerical or discrete spectral entropy is the most interesting since it fully captures deformation behavior in a continuum body according to the Saint Venant's principle.

4.9 Conclusions

In this chapter, the Parseval's theorem in digital analysis has been shown to be a novel way of understanding the transformation of mechanical deformation in continuum mechanics. The spectral form of the strain energy density (SESD) obtained from the Parseval's theorem has the same quadratic formulation as the volumetric or spatial strain energy and presents a spectrum that shows how strain energy evolves inside the material according to the Fourier harmonics available depending on a spatial coordinate in the case of a plane solid.

The SESD was seen to be an important parameter for calculating the strain energy spectral entropy (SESE) which has a very useful purpose for deformation pattern recognition. The differential or spectral entropy expression developed has a similar definition to the Shannon's entropy measure in information theory and is efficient in communicating information about surface loads at each point inside the continuum material. For practical use, a numerical or discrete spectral entropy (4-26) was also developed due to the unbound nature of

the differential or spectral entropy and the availability of sophisticated FEA programs to ease calculation of deformations and strains in a continuum body. Notwithstanding, a benchmark is provided to correlate results of the differential spectral and discrete or numerical.

In this study, an example of a Gauss-type load is presented, in which analytical forms of the strain energy spectral density (SESD) and strain energy spectral entropy (SESE) measures are derived. The Saint Venant edge effect in a plane solid is demonstrated by the narrowing of SESD and the decay of SESE along material spatial coordinate. This means information about surface loads inside the plane-solid material is preserved at small distances from the boundary surface where the load is applied and at great distances away from the load information is lost. The spectral strain energy entropy at large distances approached the negative entropy zone but for the numerical or discrete entropy it approached zero and therefore a better measure for energy studies in mechanics.

The discussion provided in this chapter enhances the field of transformation mechanics and can be proposed for energy and entropy studies for periodic lattices or architected materials, composite materials etc. [24,29,30] which have been shown to possess exotic properties such as the reverse Saint Venant edge effect and strain energy storing capabilities.

CHAPTER 4 REFERENCES

- [1] Frocht, M. M.; Photoelasticity. *J. Wiley and Sons, London*. **1965**.
- [2] Post, D. Photoelasticity, *Exp. Mechanics*. **1979**, 19 (5), 176-192
- [3] Sutton, M. A.; Orteu, J. J.; Schreier, H. W. Image Correlation for Shape, Motion and Deformation Measurements: Basic Concepts, Theory and Applications. (*Springer*), **2009**, p. 322
- [4] Bigoni, D.; Noselli, G. Localized stress percolation through dry masonry walls. *Part I - Experiments Eur. J of Mechanics & Solids*. **2010**, 29, 291-298
- [5] Ayatollahi, M. R.; Mirsayar, M. M.; Dehghany, M. Experimental determination of stress field parameters in bi-material notches using photoelasticity. *Materials & Design*. **2011**, 32, 4901–4908.
- [6] Hrennikoff, A. Solution of Problems of Elasticity by the Framework Method. *ASME J. Appl. Mech.* **1941**, 12, pp. 169–175.

- [7] Herrmann, H. J. Introduction to Modern Ideas on Fracture Patterns. *Random Fluctuations and Pattern Growth: Experiments and Models*, H. E. Stanley and N. Ostrowsky, eds., Kluwer Academic, Dordrecht, The Netherlands. **1988**, pp. 149–160.
- [8] Schlangen, E.; van Mier, J. G. M. 1992, Experimental and Numerical Analysis of Micromechanisms of Fracture of Cement-Based Composites. *Cem. Concr. Compos.* **1992**, *14*(2), pp. 105–118.
- [9] Tankasala, H.C.; Deshpande, V.S.; Fleck, N.A., Koiter medal paper: crack-tip fields and toughness of two-dimensional elastoplastic lattices. *J. Appl. Mech.* **2015**, *82*(9), p.091004.
- [10] Rade, L.; Westergren, B. *Mathematics Handbook for Science and Engineering. 5th ed, Springer.* **2004**.
- [11] Gradshteyn, I. S.; Ryzhik, I. M.; *Tables of Integrals, Series and Products, 6th ed, Academic Press.* **2000**.
- [12] Tolstov, G. P. *Fourier Series, Prentice-Hall, Inc.* **1962**.
- [13] Shannon, C. E. A mathematical theory of communication. *Bell System Technical Journal.* **1948**, *27*, 379–423.
- [14] Hankerson, D. R.; Harris, G. A.; Johnson, P. D. *Introduction to Information Theory and Data Compression. 2nd edition, CRC Press.* **2003**.
- [15] Vajapeyam, S. Understanding Shannon’s Entropy metric for Information. *arXiv preprint arXiv.* **2014**, 1405.2061.
- [16] Robinson, D. W. Entropy and uncertainty. *Entropy.* **2008**, *10*(4), 493–506
- [17] Lakes, R. Foam Structures with a negative Poisson's ratio. *Science.* *1987*, *235*, 1038-1040.
- [18] Nicolaou, Z. G.; Motter, A. E. Mechanical metamaterials with negative compressibility transitions. *Nature Materials.* **2012**, *11*, 608–613.
- [19] Schenk, M.; Guest, S. D. Geometry of Miura-Folded Metamaterials. *PNAS.* **2013**, *110*, 3276–3281.
- [20] Jiang, J. W.; Park, H. S. Negative Poisson’s ratio in single-layer black phosphorus. *Nature Communications.* **2014**, *5*, 4727.
- [21] Chen, M. L.; Karpov, E. G. Bistability and thermal coupling in elastic metamaterials with negative compressibility. *Physical Review E.* **2014**, *90*, 033201.
- [22] Karpov, E. G.; Danso, L. A.; Klein, J. T. Negative extensibility metamaterials: Occurrence and design space topology. *Physical Review E.* **2017**, *96*, 023002.
- [23] Klein, J. T.; Karpov, E. G. Negative extensibility metamaterials: Phase diagram calculation. *Computational Mechanics.* **2018**, *62*(4), p.669.
- [24] Karpov, E. G. Structural metamaterials with Saint-Venant edge effect reversal. *Acta Materialia.* **2017**, *123*, 245-254.
- [25] Coullais, C.; Sounas, D.; Alu, A. Static non-reciprocity in mechanical metamaterials. *Nature.* **2017**, *542*, 461-464.
- [26] Rafsanjani, A.; Akbarzadeh, A.; Pasini, D. Snapping Mechanical Metamaterials under Tension. *Advanced Materials.* **2015**, *27*, 5931–5935.
- [27] Ekštejn, K.; Pavelka, T. 2004. Entropy and Entropy-based Features In Signal Processing. *In Proceedings of*

PhD Workshop Systems & Control, Balatonfüred. 2004.

[28] Sadd, M. H. *Elasticity: Theory, Applications and Numerics. Elsevier, 2005.*

[29] Shan, S.; Kang, S.; Raney, J. R.; Wang, P.; Fang, L.; Candido, F.; Lewis, J. A.; Bertoldi, K. Multistable architected materials for trapping elastic strain energy. *Advanced Materials. 2015, 27, 4296–4301.*

[30] Karpov, E. G.; Stephen, N. G.; Dorofeev, D. L. On static analysis of finite repetitive structures by discrete Fourier Transform. *International Journal of Solids and Structures. 2002, 39, 4291-4310.*

CHAPTER 4 APPENDIX

A common form of the Parseval's theorem with a scalar function,

$$\int_{-\infty}^{\infty} |f(y)|^2 dy = \frac{1}{2\pi} \int_{-\infty}^{\infty} |\hat{f}(q)|^2 dq \quad (4-A.1)$$

means that information is not lost in the Fourier transform of this function,

$$\hat{f}(q) = \int_{-\infty}^{\infty} f(y) e^{-iqy} dy \quad (4-A.2)$$

Fourier transform properties:

$$f(y) = \frac{1}{2\pi} \int_{-\infty}^{\infty} \hat{f}(q) e^{iqy} dq \quad (4-A.3)$$

$$\int_{-\infty}^{\infty} \partial_y f(y) e^{-iqy} dy = iq \hat{f}(q) \quad (4-A.4)$$

Partial and full Fourier transforms of a function of several variables:

$$\tilde{f}(x, q, z) = \int_{-\infty}^{\infty} f(x, y, z) e^{-iqy} dy \quad (4-A.5)$$

$$\int_{-\infty}^{\infty} \partial_x f(x, y, z) e^{-iqy} dy = \partial_x \tilde{f}(x, q, z) \quad (4-A.6)$$

$$\hat{f}(q_1, q_2, q_3) = \int_V f(x, y, z) e^{-i(q_1x + q_2y + q_3z)} dV \quad (4-A.7)$$

Properties of the Dirac delta function δ (y, q and q_0 are real):

$$\int_{-\infty}^{\infty} e^{iq'y} e^{-iqy} dy = 2\pi \delta(q - q') \quad (4-A.8)$$

$$\int_{-\infty}^{\infty} \delta(q - q') f(q') dq' = f(q) \quad (4-A.9)$$

Variants of the Parseval's theorem of mechanics (4-8) with a general energy density $W(x, y, z)$ and multiple integrals:

$$\int_{-\infty}^{\infty} W(x, y, z) dy = \frac{1}{2\pi} \int_{-\infty}^{\infty} \tilde{W}(x, q, z) dq \quad (4-A.10)$$

$$\int_{-\infty}^{\infty} \int_{-\infty}^{\infty} W(x, y, z) dy dz = \frac{1}{4\pi^2} \int_{-\infty}^{\infty} \int_{-\infty}^{\infty} \tilde{W}(x, q_1, q_2) dq_1 dq_2 \quad (4-A.11)$$

$$\int_V W(x, y, z) dV = \frac{1}{8\pi^3} \int_Q \widehat{W}(q_1, q_2, q_3) dQ \quad (4-A.12)$$

Sign function:

$$\text{sgn}(q) = \begin{cases} 1, & q > 0 \\ 0, & q = 0 \\ -1, & q < 0 \end{cases} \quad (4-A.13)$$

Complementary error function:

$$\text{erfc } z = \frac{2}{\sqrt{\pi}} \int_z^\infty e^{-\alpha^2} d\alpha \quad (4-A.14)$$

Plane stress (σ) and plane strain (ε) constitutive matrices with Young's modulus E and Poisson's ratio ν :

$$\mathbf{E}_\sigma = \frac{E}{1-\nu^2} \begin{bmatrix} 1 & \nu & 0 \\ \nu & 1 & 0 \\ 0 & 0 & \frac{1}{2}(1-\nu) \end{bmatrix} \quad \mathbf{E}_\varepsilon = \frac{E}{(1+\nu)(1-2\nu)} \begin{bmatrix} 1-\nu & \nu & 0 \\ \nu & 1-\nu & 0 \\ 0 & 0 & \frac{1}{2}-\nu \end{bmatrix} \quad (4-A.15)$$

Discrete Fourier transform of a discrete periodic sequence g_m , such that $g_{m+M} = g_m$:

$$\tilde{g}_\mu = \sum_{m=-M/2}^{M/2-1} g_m e^{-i2\pi\mu m/M}, \quad \mu = 0, \pm 1, \dots, \pm M/2 \quad (4-A.16)$$

$$g_m = \frac{1}{M} \sum_{\mu=-M/2}^{M/2-1} \tilde{g}_\mu e^{i2\pi\mu m/M}, \quad m = 0, \pm 1, \dots, \pm M/2 \quad (4-A.17)$$

Discrete Fourier transform of a Kronecker delta:

$$\sum_{m=-M/2}^{M/2-1} \delta_{m0} e^{-i2\pi\mu m/M} = 1 \quad (4-A.18)$$

where

$$\delta_{mm'} = \begin{cases} 1, & m = m' \\ 0, & m \neq m' \end{cases} \quad (4-A.19)$$

5 NONLOCAL MECHANICAL METAMATERIAL

(This chapter is based on a material previously published as Danso, L. A.; Karpov, E.G. Reprogramming Static Deformation Patterns in Mechanical Metamaterials. Materials. 2018, 11, 2050 and Karpov, E. G., Danso, L. A., Klein J.T. Anomalous Strain Energy Transformation Pathways in Mechanical Metamaterials. Proceedings of the Royal Society A. 2019, 2019004.)

5.1 Introduction

Mechanical Metamaterials are controlled materials with preconceived elastic properties that is not seen in natural materials. Earliest example of mechanical metamaterials was the auxetic material with negative Poisson's ratio [1-5]. Other interesting examples are materials with negative stiffness [6-8], reconfigurable origami structures [9-11], negative compressibility materials [12-15], pentamode metamaterials [16-18], topological metamaterial [19-22] and reverse Saint-Venant edge effect lattice materials [23]. These mechanical metamaterials possess extreme functionalities with their performance generally defined by material's response to deformation.

Even though the theory of nonlocality [24] in continuum materials has been exploited in fracture and failure analysis, nonlocality is for the first time studied in lattices [23] to account for the unusual RSV metamaterial behavior and there is a vivid illustration of how material responses such as stress, strain, etc due to mechanical deformation could be reprogrammed in a (1D) degree of freedom non-local lattice material. The presence of badgaps in the deformation decay spectrum of the non-local lattice ensures blockage of a static Raleigh mode of the coinciding wave number and coarse modes decaying faster inside a non-local material than even modes. Expanding this study by Karpov [23] on the reverse Saint Venant edge effect in non-local lattice materials to multiple degrees of freedom and employing principles of the Parseval's theorem [25-27] and entropy [28-31] that were developed fully in Chapter 4 for a mechanics problem, it is possible to fully understand strain energy behavior in these nonlocal materials.

Our interest in non-local lattice material is driven by the potential to program them to exhibit exciting functionalities like static load induced deformation pattern recognition and localization and strain energy redistribution. The geometrical periodicity of a non-local lattice material allows for efficient design and

analysis which is the case for engineered periodic structural systems and extremely reduces production cost and time.

The solution of periodic or repetitive structures presented in earlier studies [32-33] involved using the discrete field analysis method to solve a system of governing equations made up of a set of finite difference equations. The governing system of equations was shown to be rewritable as a compact matrix [34] by applying a discrete convolution operator and using such a matrix form, the discrete Fourier transform (DFT) approach has been useful in developing Green's function solution operators [35] for analyzing lattice structures under arbitrary force boundary conditions. An important application of the Green's function operator solution method is seen in molecular dynamics where they are employed to build interfaces that minimize boundary reflection [36-39].

The transfer matrix method of analyzing the lattice system of governing equations and other approaches have been similarly used to derive lattice response under quasi-static loading [41-43]. On analyzing 1D beam-like structures under self-equilibrated end loads [43], an interesting observation was made that system's solution could be composed of exponential decay of loads and polynomial mode terms that define a structure in tension and bending. On examination, the illustrated exponential decay solution exemplified material's response to forces in continuum mechanics governed by the Saint-Venant principle and that for a discrete mechanics problem, the rate of decay was a function of the transfer matrix eigenvalues.

Lattice metamaterial research has over the past decade gained a great significance due to the advancements in additive manufacturing technology and hence drives the need for analytical and computational methods to effectively model 2D and 3D discrete materials or structures. In [23], a fundamental solution was presented for a discrete system based on a combined approach of the DFT and the transfer matrix methods. The solution typified a static or harmonic surface mode whose amplitude decayed exponential at a rate characteristic of the eigenvalue $\lambda < 1$ of the Fourier parameter $q \in (-\pi, \pi)$ and the deformation inside the material with no mode variance:

$$\mathbf{d}_{nm} = C(q)\mathbf{h}(q)\lambda^n(q)e^{iqm} \quad (5-1)$$

The above fundamental solution also represents a Raleigh wave with material's vertical edge discrete dimension m and horizontal edge discrete dimension n and an arbitrary constant amplitude $C(q)$. The terms $\mathbf{h}(q)$ and $\lambda(q)$ are the polarization vector or half-eigenvector and decay rate or eigenvalue respectively obtained for the lattice for the representative Raleigh wave number or Fourier parameter q . Therefore, the solution \mathbf{d}_{nm} would be composed of both real and imaginary parts of the displacement components that describe the Raleigh wave in the lattice material. The Saint-Venant principle is observed in a discrete elastic medium when the decay rate $\lambda(q)$ has a constant or monotonous increase with increase in the Fourier parameter, q or as the evenness of the Raleigh mode increases. The value of the mean square deformation gradient of the Raleigh mode in the m discrete dimension is q^2 and so equivalently modes of high parameter q are more even with smaller decay rate compared to modes of lower q values which are coarser. In the reverse Saint Venant study in [23], we see an anomalous behavior of the decay rate $\lambda(q)$ for an x-braced discrete nonlocal lattice where modes of high parameter q rather decay faster compared to coarser modes due to the presence of asymptotic bandgaps in the lattice deformation decay spectrum. *The reversal in the decay rates as evenness or Fourier parameter q increases is a metamaterial behavior termed the Reverse Saint-Venant edge effect (RSV).* The asymptotic bandgaps provide a way to detain any static Raleigh mode with the coincident q .

The potential applications of the RSV metamaterial behavior are great if a structured analytical and numerical procedures are developed to understand deformation and strain energy patterns in discrete lattice materials for identifiable boundary conditions seen in practical mechanics problems. This chapter will therefore present a detailed outlook on analyzing a 2D discrete lattice problem. Method of constructing fundamental solutions for a 2D problem would be detailed: formulating a semi-analytical method for both applied essential and natural boundary conditions, a method of reprogramming static deformation and strain energy patterns using a bandgap design map and the case of polarizing structures in the case repeated zero-eigenvalues will be illustrated. Several examples will be presented for the non-local x-braced lattice to explain the RSV effect in 2D discrete lattices including cases where principles of

the strain energy spectral density (SESD) and strain energy spectral entropy (SESE) from chapter 4 are applied to monitor anomalous strain energy behavior.

5.2 Transfer Matrix and Polarization Vectors for A 2D Non-Local Lattices

The displacement transfer matrix formulation would require first writing down the system of governing equations which for a non-local periodic lattice is written compactly using a convolution operator [23, 35] as

$$(\mathbf{k} * \mathbf{d})_{nm} = \sum_{n'm'} \mathbf{k}_{n-n'm-m'} \mathbf{d}_{n'm'} = \mathbf{f}_{nm} \quad (5-2)$$

Where the stiffness kernel \mathbf{k} for is a chosen repetitive part of a periodic lattice called the associate substructure or cell [See Fig. 5.1] that represents all the elastic interactions between the current node (n, m) and neighboring nodes (n', m') . Periodicity of the lattice ensures \mathbf{k} is dependent only on the current and neighbor nodal differences $(n-n', m-m')$ and not requiring separate dependencies in the case of non-periodic lattices. The expression in (5-2) can evaluate the vector of displacements \mathbf{d}_{nm} at any arbitrary node comprising the periodic lattice given the external force vector \mathbf{f}_{nm} on the lattice. For the operator function in (5-2), summation along the n index is allowed for the limits of $n - 1$ to $n + 1$ but range for the m index can be arbitrary.

Assuming a point in a periodic lattice where $n = 0$, the boundary condition \mathbf{d}_{0m} or \mathbf{f}_{0m} is established then it is possible to determine the static deformation configuration inside the lattice material when $n > 0$ by evaluating the displacement solution \mathbf{d}_{nm} of lattice nodal points. When $n > 0$, the governing equation in (5-2) is rewritten as

$$\sum_{n'm'} \mathbf{k}_{n-n'm-m'} \mathbf{d}_{n'm'} = \mathbf{0} \quad (5-3)$$

Performing the n' index summation in (5-3) from -1 to 1 :

$$\sum_{m'} \mathbf{k}_{1m-m'} \mathbf{d}_{n-1 m'} + \mathbf{k}_{0m-m'} \mathbf{d}_{n m'} + \mathbf{k}_{-1m-m'} \mathbf{d}_{n+1 m'} = \mathbf{0} \quad (5-4)$$

A discrete Fourier transform (DFT) of each term in (5-4) over the index m results in

$$\mathbf{K}_1(q) \mathbf{d}_{n-1}(q) + \mathbf{K}_0(q) \mathbf{d}_n(q) + \mathbf{K}_{-1}(q) \mathbf{d}_{n+1}(q) = \mathbf{0} \quad (5-5)$$

$$\mathbf{H}(q) \begin{Bmatrix} \mathbf{d}_{n-1}(q) \\ \mathbf{d}_n(q) \end{Bmatrix} = \begin{Bmatrix} \mathbf{d}_n(q) \\ \mathbf{d}_{n+1}(q) \end{Bmatrix}$$

(5-6)

$$\mathbf{H}(q) = \begin{bmatrix} \mathbf{0} & \mathbf{I} \\ -\mathbf{K}_{-1}(q)^{-1}\mathbf{K}_1(q) & -\mathbf{K}_{-1}(q)^{-1}\mathbf{K}_0(q) \end{bmatrix}$$

The next step is to obtain the eigensystem of $\mathbf{H}(q)$ which are needed to construct fundamental solution in (5-1). Generally, the transfer matrix $\mathbf{H}(q)$ will have the dimension $2R \times 2R$, R denoting the number of degrees of freedom at each nodal point in the periodic lattice and so the number of eigenvalues $\lambda(q)$ will be $2R$. The transfer matrix $\mathbf{H}(q)$ conforms to the nature of a symplectic matrix whose eigenvalues are sets of reciprocal pairs of $\lambda(q)$ and $1/\lambda(q)$ [44-46]. However, only eigenvalues where $|\lambda(q)| \leq 1$ are of interest assures solution (5-1) convergence. It must be noted that eigenvalues could be real or complex valued depending on lattice stiffness properties and also complex eigenvalues are always obtained in conjugate pairs, $\lambda(q) = \mu \pm \omega i$.

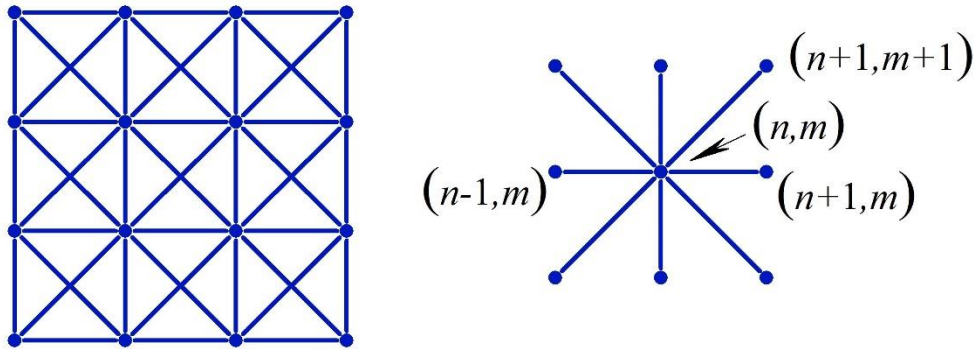


Figure 5.1 A sample model of a periodic x-braced lattice, and its associate substructure

There will be $2R$ corresponding number of eigenvectors and they will have a vector component form

$\begin{Bmatrix} \mathbf{h}(q) \\ \lambda(q)\mathbf{h}(q) \end{Bmatrix}$. Meaning matrices of the form $\mathbf{H}(q)$ have their bottom component of each eigenvector equal to

the top component eigenvector multiplied by the corresponding eigenvalue $\lambda(q)\mathbf{h}(q)$ [23].

For a 2D x-braced periodic nonlocal lattice the displacement transfer matrix $\mathbf{H}(q)$ is a 4×4 matrix given in parametric form as

$$\mathbf{H}(q) = \begin{bmatrix} 0 & 0 & 1 & 0 \\ 0 & 0 & 0 & 1 \\ \beta_1 & \beta_3 i & \beta_4 & \beta_6 i \\ \beta_2 i & \beta_1 & \beta_5 i & \beta_7 \end{bmatrix} \quad (5-7)$$

$$\beta_1 = -\frac{(\sqrt{2} \cos q + k \cos 2q)}{k + \sqrt{2} \cos q}, \quad \beta_2 = \frac{2(\sqrt{2} + k \cos q) \sin q}{k + \sqrt{2} \cos q}, \quad \beta_3 = \frac{k \sin q}{k + \sqrt{2} \cos q}, \quad \beta_4 = \frac{2(\sqrt{2} + k) \cos q}{k + \sqrt{2} \cos q}$$

$$\beta_5 = -\frac{2(\sqrt{2} + k) \sin q}{k + \sqrt{2} \cos q}, \quad \beta_6 = -\frac{2(k - \sqrt{2}(k \cos q - 1)) \sin q}{k + \sqrt{2} \cos q}, \quad \beta_7 = \frac{(2 + k\sqrt{2} - 2 \cos q)(2 + \sqrt{2} k \cos q)}{k + \sqrt{2} \cos q}$$

Here, the relative stiffness parameter k is the ratio of the stiffness of a diagonal bar over the stiffness of a vertical or horizontal bar and q represents the Fourier parameter or Raleigh mode wave number. Applying the

equation $(\mathbf{H}(q) - \lambda \mathbf{I}(q)) \begin{Bmatrix} \mathbf{h}(q) \\ \lambda(q) \mathbf{h}(q) \end{Bmatrix} = \mathbf{0}$ for an eigenvalue problem and solving, the non-zero eigenvector

$\begin{Bmatrix} \mathbf{h}(q) \\ \lambda(q) \mathbf{h}(q) \end{Bmatrix}$ is derived in (See in Appendix 5-A1- 5-A4):

$$\begin{Bmatrix} \mathbf{h}(q) \\ \lambda(q) \mathbf{h}(q) \end{Bmatrix} = C(q) \begin{Bmatrix} i(\beta_3 + \beta_6 \lambda) \\ \lambda^2 - \beta_4 \lambda - \beta_1 \\ i \lambda(\beta_3 + \beta_6 \lambda) \\ \lambda(\lambda^2 - \beta_4 \lambda - \beta_1) \end{Bmatrix} \quad (5-8)$$

Where the constant $C(q)$ is any arbitrary real or complex number that could be varied to achieve a certain boundary effect or polarization vector normalization $|\mathbf{h}(q)| = 1$. Looking at the right-hand side of (5-8), the eigenvector component form $\begin{Bmatrix} \mathbf{h}(q) \\ \lambda(q) \mathbf{h}(q) \end{Bmatrix}$ of $\mathbf{H}(q)$ is shown.

Therefore, a standard polarization vector $\mathbf{h}(q)$ of a given conjugate pair of complex eigenvalues $\lambda(q) = \mu \pm \omega i$ is evaluated by substituting into the top half-vector of (5-8) to get

$$\mathbf{h}(q) = \begin{Bmatrix} a \pm ib \\ -c + id \end{Bmatrix} \quad (5-9)$$

$$a = -\beta_6 \omega, \quad b = (\beta_3 + \beta_6 \mu), \quad c = (-\beta_1 - \beta_4 \mu + \mu^2 - \omega^2), \quad d = (2\mu \omega - \beta_4 \omega)$$

Likewise, for a given real eigenvalue $\lambda(q)$ where $\omega = 0$, we obtain the polarization vector from (5-9) as

$$\mathbf{h}(q) = \begin{Bmatrix} ib \\ c \end{Bmatrix} \quad (5-10)$$

5.3 Constructing A 2D Problem Raleigh Wave Solution

Periodic structures or lattices maintain symmetry of response characteristics about symmetry plane which for the ongoing studies is along the midpoint of index m and solution (5-1) will obey the symmetry rule:

$$\mathbf{d}_{nm} = \begin{Bmatrix} U_{nm} \\ V_{nm} \end{Bmatrix} = \begin{Bmatrix} U_{nm} \\ -V_{nm} \end{Bmatrix} \quad (5-11)$$

Hence, constructing a real-cyclic Raleigh wave solution should meet the conditions in (5-11). For example, to construct the Raleigh mode solution \mathbf{d}_{nm} , $\lambda(q)$ and $\mathbf{h}(q)$ are substituted into (5-1) that results in a complex valued solution where both real and imaginary parts are possible solutions. The part satisfying the symmetry test condition in (5-11) is considered the real-cyclic Raleigh mode solution. In case of a conjugate pair of complex eigenvalues $\lambda(q) = \mu \pm \omega i$, their polar coordinate counterpart $\lambda(q) = \rho e^{i\theta}$ is used to simplify algebraic operations. Here we have a modulus $\rho = |\lambda(q)|$ and an argument $\theta = \text{Arg}(\lambda(q))$. Four possible solutions (2 real and 2 imaginary components) are obtained after substituting the polar form of each eigenvalue into the conjugate pair and corresponding polarization vectors $\mathbf{h}(q)$, but none would satisfy the symmetry test. A real-cyclic solution (5-12) meeting the symmetry test is constructed by summing corresponding real components and imaginary components. The Raleigh mode solutions \mathbf{d}_{nm} constructed for both complex and real eigenvalues are as follows (See in Appendix 5-A5 - 5-A12):

Complex Eigenvalue:

$$\mathbf{h}(q) = \begin{Bmatrix} a \pm ib \\ -c + id \end{Bmatrix}; \quad \mathbf{d}_{nm} = \begin{Bmatrix} C_1 \rho^n(q) \begin{Bmatrix} a \cos qm \\ -d \sin qm \end{Bmatrix} \\ C_1 \rho^n(q) \begin{Bmatrix} b \cos qm \\ c \sin qm \end{Bmatrix} \end{Bmatrix} \quad (5-12)$$

Real Eigenvalue:

$$\mathbf{h}(q) = \begin{Bmatrix} ib \\ c \end{Bmatrix}; \quad \mathbf{d}_{nm} = C_2 \lambda^n(q) \begin{Bmatrix} b \cos qm \\ c \sin qm \end{Bmatrix} \quad (5-13)$$

Therefore, the coefficients a, b, c, d in \mathbf{d}_{nm} of equations (5-12) and (5-13) are the only components of a polarization vector $\mathbf{h}(q)$ that constructs a real-cyclic Raleigh wave solution (5-1)

5.4 Non-Raleigh Wave Solution: Essential Boundary Condition

Since most deformations (impact, Gaussian, triangular etc.) sustained by materials or mechanical components are non-Raleigh wave modes, a semi-analytical approach is presented in this section to deal with such special boundary scenarios. A general solution can be written for an arbitrary essential boundary solution as a summation operation of all possible Raleigh modes (5-1) of q :

$$\mathbf{d}_{nm} = \frac{1}{M} \sum_{q=0}^{M-1} [\mathbf{h}_1(q) \quad \mathbf{h}_2(q)] \begin{bmatrix} \lambda_1(q) & 0 \\ 0 & \lambda_2(q) \end{bmatrix}^n \begin{Bmatrix} C_1(q) \\ C_2(q) \end{Bmatrix} e^{iqm} \quad (5-14)$$

The solution above is written in matrix form so that $[\mathbf{h}_1(q) \quad \mathbf{h}_2(q)]$ is a matrix composed of components of column vectors. In (5-14), $\mathbf{h}(q)$ and $\lambda(q)$ are known from the eigensystem of the lattice transfer matrix except for the Fourier coefficients $C_1(q)$ and $C_2(q)$ which must be determined to analyze a lattice with an imposed arbitrary essential boundary condition \mathbf{d}_{0m} . To do this, we first multiply through solution \mathbf{d}_{0m} from (5-14) at $n = 0$ with $\mathbf{h}_1^*(q')$, representing the normalized conjugate transpose of the polarization vector $\mathbf{h}_1(q)$ and a after a DFT operation on both sides of (5-14):

$$\frac{1}{M} \sum_{m=0}^{M-1} \mathbf{h}_1^*(q') \mathbf{d}_{0m} e^{-iq'm} = \frac{1}{M^2} \sum_{m=0}^{M-1} \sum_{q=0}^{M-1} \{ \mathbf{h}_1^*(q') \mathbf{h}_1(q) \quad \mathbf{h}_1^*(q') \mathbf{h}_2(q) \} \begin{Bmatrix} C_1(q) \\ C_2(q) \end{Bmatrix} e^{iqm} e^{-iq'm} \quad (5-15)$$

Applying summation rules,

$$\sum_{m=0}^{M-1} \mathbf{h}_1^*(q') \mathbf{d}_{0m} e^{-iq'm} = \frac{1}{M} \sum_{q=0}^{M-1} \left(\sum_{m=0}^{M-1} e^{-iq'm} e^{iqm} \right) \{ \mathbf{h}_1^*(q') \mathbf{h}_1(q) \quad \mathbf{h}_1^*(q') \mathbf{h}_2(q) \} \begin{Bmatrix} C_1(q) \\ C_2(q) \end{Bmatrix} \quad (5-16)$$

According to

$$\sum_{m=0}^{M-1} e^{-iq'm} e^{iqm} = M \delta_{qq'} \quad \text{and} \quad \mathbf{h}_1^*(q') \mathbf{h}_1(q) = 1 \quad (5-17)$$

Equation (5-16) is rewritten as

$$\sum_{m=0}^{M-1} \mathbf{h}_1^*(q) \mathbf{d}_{0m} e^{-iqm} = \{ 1 \quad \mathbf{h}_1^*(q) \mathbf{h}_2(q) \} \begin{Bmatrix} C_1(q) \\ C_2(q) \end{Bmatrix} \quad (5-18)$$

Again, the procedure in (5-15 – 5-18) is repeated for $\mathbf{h}_2^*(q')$ to obtain a matrix expression for finding the Fourier coefficients $C_1(q)$ and $C_2(q)$ as

$$\begin{Bmatrix} C_1(q) \\ C_2(q) \end{Bmatrix} = \begin{bmatrix} 1 & \mathbf{h}_2^*(q) \mathbf{h}_1(q) \\ \mathbf{h}_1^*(q) \mathbf{h}_2(q) & 1 \end{bmatrix}^{-1} \begin{bmatrix} \mathbf{h}_1^*(q) \\ \mathbf{h}_2^*(q) \end{bmatrix} \mathbf{d}_0(q) \quad (5-19)$$

Here, $\mathbf{d}_0(q)$ is obtained from the DFT operation of the non-Rayleigh boundary condition as $\sum_{m=0}^{M-1} \mathbf{d}_{0m} e^{-iqm}$.

Hence, a general solution for any static deformation of a periodic lattice under an arbitrary essential boundary condition is found by substituting $C_1(q)$ and $C_2(q)$ into Equation (5-14).

5.5 Non-Raleigh Wave Solution: Natural Boundary Condition

In this section, we develop a semi-analytical methodology for analyzing periodic lattices with a natural or forced boundary condition which is the more ideal case in mechanics. For periodic lattice with a forced condition at $n = 0$, the equilibrium governing equation (5-2) is rewritten in Fourier form as

$$\begin{aligned} \frac{1}{2} \mathbf{K}_0(q) \mathbf{d}_0(q) + \mathbf{K}_{-1}(q) \mathbf{d}_1(q) &= \mathbf{f}_0(q) \\ \mathbf{d}_0(q) = \{C_1(q) \quad C_2(q)\} \begin{Bmatrix} \mathbf{h}_1(q) \\ \mathbf{h}_2(q) \end{Bmatrix}, \quad \mathbf{d}_1(q) = \{C_1(q)\lambda_1(q) \quad C_2(q)\lambda_2(q)\} \begin{Bmatrix} \mathbf{h}_1(q) \\ \mathbf{h}_2(q) \end{Bmatrix} \end{aligned} \quad (5-20)$$

Here, $\mathbf{f}_0(q)$ is obtained from the DFT operation of the natural boundary condition as $\sum_{m=0}^{M-1} \mathbf{f}_{0m} e^{-iqm}$.

Equation (5-20) assumes that the nodal set to left of $n = 0$ where force is applied is non-existent and the term $\frac{1}{2} \mathbf{K}_0(q)$ eliminates stiffness interaction due to that set of nodes. Using the decomposed forms of $\mathbf{d}_0(q)$ and $\mathbf{d}_1(q)$ into (5-20), we solve for the Fourier coefficients $C_1(q)$ and $C_2(q)$:

$$\begin{Bmatrix} C_1(q) \\ C_2(q) \end{Bmatrix} = \left[\frac{1}{2} \mathbf{K}_0(q) \begin{Bmatrix} \mathbf{h}_1(q) \\ \mathbf{h}_2(q) \end{Bmatrix} + \mathbf{K}_{-1}(q) [\mathbf{h}_1(q) \quad \mathbf{h}_2(q)] \begin{bmatrix} \lambda_1(q) & 0 \\ 0 & \lambda_2(q) \end{bmatrix} \right]^{-1} \mathbf{f}_0(q) \quad (5-21)$$

Hence, a general solution for any static deformation of a periodic lattice under an arbitrary natural boundary condition is found by substituting $C_1(q)$ and $C_2(q)$ into (5-14) and adding the term $\mathbf{G}(n) = n \mathbf{K}_{-1}(0)^{-1} \tilde{\mathbf{f}}_0(q)$ that accounts for uniform deformation [43]:

$$\mathbf{d}_{nm} = \frac{1}{M} \sum_{q=0}^{M-1} [\mathbf{h}_1(q) \quad \mathbf{h}_2(q)] \begin{bmatrix} \lambda_1(q) & 0 \\ 0 & \lambda_2(q) \end{bmatrix}^n \begin{Bmatrix} C_1(q) \\ C_2(q) \end{Bmatrix} e^{iqm} + \mathbf{G}(n) \quad (5-22)$$

5.6 Bandgap Design: Raleigh Wave Mode

Since the transfer matrix $\mathbf{H}(q)$ eigensystem of a periodic lattice is dependent on the Fourier parameter q , a relationship plot can be drawn between the q and a decay parameter $\eta(q) = -\log \lambda(q)$ known as the *deformation decay spectrum* [23] that describes the relative rate of decay of static Raleigh mode deformation across all q ranging from $-\pi$ to π . For a usual material the decay parameter $\eta(q)$ decreases with increase in q that corresponds with increase in fineness of a Raleigh mode. In the case of an RSV metamaterial, there exist asymptotic bandgaps (See Fig. 5.4) in the deformation decay spectrum when $\lambda(q) = 0$ leading to the reversal in the decrease in $\eta(q)$ as q increases or growth in fineness of Raleigh mode. Therefore, a

Raleigh mode associated with the Fourier parameter q at the point of the bandgap would be localized when applied at a boundary of a metamaterial lattice because of its zero eigenvalue $\lambda(q) = 0$.

So in this section we present system parametric design maps that would guide in formulating Raleigh mode solutions (5-1) for a Fourier parameter q and would be blocked when applied on the lattice boundary at $n = 0$. In accordance with Vieta's rule where $\det \mathbf{H}(q) = \prod_{i=1}^n \lambda_i(q)$, a zero eigenvalue $\lambda(q) = 0$ exists when $\det \mathbf{H}(q) = 0$. Therefore, to develop system parametric relationship for occasions when bandgaps ($\lambda(q) = 0$) exists for the 2D x-braced periodic lattice, we employ the condition $\det \mathbf{H}(q) = 0$ (A13-14):

$$k + \sqrt{2} \cos q = 0 \quad (5-23)$$

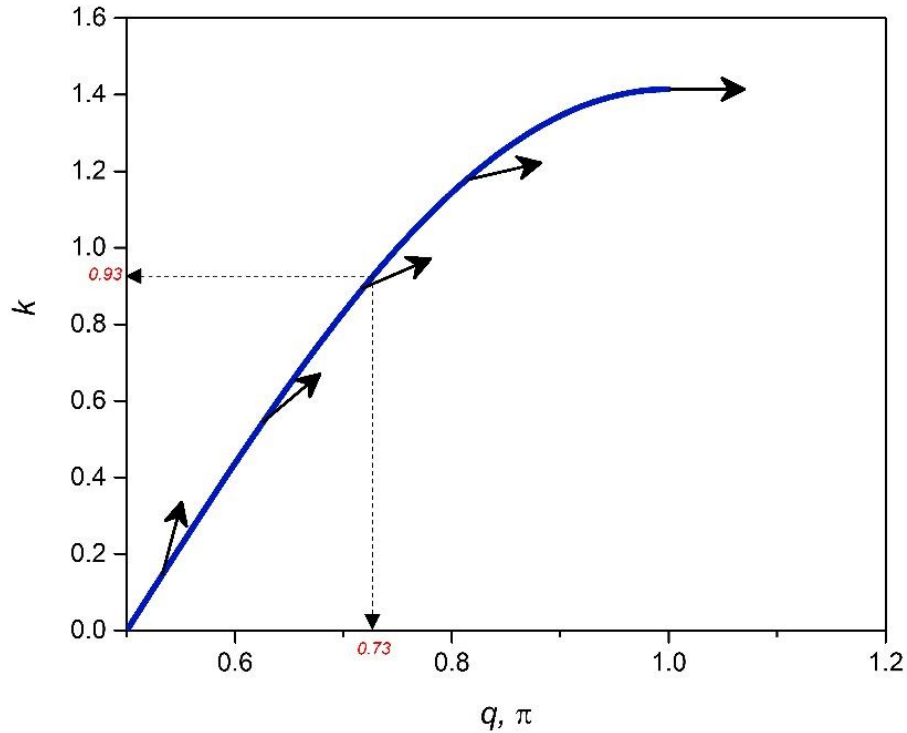


Figure 5.2 Occurrence of zero eigenvalues in the (q, k) -parameter space of Fig.1 lattice. Arrows represent orientation of their corresponding polarization vectors $\mathbf{h}(q)$.

From (5-23), a plot of the relationship between the stiffness parameter k and Fourier q is presented in Fig. 5.2 that gives those tenable q of a Raleigh mode and the k value of the x-braced lattice required to localize or block

the Raleigh mode at $n = 0$. The direction of the polarization vectors $\mathbf{h}(q)$ to construct the Raleigh mode solution to be blocked are shown as the dark arrows in Fig. 5.2.

Alternatively, we can introduce the x-braced unit cell aspect ratio α into the displacement transfer matrix $\mathbf{H}(q)$ as a system parameter and solve for the condition $\det \mathbf{H}(q) = 0$ as

$$2k\alpha^3\sqrt{1+\alpha^2} + \cos q + 2\alpha^2 \cos q + \alpha^4 H \cos q = 0 \quad \alpha = \frac{\text{breadth}}{\text{height}} \quad (5-24)$$

Considering (5-24) to be in equilibrium and using a degenerate point or inflection point condition approach (See Chapters 2 and 3) all the points when the equilibrium of the function in (5-24) is neither maximum or minimum is plotted as the bandgap phase diagram in Fig. 5.3 of the x-braced design parameters α and k .

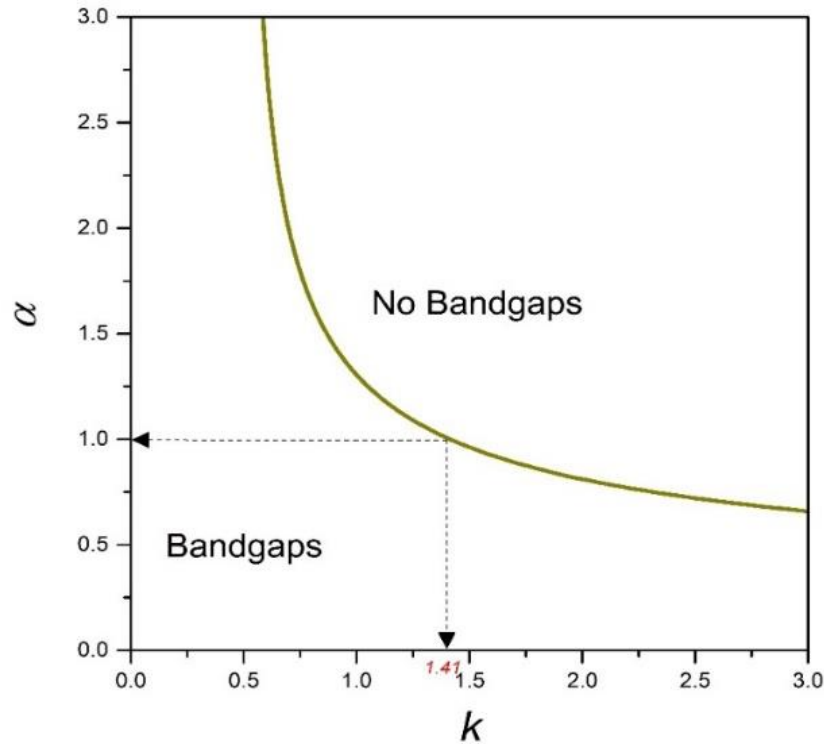


Figure 5.3 A Phase Diagram of the lattice material of Fig. 5.1.

From Fig. 5.3, the ranges and points of transition for the condition of an x-braced lattice when bandgaps exist to the condition of no bandgaps are deduced. For example, the ideal x-braced lattice with $\alpha = 1$ that was

analyzed in (5-23) had its k values for which a bandgap exists to be in the range 0-1.41 (See Fig. 5.2) which is true as seen in Fig. 5.3. Looking at Fig. 5.3, suggestions for bandgap design optimization would be to limit the aspect ratio α within the range 0 - 0.5 and for such a case there is no limitation on the range stiffness parameter values since $k \rightarrow \infty$ for bandgaps exists for an x-braced lattice.

5.7 Periodic Lattice with Repeated Zero Eigenvalues ($\lambda_1 \& \lambda_2 \rightarrow 0$)

In the discussions above, we were concerned with the feature of Raleigh mode blockage at $n = 0$ due to a single zero-eigenvalue $\lambda(q) = 0$ solution (5-1) but there could be instances when a periodic lattice would have deformation decay spectrum with coincident bandgaps ($\lambda_1 \& \lambda_2 \rightarrow 0$) at a Fourier parameter q and that from initial studies according to our exponential decay Raleigh mode solution (5-1) suggests that any polarization vector would be localized at $n = 0$. However, that is not the case for a repeated zero-eigenvalues but rather such periodic lattices behave as *polarizing structures*, converting an arbitrary polarization vector $\hat{\mathbf{h}}(q)$ at $n = 0$ into the required polarization vector $\mathbf{h}(q)$ and subsequently causing deformation block at $n = 1$. Since with a robust numerical search, 2D polarizing structures instead of two produce only a single independent eigenvector $\left\{ \begin{array}{l} \mathbf{h}(q) \\ \lambda(q)\mathbf{h}(q) \end{array} \right\}$ and so the Jordan canonical form [32] of $\mathbf{H}(q)$ is only written as

$$\mathbf{J} = \begin{bmatrix} 0 & 1 \\ 0 & 0 \end{bmatrix} \quad (5-25)$$

The Jordan canonical structure in (5-25) possess two (2) solution modes which are stated below:

$$\mathbf{j}_n^{(1)} = 0^n \mathbf{h} \quad (5-26)$$

$$\mathbf{j}_n^{(2)} = 0^n \mathbf{g} + n0^{n-1} \mathbf{h} \quad (5-27)$$

In the above equations, \mathbf{h} and \mathbf{g} are the independent eigenvector and the generalized eigenvectors respectively for the displacement transfer matrix $\mathbf{H}(q)$. From finite element simulations, we observed that when the appropriate polarization vector $\mathbf{h}(q)$ obtained for the Fourier parameter q at the point of the repeated zero-eigenvalues was applied, the exponential deformation mode in (5-26) controlled static displacements in the periodic lattice and blockage is seen at $n = 0$. For the case of an arbitrary polarization vector $\hat{\mathbf{h}}(q)$, a

combination of the exponential and polynomial mode as in (5-27) controlled static deformation pattern while deformation is localized at $n = 1$. The case of the arbitrary polarization vector $\hat{\mathbf{h}}(\mathbf{q})$, is explained when we consider the second mode in (5-27) at $n = 1$ and $n = 2$:

At $n = 1$,

$$\mathbf{j}_1^{(2)} = 0 \mathbf{g} + \mathbf{h} = \mathbf{h} \quad (5-28)$$

At $n = 2$,

$$\mathbf{j}_2^{(2)} = 0 \mathbf{g} + 2 \times 0 \mathbf{h} = \mathbf{0} \quad (5-29)$$

Hence, polarizing structures can transform an arbitrary polarization vector at $n = 0$ into the desired polarization vector at $n = 1$ (5-28) which localizes the static deformation at this point and that curtails deformation propagation inside the lattice (5-29).

5.8 Strain Energy Density of Periodic Lattices

A study of the anomalous strain energy behavior in a periodic lattice metamaterial using principles of the strain energy spectral density (SESD) and strain energy spectral entropy (SESE) seen in Chapter 4, would require a formulation of the strain energy $W_{n,m}$ at a point in the lattice material. This is done by considering the total strain energy in an associate substructure (See Fig. 5.1) of the periodic lattice which from finite element analysis of a truss system is represented as

$$W = \frac{1}{2} \sum_i \mathbf{d}_i^T \mathbf{K}_i \mathbf{d}_i \quad (5-30)$$

$$\mathbf{K} = \begin{bmatrix} \mathbf{k}_{nm} & -\mathbf{k}_{nm} \\ -\mathbf{k}_{nm} & \mathbf{k}_{nm} \end{bmatrix} \quad \mathbf{d} = \begin{pmatrix} \mathbf{u}_{nm} \\ \mathbf{u}_{n'm'} \end{pmatrix}$$

$$\mathbf{k}_{nm} = \begin{bmatrix} C^2 & CS \\ CS & S^2 \end{bmatrix} \quad C = \text{Cos } \theta \quad S = \text{Sin } \theta$$

Where i is the i th bar in the associate substructure and \mathbf{K} and \mathbf{d} are the i th bar's stiffness matrix and nodal displacements respectively. For an associate substructure, the discrete convolution operator is employed like that used in (5-2) to rewrite and simplify (5-30) resulting in

$$W_{nm} = \frac{1}{2} \sum_{n'm'} (\mathbf{u}_{n'm'}^* - \mathbf{u}_{nm}^*) \mathbf{k}_{n-n'm-m'} (\mathbf{u}_{n'm'} - \mathbf{u}_{nm}) \quad (5-31)$$

Expanding the expression in (5-31) and simplifying further we obtain the final strain energy form at a point in a lattice as

$$W_{nm} = \frac{1}{2} \sum_{n'm'} \mathbf{u}_{n'm'}^* \mathbf{k}_{n-n'm-m'} \mathbf{u}_{n'm'} \quad (5-32)$$

The strain energy density formulation obtained in equation (5-32) therefore defines the strain energy contained in the associate substructure of any nonlocal lattice. The sum of these localized strain energies across the spatial index m is the internal strain energy or volumetric strain energy at the spatial index n :

$$\sum_m W_{nm} = \frac{1}{2} \sum_m \sum_{n'm'} \mathbf{u}_{n'm'}^* \mathbf{k}_{n-n'm-m'} \mathbf{u}_{n'm'} \quad (5-33)$$

Having developed an expression for the volumetric strain energy at the index n , we can proceed to find the relationship between the strain energy and the spectral strain energy at a point in a lattice termed the mechanics analogue of the Parseval theorem (See Chapter 4). Rewriting (5-33) in an alternative form we obtain

$$\sum_m W_{nm} = \frac{1}{2} \sum_m \sum_{n'm'} \mathbf{u}_{n-n'm-m'}^* \mathbf{k}_{n'm'} \mathbf{u}_{n-n'm-m'} \quad (5-34)$$

Expressing $\mathbf{u}_{n-n'm-m'}$ and $\mathbf{u}_{n-n'm-m'}^*$ in (5-34) using inverse discrete Fourier transform (IDFT) of their Fourier forms and substituting back into (5-34):

$$\sum_m W_{nm} = \frac{1}{2} \sum_m \sum_{n'm'} \left(\frac{1}{M} \sum_{q_1} \tilde{u}(q)_{n-n'}^* e^{-iq_1 m - m'} \right) k_{n'm'} \left(\frac{1}{M} \sum_{q_2} \tilde{u}(q)_{n-n'} e^{-iq_2 m m'} \right) \quad (5-35)$$

$$m = 0, \pm 1, \dots, \pm M/2 \quad q_\mu = \frac{2\pi\mu}{M}, \quad \mu = 0, \pm 1, \dots, \pm M/2$$

Equation (5-35) above can be reconstructed to satisfy summation rules as

$$\sum_m W_{nm} = \frac{1}{2M^2} \sum_{n'm'} \sum_{q_1} \sum_{q_2} \left(\sum_m e^{-iq_1 m} e^{iq_2 m} \right) \tilde{u}(q)_{n-n'}^* e^{iq_1 m'} k_{n'm'} \tilde{u}(q)_{n-n'} e^{-iq_2 m'} \quad (5-36)$$

Since $\sum_m e^{-iq_1 m} e^{iq_2 m} = M \delta_{q_1 q_2}$, equation (5-36) simplifies to

$$\sum_m W_{nm} = \frac{1}{2M} \sum_{n'm'} \sum_{q_1} \sum_{q_2} \delta_{q_1 q_2} \tilde{u}(q)_{n-n'}^* e^{iq_1 m'} k_{n'm'} \tilde{u}(q)_{n-n'} e^{-iq_2 m'} \quad (5-37)$$

The Kronecker delta function $\delta_{q_1 q_2}$ then reduces (5-37) into

$$\sum_m W_{nm} = \frac{1}{2M} \sum_q \sum_{n'} \tilde{u}(q)_{n-n'}^* (\sum_{m'} k_{n'm'}) \tilde{u}(q)_{n-n'} \quad (5-38)$$

However, $\sum_{m'} k_{n'm'}$ represents the DFT of $k_{n',m'}$ when $q = 0$ ($\tilde{k}(0)_{n-n'}$) therefore the total strain energy at index n (5-32) can be completely written in spectral form as

$$\sum_m W_{nm} = \frac{1}{2M} \sum_q \sum_{n'} \tilde{u}(q)_{n-n'}^* \tilde{k}(0)_{n'} \tilde{u}(q)_{n-n'} \quad (5-39)$$

An alternative form of (5-39) is written by redefining summation indices:

$$\sum_m W_{nm} = \frac{1}{M} \sum_q \frac{1}{2} \sum_{n'} \tilde{u}(q)_{n-n'}^* \tilde{k}(0)_{n-n'} \tilde{u}(q)_n \quad (5-40)$$

The expression in (5-40) is significant in the sense that it justifies the Parseval's theorem for periodic lattice systems where summation of strain energy in spatial domain, $\sum_m W_{nm}$ is equal to summation of strain energy in Fourier domain, $\frac{1}{M} \sum_q \tilde{W}_{nq}$:

$$\sum_m W_{nm} = \frac{1}{M} \sum_q \tilde{W}_{nq} \quad (5-41)$$

$$W_{nm} = \frac{1}{2} \sum_{n'm'} \mathbf{u}_{n'm'}^* \mathbf{k}_{n-n' m-m'} \mathbf{u}_{n'm'}$$

$$\tilde{W}_{nq} = \frac{1}{2} \sum_{n'} \tilde{u}(q)_{n-n'}^* \cdot \tilde{k}(0)_{n-n'} \cdot \tilde{u}(q)_n$$

Where W_{nq} represents the spectral strain energy at a point in a periodic lattice analogous to the strain energy spectral density (SESD) term seen in Chapter 4. The spectral strain energy \tilde{W}_{nq} would help us to monitor strain energy transformation in a periodic lattice as well as calculate the spectral entropy of deformation, approaches as seen for continuum materials are necessary to fully understand the behavior and potential of mechanical metamaterials. Therefore, using the spectral strain energy at a point in a periodic lattice \tilde{W}_{nq} , the spectral entropy of deformation for a periodic lattice can be calculated from the discrete or numerical strain energy spectral entropy $h(\mathbf{x})$ expressions developed in Chapter 4 after replacing the x variable with the spatial index n as follows:

$$h(n) = -\frac{1}{\ln M} \sum_{\mu=-M/2}^{M/2-1} p_{\mu}(n) \ln p_{\mu}(n) \quad (5-42)$$

$$\tilde{w}(n, q_{\mu}) = \frac{\tilde{W}_{nq}}{\sum_q \tilde{W}_{nq}} \quad p_{\mu}(n) = \tilde{w}(n, q_{\mu})$$

5.9 Illustrative Examples

We start by constructing a Raleigh mode solution for both real and complex eigenvalues for a 2D periodic x-braced lattice with a stiffness parameter $k = 0.93$ and Raleigh mode decay rates defined the deformation decay spectrum shown in Fig. 5.4. Considering a Fourier parameter $q = \frac{4}{5}\pi$, the displacement transfer matrix $\mathbf{H}(q)$ generates the real eigenvalues, $\lambda_1 = 0.10$ and $\lambda_2 = -0.06$ and their associated eigenvectors are $\mathbf{h}_1 = \begin{Bmatrix} 0.9335 \\ -0.3442i \end{Bmatrix}$ and $\mathbf{h}_2 = \begin{Bmatrix} 0.4870i \\ 0.8710 \end{Bmatrix}$ that constructs real-valued cyclic solutions (5-13) as follows:

$$\mathbf{d}_{nm}^{(1)} = C_2 \lambda_1^n(q) \begin{Bmatrix} b \cos qm \\ -c \sin qm \end{Bmatrix} = 0.10^n \begin{Bmatrix} 0.9335 \cos \frac{4}{5}\pi m \\ 0.3442 \sin \frac{4}{5}\pi m \end{Bmatrix} \quad (5-43)$$

$$\mathbf{d}_{nm}^{(2)} = C_2 \lambda_2^n(q) \begin{Bmatrix} b \cos qm \\ c \sin qm \end{Bmatrix} = (-0.06)^n \begin{Bmatrix} 0.4870 \cos \frac{4}{5}\pi m \\ 0.8710 \sin \frac{4}{5}\pi m \end{Bmatrix} \quad (5-44)$$

The solutions in (43-44) are presented in Fig. 5.5 for an x-braced lattice with spatial lengths of $M = 10$ for the index m and $N = 4$ along index n . Next, we assume a Fourier parameter $q = \frac{1}{5}\pi$ for the stiffness parameter $k = 0.93$ and so obtain a conjugate pair of complex eigenvalues $\lambda = 0.5439 \pm 0.1425i$ and their conjugate eigenvectors $\mathbf{h} = \begin{Bmatrix} 0.7537 \pm 0.4554i \\ -0.8903 - 0.6572i \end{Bmatrix}$ to construct the featured real-cyclic solution (5-12) in the following:

$$\mathbf{d}_{nm}^{(1)} = C \rho^n(q) \begin{Bmatrix} a \cos qm \\ -d \sin qm \end{Bmatrix} = 0.32^n \begin{Bmatrix} 0.7537 \cos \frac{1}{5}\pi m \\ 0.6572 \sin \frac{1}{5}\pi m \end{Bmatrix} \quad (5-45)$$

$$\mathbf{d}_{nm}^{(2)} = C \rho^n(q) \begin{Bmatrix} b \cos qm \\ c \sin qm \end{Bmatrix} = 0.32^n \begin{Bmatrix} 0.4554 \cos \frac{1}{5}\pi m \\ -0.8903 \sin \frac{1}{5}\pi m \end{Bmatrix} \quad (5-46)$$

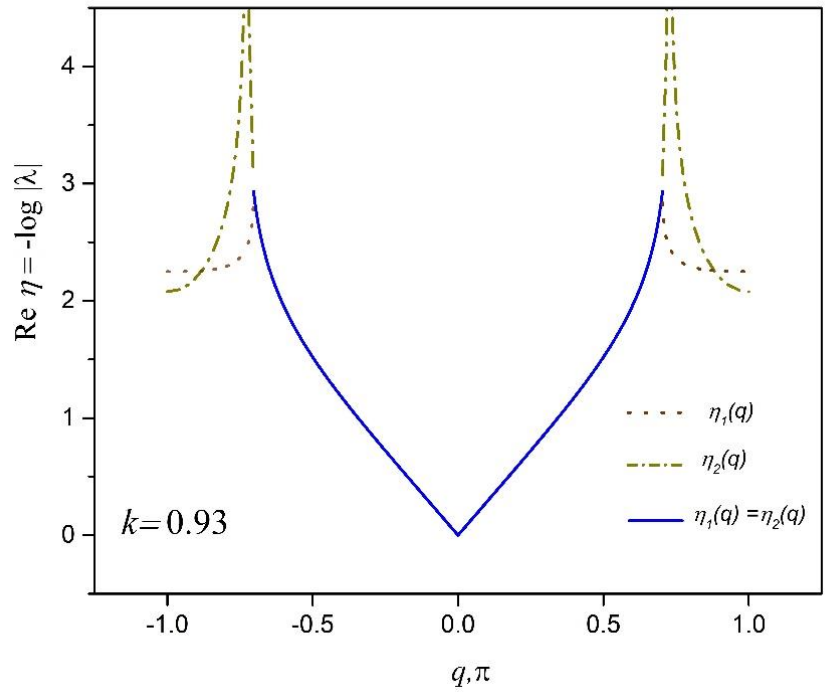


Figure 5.4 Deformation decay spectrum for an x-braced lattice (Fig.1) at $k = 0.93$

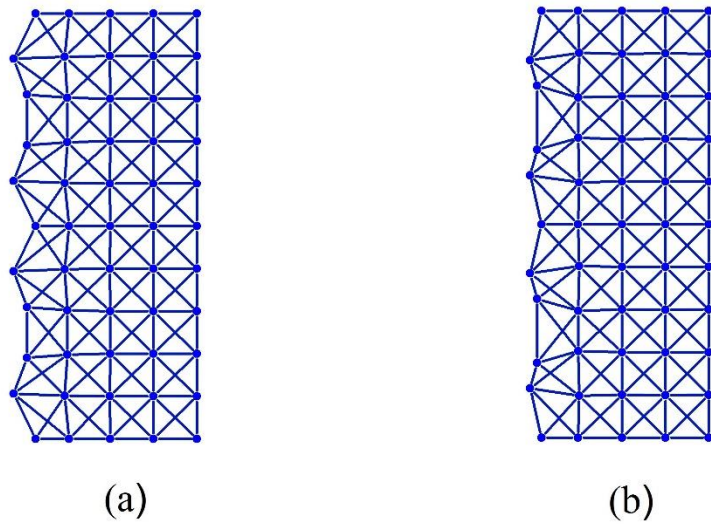


Figure 5.5 Deformation configuration (scaled) of 2DoF x-braced lattice ($k = 0.93$, $q = \frac{4}{5}\pi$, $m = 0 \rightarrow 10$, $n = 0 \rightarrow 4$) given by the analytical solutions (5-43) and (5-44) in (a) and (b) respectively.

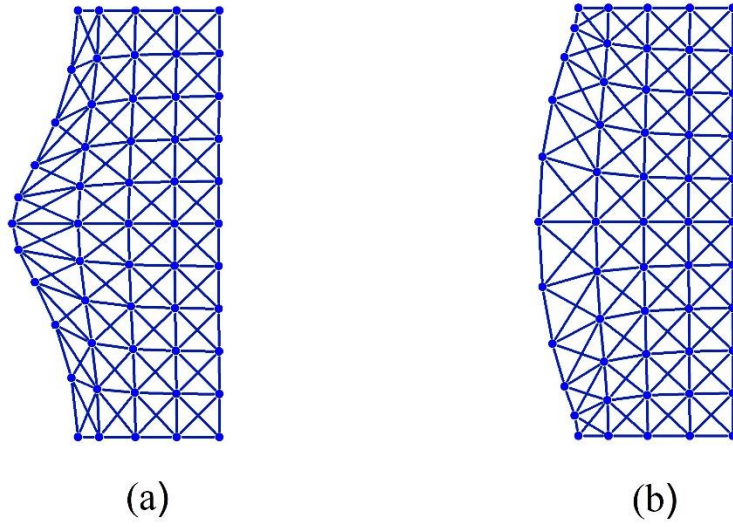


Figure 5.6 Deformation configuration (scaled) of 2DoF x-braced lattice ($k = 0.93$, $q = \frac{1}{5}\pi$, $m = 0 \rightarrow 10$, $n = 0 \rightarrow 4$) given by the analytical solutions (5-45) and (5-46) in (a) and (b) respectively.

The solutions in (5-45 – 5-46) are presented in Fig. 5.6 for the x-braced lattice spatial lengths of $M = 10$ for the index m and $N = 4$ along index n .

Now we will demonstrate the Raleigh mode blockage or localization and the RSV effect in a periodic x-braced lattice by considering the deformation decay spectrum in Fig. 5.4 when the Fourier parameter $q = \frac{8\pi}{11} \approx 0.73$ coincides with the bandgap and the Fourier parameters $q = \frac{9\pi}{11}$ and $q = \frac{10\pi}{11}$ are represented on the reverse decay branches after the bandgap. The Raleigh mode solutions of the three cases are as follows:

$$q = \frac{8\pi}{11}: \quad \mathbf{d}_{nm} = 0.0015^n \begin{pmatrix} 0.6609 \cos \frac{8}{11}\pi m \\ 0.7504 \sin \frac{8}{11}\pi m \end{pmatrix} \quad (5-47)$$

$$q = \frac{9\pi}{11}: \quad \mathbf{d}_{nm} = -0.0756^n \begin{pmatrix} 0.4495 \cos \frac{9}{11}\pi m \\ 0.8901 \sin \frac{9}{11}\pi m \end{pmatrix} \quad (5-48)$$

$$q = \frac{10\pi}{11}: \quad \mathbf{d}_{nm} = 0.1039^n \begin{pmatrix} 0.9823 \cos \frac{10}{11}\pi m \\ 0.1524 \sin \frac{10}{11}\pi m \end{pmatrix} \quad (5-49)$$

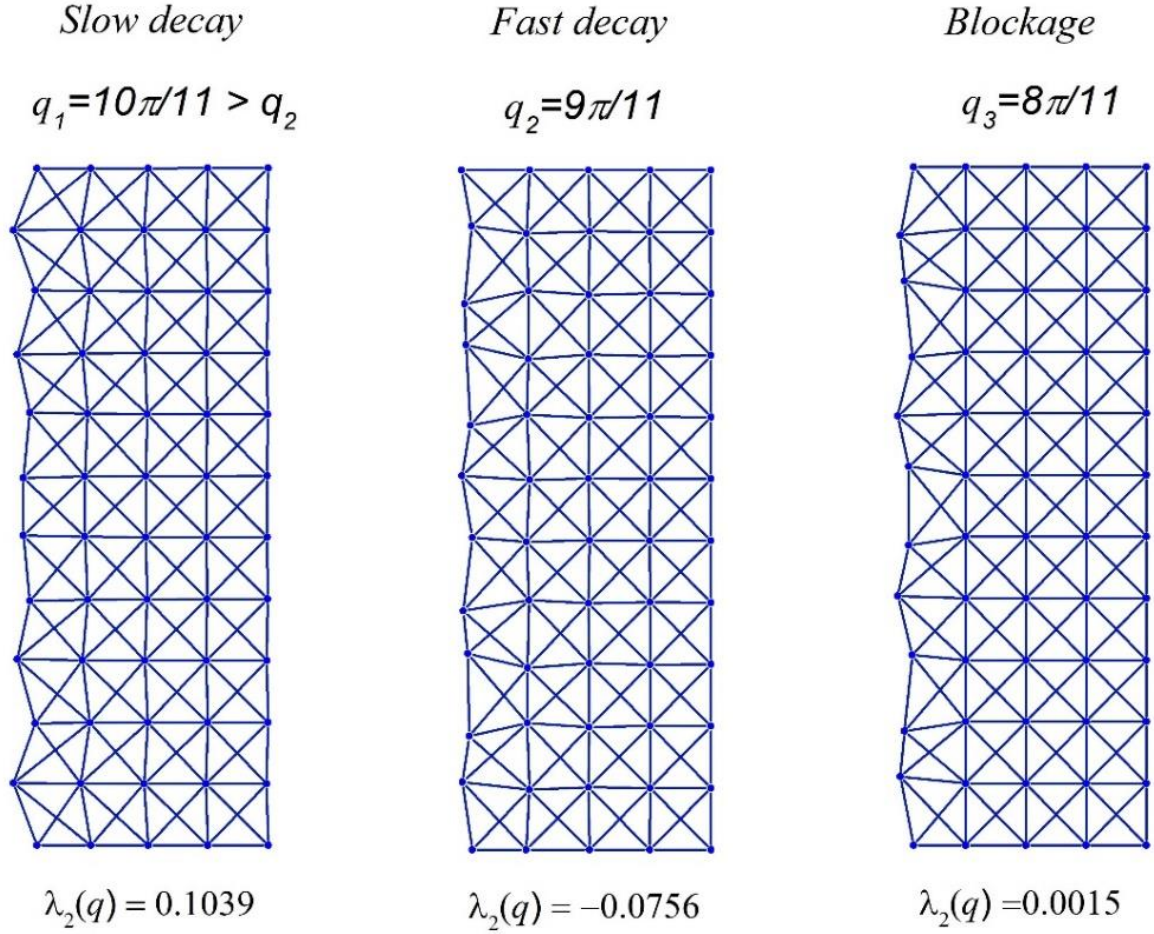


Figure 5.7 Deformation configuration (scaled) of the analytical solutions (5-47), (5-48) and (5-49) respectively for half-cyclic domain of an x-braced lattice ($k = 0.93$, $m = 0 \rightarrow 11$, $n = 0 \rightarrow 4$).

The solutions in (5-47 – 5-49) are presented in Fig. 5.7 for the x-braced lattice spatial length of $M = 22$ for the index m and $N = 4$ along the index n . Fig. 5.7 confirms that blockage of the Raleigh mode due to the zero-eigenvalue at $q = \frac{8\pi}{11}$ and the RSV effect in the Raleigh mode solutions corresponding to the Fourier parameters $q = \frac{9\pi}{11}$ and $q = \frac{10\pi}{11}$. For a coarser mode at $q = \frac{9\pi}{11}$, we see in Fig. 5.7 a faster decay due to a decline in the $\eta(q)$ values (See Fig. 5.4) and for a finer mode at $q = \frac{10\pi}{11}$ we observe a slower decay and so these reverse mode effects establish the x-braced lattice as a RSV metamaterial.

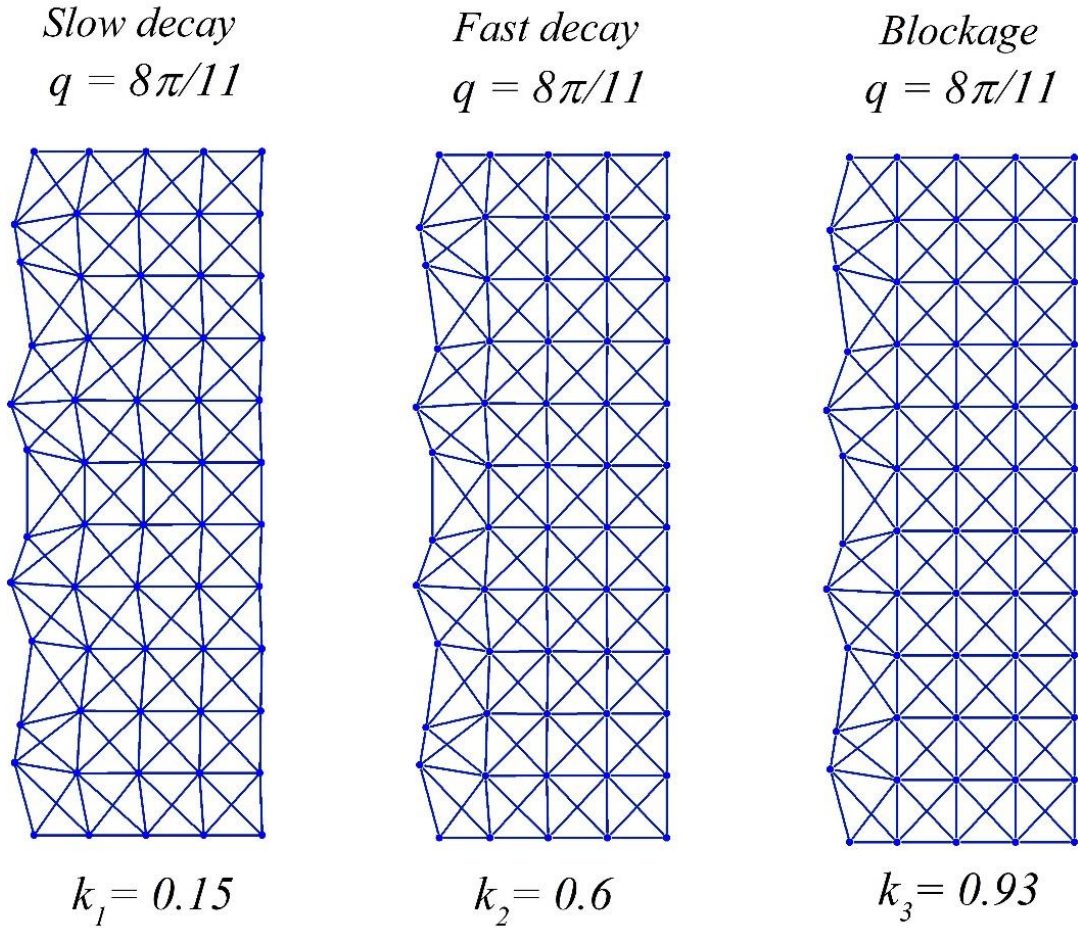


Figure 5.8 Deformation configurations (scaled) of different stiffness parameters under a Raleigh mode solution for $q = \frac{8\pi}{11}$ in a half-cyclic domain of the x-braced lattice ($m = 0 \rightarrow 11, n = 0 \rightarrow 4$).

An example of the Raleigh mode deformation programming is also presented in Fig. 5.8 by considering different stiffness parameters k and applying the same Raleigh mode at $q = \frac{8\pi}{11}$. On tuning k from 0.15 – 0.93, we see a gradual decrease in the decay rate of the Raleigh mode till the complete blockage when $k = 0.93$ which the relative stiffness required for bandgap to exist at $q = \frac{8\pi}{11}$.

In Fig. 5.9, we show a plot of the volumetric strain energy $\sum_m W_{nm}$ (5-33) along the lattice index n for the example seen in Fig. 5.7.

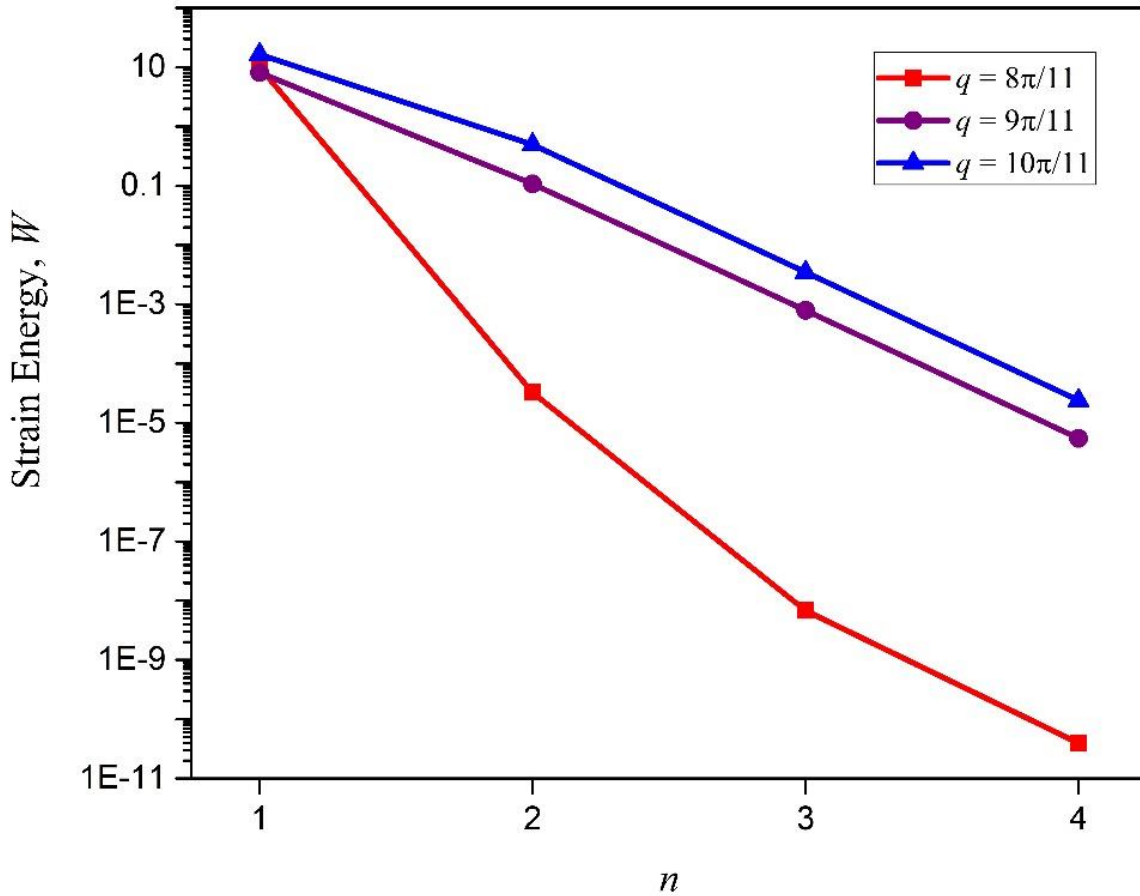


Figure 5.9 Strain Energy along index n in an x-braced lattice with $k = 0.93$: The fastest total strain energy decay occurs at $q = \frac{8}{11}\pi$, followed by $q = \frac{9}{11}\pi$ and then $q = \frac{10}{11}\pi$ due to the RSV.

Since the strain energy (5-32) is dependent on the amount of static deformation, Fig. 5.9 shows a decay in volumetric strain energy corresponding to that shown in Fig. 5.7 where the high drop in energy of Raleigh mode of $q = \frac{8\pi}{11}$ is related to its fast decay because of the associated zero-eigenvalue ($\lambda = 0$) and the slow decay in Raleigh mode of $q = \frac{10\pi}{11}$ sustaining the highest strain energy due to the reversal in the decay rate pattern (RSV). To give a comprehensive illustration of the RSV and how it impacts strain energy decay, a plot of volumetric strain energies along index n is normalized with the volumetric strain at $n = 1$ for an x-braced lattice dimensioned as those in Fig. 5.7 for all possible Raleigh modes is shown in Fig. 5.10. The figure shows that as we increase the Fourier parameter q of the Raleigh mode there is increase in the rate of decay of relative

strain energy, depicted by the increase in slope of curves for each index n until the Raleigh for $q = \frac{8\pi}{11}$ which manifests the lowest values in relative strain energies due to the associated zero-eigenvalue ($\lambda = 0$). The presence of the bandgap at $q = \frac{8\pi}{11}$ reverses the order of decay rate such that we begin to see an increase in values of the relative strain energies and that explains RSV behavior in the x-braced lattice.

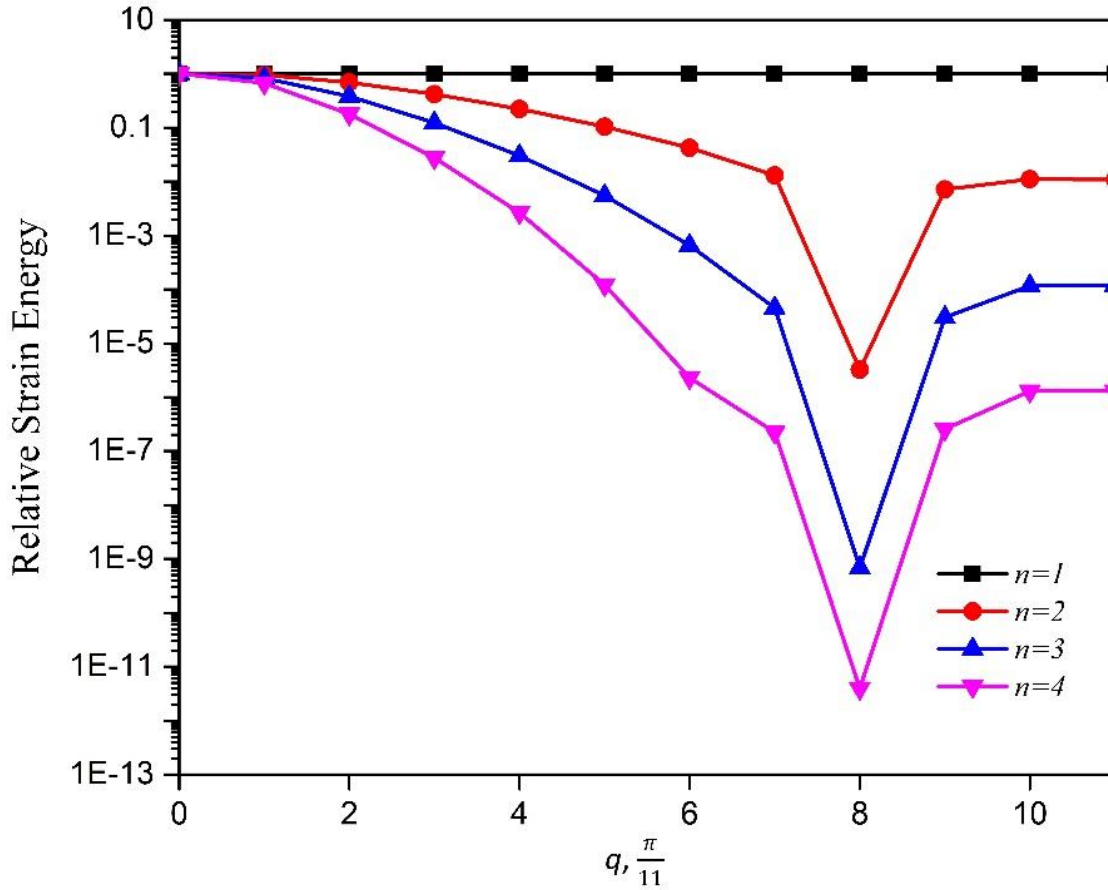


Figure 5.10 Relative Strain Energy against Fourier parameter q . A plot of strain energy at n relative to strain energy at $n = 1$ against the Fourier parameter q .

To conclude the examples on 2D x-braced lattices under static Raleigh modes, we illustrate the behavior of polarizing lattice structures detailed in Section 5.7. Two x-braced lattices of equal spatial length of $M = 20$ for the index m and $N = 4$ along the index n having different stiffness parameters of $k = 0.4714$ and $k = 1.0834$ are analyzed. The deformation decay spectrum for the two lattices are presented in Fig. 5.11 which shows that

at the Fourier parameter $q = \frac{7}{9}\pi$ there exist no zero-eigenvalue ($\lambda_1 > 0$ and $\lambda_2 < 0$) for $k = 0.4714$ while we find repeated zero-eigenvalues ($\lambda_1 \approx 0$ and $\lambda_2 \approx 0$) for $k = 1.0834$. At this instance, if we desired to build a Raleigh mode solution (5-1) that would be arrested at $n = 0$ for $k = 1.0834$, the required polarization vector $\mathbf{h} = \begin{Bmatrix} 0.7677 \\ 0.6408 \end{Bmatrix}$ corresponding to the repeated zero-eigenvalues must apply but we rather apply an arbitrary vector $\hat{\mathbf{h}} = \begin{Bmatrix} 0.5139 \\ 0.8579 \end{Bmatrix}$ to the two x-braced lattices. In Fig. 5.12, we see deformation propagating in the deformation for the case of $k = 0.4714$ since its eigenvalues are not zero and localization of deformation at $n = 1$ for the case $k = 1.0834$ which distinguishes it as a polarizing periodic lattice structure just as detailed earlier. Further analysis of displacements in the polarizing lattice $n = 1$ juxtaposed with the Raleigh mode solution in (5-1) reveal the true polarization vector \mathbf{h} concurring with the definition in Section 5.7.

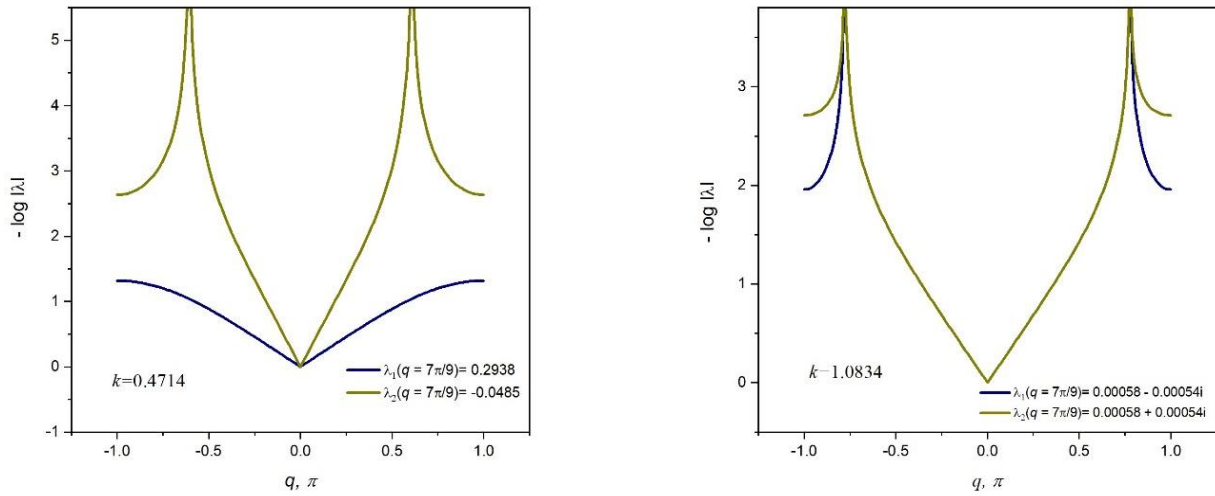


Figure 5.11 Deformation decay spectrum for $k = 0.4714$ and $k = 1.0834$ respectively

To complete the set of examples, we study the distribution of volumetric strain energy, spectral strain energy and strain energy spectral entropy in a periodic lattice compared to an L -periodic approximation of a continuum material under a Gaussian load by applying a point load $\mathbf{f}_{0m} = \begin{Bmatrix} 1 \\ 0 \end{Bmatrix} \delta_{m0}$ at the midpoint of an x-braced lattice. Three x-braced lattices $k = 0.5$, $k = 1.1$ and $k = 9$ are analyzed having spatial lengths of $M = 144$ in the index

m direction and $N = M$ along index n direction. The deformation decay spectrums for the three x-braced designs and the continuum are presented in Fig. 5.13.

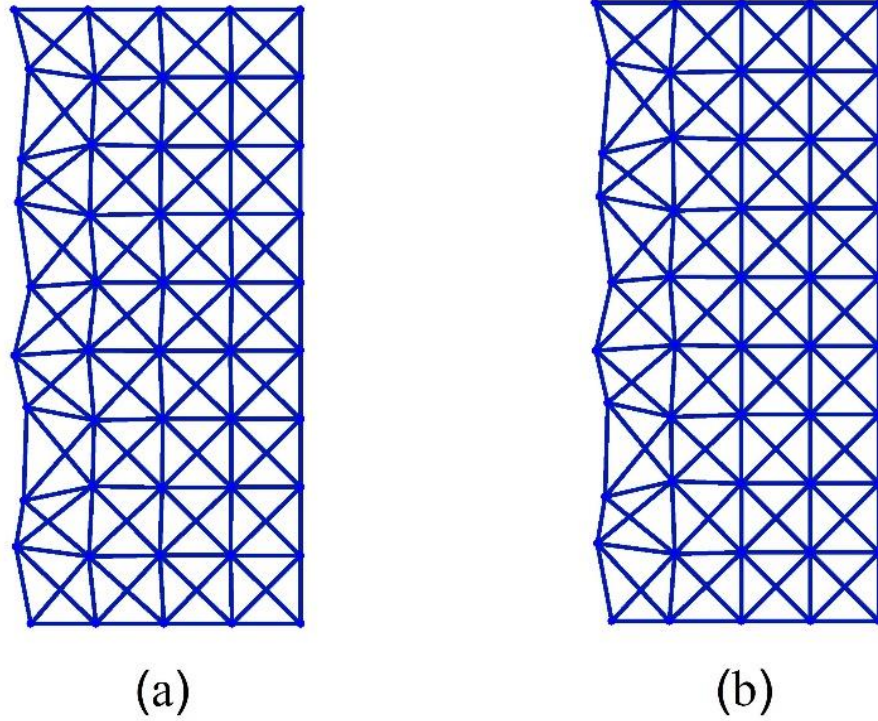


Figure 5.12 Deformation configurations (scaled) for a half-cyclic domain of the x-braced lattice ($m = 0 \rightarrow 9$, $n = 0 \rightarrow 4$) at $k = 0.4714$ (a), and $k = 1.0834$ (b).

The displacement solutions for the described natural boundary condition for the x-braced lattices are obtained from equations (5-20 – 5-22) and their normalized strain energy $w_{nm} = W_{nm} / \sum_m W_{nm}$ distribution (See Fig. 5.14b - d), normalized spectral strain energy $w_{nm} = W_{nq} / \frac{1}{M} \sum_q W_{nq}$ distribution (See Fig. 15b-d) and the strain energy spectral entropy $h(n)$ are calculated from equations (5-41 – 5-42) (See Fig. 5.16). In case of the continuum, the normalized volumetric and spectral energy density distributions (See Fig. 5.14a - 5.15a) and spectral entropy (See Fig. 5.16) are calculated from the L -periodic forced boundary approximations below derived in Chapter 4:

$$w_L(x, y) = \frac{(e^{4\pi x/L} - 1)/L}{1 + e^{4\pi x/L} - 2e^{4\pi x/L} \cos 2\pi x/L} \quad (5-50)$$

$$\tilde{w}_L(x, \mu) = \frac{(2 - \delta_{\mu 0})x e^{-2|\mu|x}}{2 \coth 2\pi x/L - 1} \quad (5-51)$$

$$S_L(x) = -\frac{4 \ln 2}{3 + e^{4\pi x/L}} + \ln(2 \coth 2\pi x/L - 1) + \frac{8\pi x/L}{1 - \cosh 4\pi x/L + 2 \sinh 4\pi x/L} \quad (5-52)$$

From Fig. 5.13 and Fig. 5.14, we observe that the spectral strain energy distributions are controlled by the deformation decay spectrum and therefore determine the contribution of each Raleigh wave in the distribution of volumetric strain energies in a material. The continuum material having the decay relationship $Re \eta(q) = |q|$ (Fig. 5.13a) ensure the Saint Venant effect in its spectral energy distribution (Fig. 5.14a) decay pattern since the contribution of the higher Raleigh wave numbers diminish faster compared to lower wave numbers as you move inside the material. The x-braced lattice with $k = 0.5$ has its spectral energy distribution decay pattern following the lower branch of its decay spectrum (Fig. 5.13b) without a bandgap and so we also see the Saint-Venant effect in the spectral distribution (Fig. 5.14b) but the decay rate is significantly lower for each Raleigh wave number compared to the continuum case since the decay parameters $Re \eta(q)$ of the lower branch are comparatively low. However, the deformation decay spectrum (Fig. 5.13c) for $k = 1.1$ shows a band gap in both branches at approximately $q = \pm 1.93$ with the decay pattern controlled by the lower branch. The continuum behavior is observed in the spectral distribution (Fig. 5.14c) for the Raleigh wave numbers to the point of the Raleigh wave number $q = \pm 1.93$ associated with the bandgap, after which the spectral strain energy contribution of the immediate wave numbers decay faster while the farer wave numbers decay slower corresponding to the RSV effect. The last x-braced lattice having $k = 9.0$ shows both branches coinciding into a single decay branch (Fig. 5.13d) like the wedge-shaped decay branch (Fig. 5.13a) of the continuum. Its spectral strain energy distribution follows a similar decay pattern but shows a slower decay rate across the wave numbers since the decay parameters $Re \eta(q)$ are relatively low.

In Fig. 5.15(a-c), the normalized spatial strain energy spectrums show energies decaying faster inside the continuum material in a concentric curves pattern compared to the two x-braced lattices ($k = 0.5$ & $k = 1.1$) as a result of the faster decaying wave numbers in the continuum material. The spatial energies in x-braced

lattice $k = 1.1$ decay faster since an entire wave number $q = \pm 2.5$ has no contribution in the energy formulation and its decay parameters $Re \eta(q)$ values are higher than that of $k = 0.5$. However, the last x-braced lattice with $k = 9.0$ even though its decay spectrum and spectral strain distribution is wedge shaped like the continuum material (Fig. 5.13d-5.14d) shows a rather anomalous strain energy distribution behavior by bifurcating the high strain energies at the neighborhood of the applied load along a 45° direction and localizing at the edges halfway into the lattice material (Fig. 5.15d). This behavior is attributed to the distribution of the imaginary part of the decay parameters $Im \eta(q) = -Arg \lambda(q)$ which accounts for phase shifts in elastic deformation at point in the lattice material. In the continuum material, $Im \eta(q) = 0$ (Fig. 5.13a) and therefore no shift in strain energies can be expected. For the x-braced lattice with $k = 9.0$, the imaginary part of the decay parameter has a distribution where $Im \eta(q) = Arg \lambda_2(q) = -Arg \lambda_1(q)$ (Fig. 5.13d) since all its eigenvalues are complex conjugates pairs and therefore ensures a symmetric shifting of maximal strain energies along the lattice vertical axis. The energy shifting behavior allows for a safe zone region close to the middle of the lattice to be created with very low spatial strain energies. The unusual energy distribution behavior introduces an interesting metamaterial behavior of an x-braced lattice significant for shielding and structure integrity applications.

Another minor feature noticeable by comparing spatial strain energy distribution of the x-braced lattices to the continuum are the bursts of very low energies (blue tones) along symmetric contour sleeves within the range of $0 - 0.25 n.a/L$.

The exponential decaying spectral entropy curve (dark color) in Fig. 5.16 confirm the fast decaying spatial strain energy in the continuum material which drifts away from the entropy of the x-braced lattices that have slower decaying strain energies due to the characteristic behaviors of their decay spectrums. We also observe in Fig. 5.16 that entropy behavior of x-braced lattices may be non-monotonic such as a decreasing entropy may show local maxima along the material axis which is clearly seen in the entropy of the x-braced lattice ($k = 9.0$) with energy deflection or rerouting metamaterial.

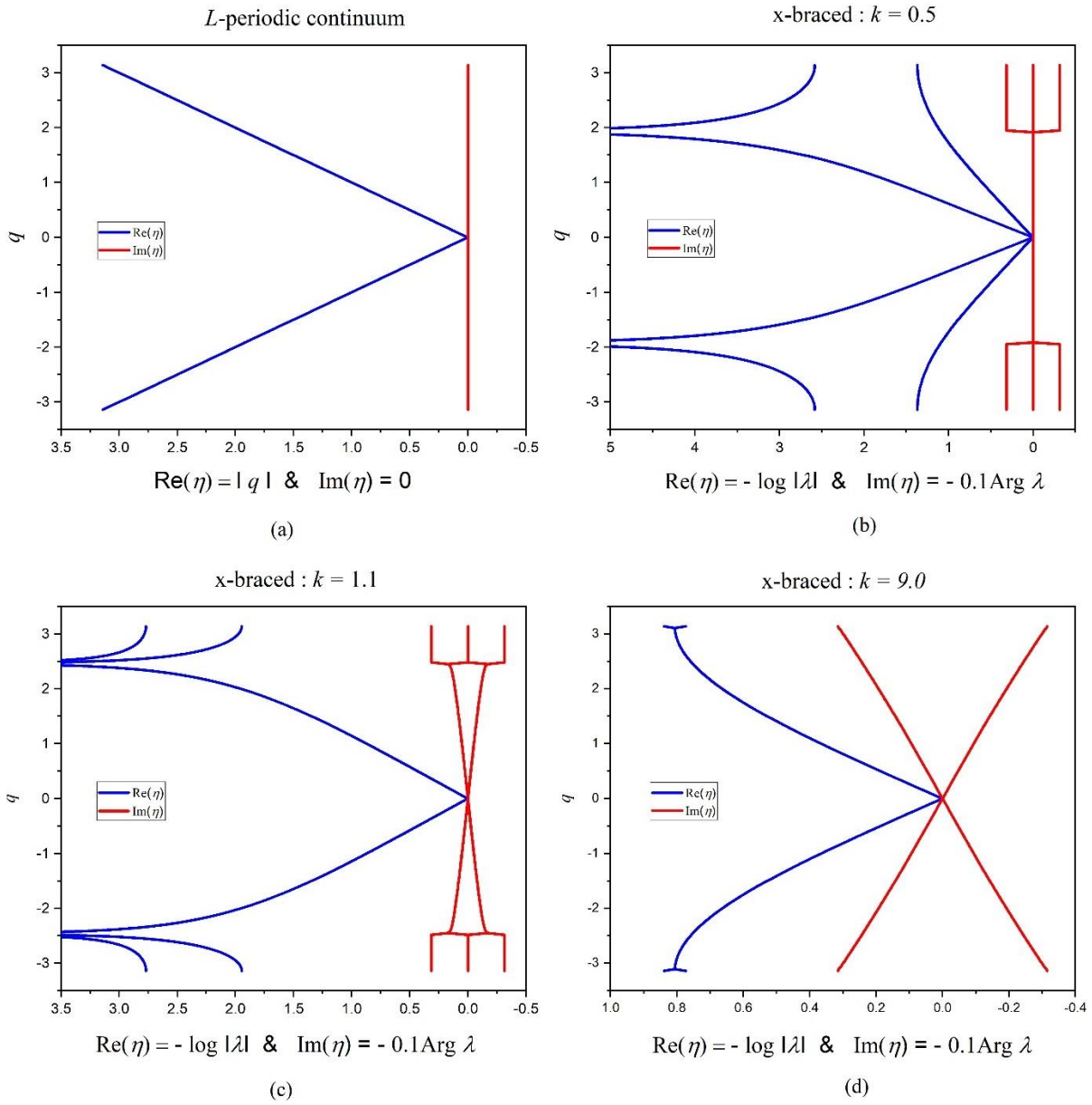


Figure 5.13 Deformation decay spectrums: (a) Continuum (b) x-braced lattice - $\kappa = 0.5$ (c) x-braced lattice - $\kappa = 1.1$ (d) x-braced lattice - $\kappa = 9.0$.

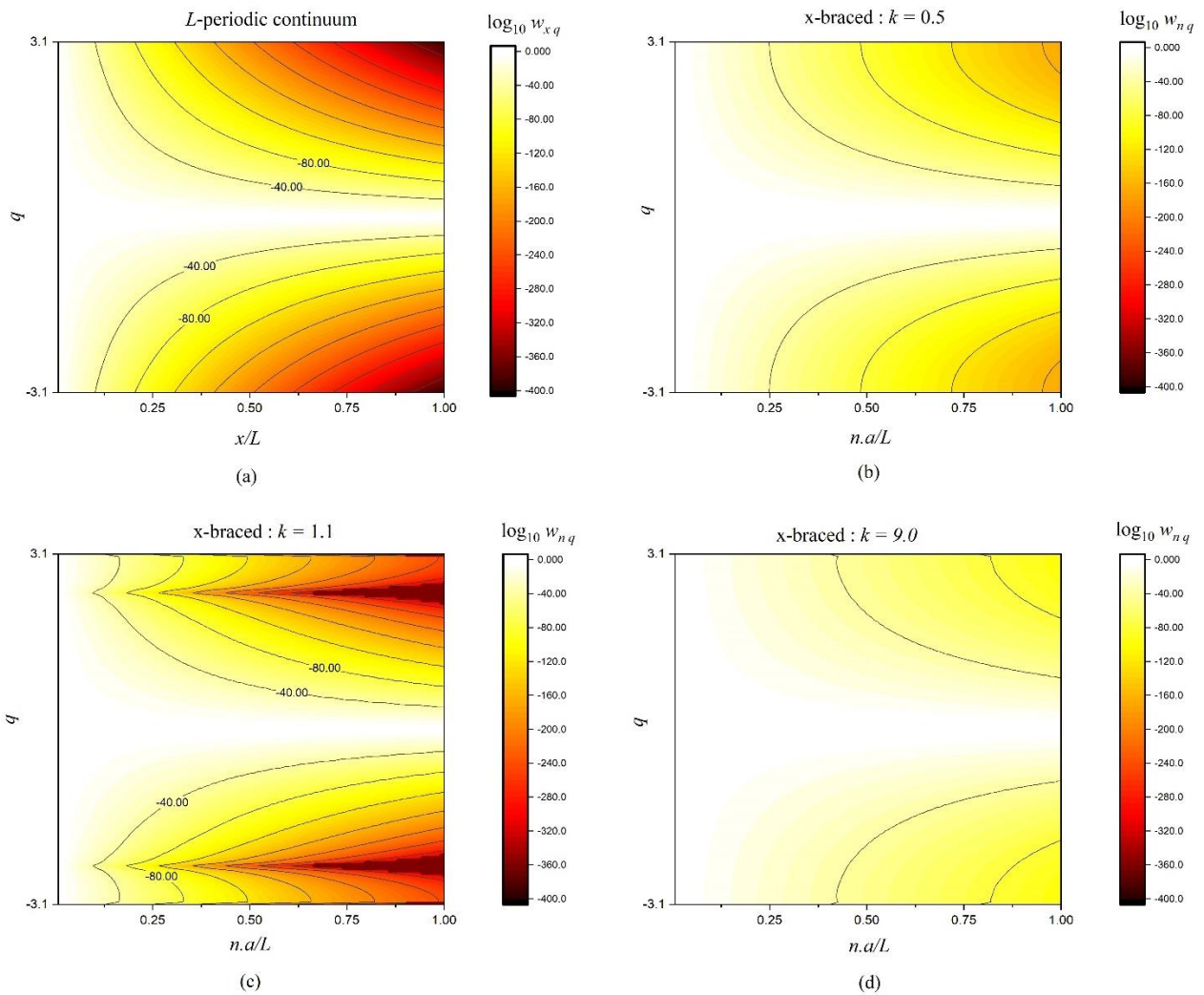


Figure 5.14 Spectral strain energy distribution contour maps: (a) Continuum (b) x-braced lattice - $\kappa = 0.5$ (c) x-braced lattice - $\kappa = 1.1$ (d) x-braced lattice - $\kappa = 9.0$. Material lengths are normalized with a lattice unit-cell length a .

It is possible to simulate the examples performed in this chapter with any FEA commercial software and such an exercise has been performed using a continuous periodic unit where the horizontal boundaries or edges were assumed to have only horizontal displacements to ensure model is cyclic. The semi-analytical methods presented in this chapter are deemed robust for practical application since the ANSYS verification results differed by an order of 10^{-6} .

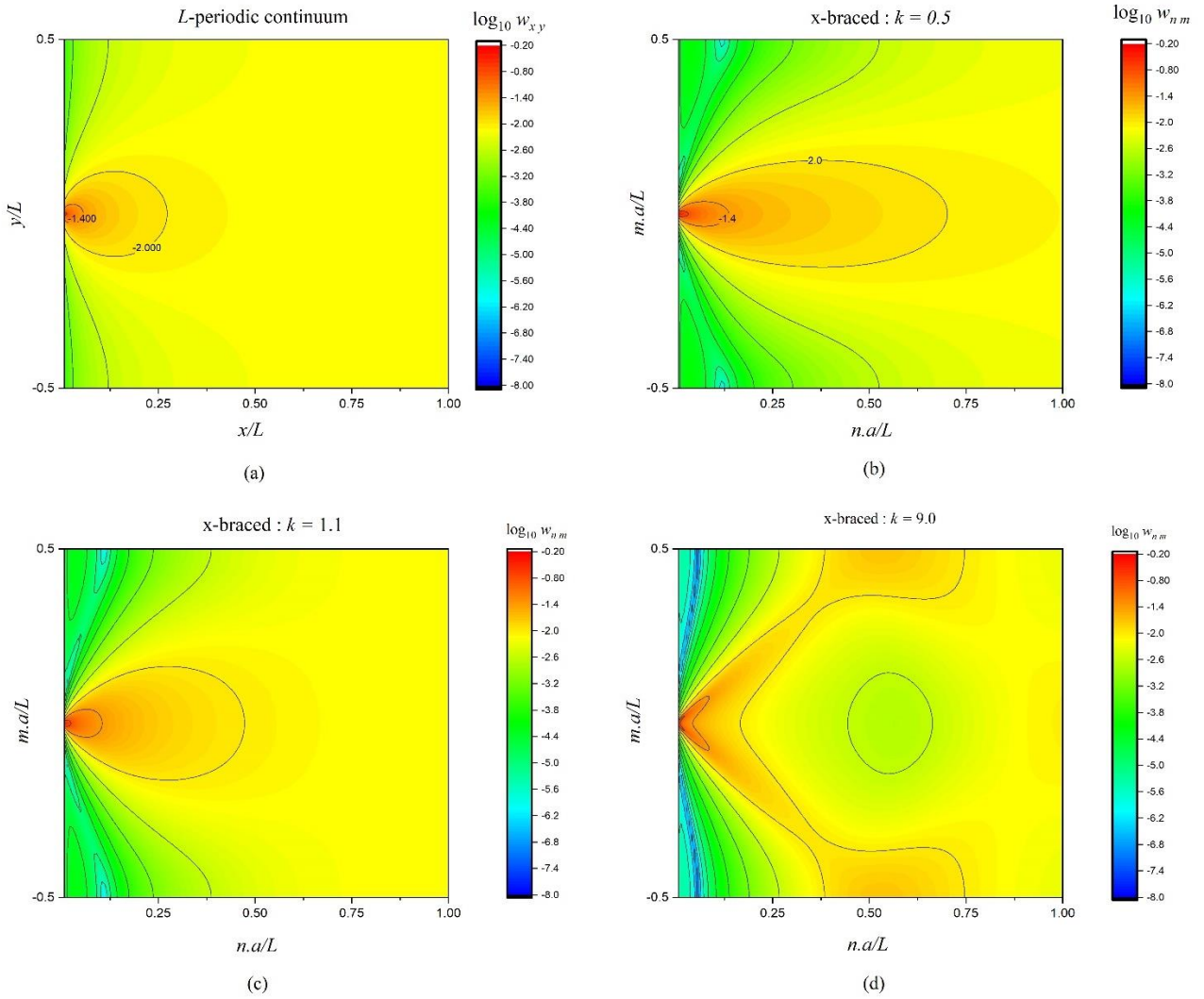


Figure 5.15 Volumetric strain energy distribution contour maps: (a) Continuum (b) x-braced lattice - $k = 0.5$ (c) x-braced lattice - $k = 1.1$ (d) x-braced lattice - $k = 9.0$. Material lengths are normalized with a lattice unit-cell length a .

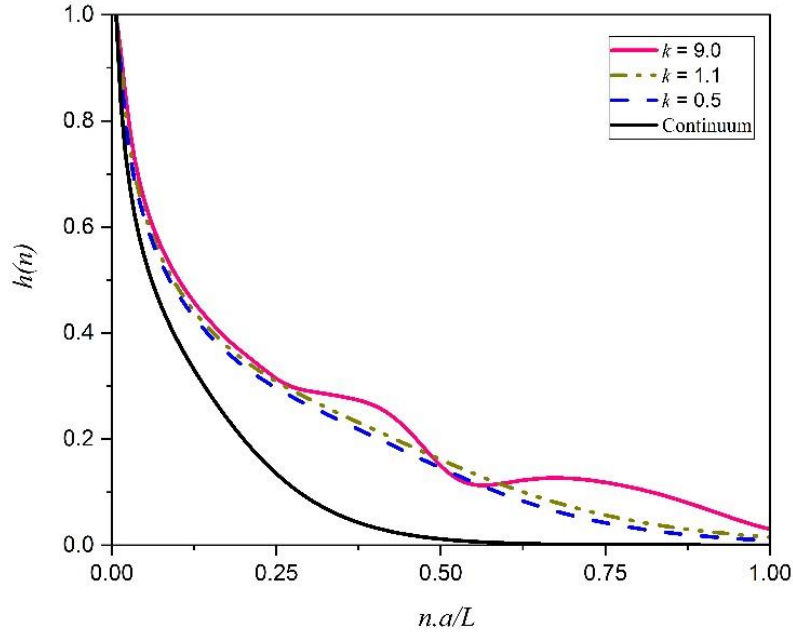


Figure 5.16 Strain energy spectral entropy plots. Material lengths are normalized with a lattice unit-cell length a .

5.10 Conclusions

In this chapter, we have provided a comprehensive outlook on the methods of constructing general 2D Raleigh mode solutions for a periodic nonlocal lattice under either an essential or natural boundary condition.

Since the RSV effect in nonlocal lattices present opportunities for deformation blockage ($\lambda = 0$), bandgap design maps showing a relationships between the lattice unit-cell aspect ratio and stiffness parameter and also a relationship between the stiffness parameter and Raleigh wave numbers are developed for effectively designing a 2D lattice to arrest a Raleigh wave modes of interest or filter out specific Raleigh modes if an applied boundary condition is a composition of Raleigh wave modes.

The possibility of repeated eigenvalues ($\lambda_1 \& \lambda_2 \rightarrow 0$) in nonlocal lattice was demonstrated to possess a unique material behavior identifying it as a polarizing lattice such that it has the functionality of polarizing any arbitrary applied boundary Raleigh wave mode ($n = 1$) for blockage at $n = 1$.

The concept of lattice spectral strain energy and spectral entropy developed in Chapter 4 for a continuum material were shown to be applicable and beneficial in the study of lattice materials. Including continuum comparisons, we have illustrated in detail how the characteristics of spectral components in a spectral strain energy conforming to the materials decay spectrum could be used in defining or programming strain energy transformation in a lattice. This energy study helped in identifying the anomalous behavior of 45° strain energy diversion or rerouting in an x-braced lattice.

The spectral entropy in lattices could be non-monotonic which could be predictive of an anomaly inherent in the energy distribution of a lattice. Lattice energy transformation was seen to be close to continuum behavior but showed slower decay rates due to complex features of spectral components, but a noticeable difference was the channeling of low energy pockets close to the boundary of lattice materials.

All rigid pin-joined periodic lattices are statically indeterminate, i.e. structurally redundant, and therefore axial forces in members determine their overall performance. A statically indeterminate structures do not translate external forces to any significant bending moments at nodes and as such lattices could be classified as stretch dominated. Therefore, replacement of link elements with axial bar elements will not amend the stress energy distributions qualitatively.

The methodologies and metamaterial behaviors described in this chapter could be a guide for studying much desired controllable materials applicable in smart materials, advanced structures and robotics with static deformation blockage or filtering, strain and stress alleviation and load pattern detection functionalities.

CHAPTER 5 REFERENCES

- [1] Kolpakov, A.G. On the determination of the averaged moduli of elastic gridworks. *Prikl. Mat. Mekh.* **1985**, 59, 969–977.
- [2] Lakes, R.S. Foam structures with a negative Poisson's ratio. *Science*. **1987**, 235, 1038–1040.
- [3] Lakes, R.S. Negative Poisson's ratio materials. *Science*. **1987**, 238, 551.

- [4] Kaminakis, N. T.; Stavroulakis, G. E. Topology optimization for compliant mechanisms, using evolutionary-hybrid algorithms and application to the design of auxetic materials. *Composites Part B: Engineering*. **2012**, *43* (6): 2655–2668.
- [5] Stavroulakis, G.E. Auxetic behaviour: Appearance and engineering applications. *Physica Status Solidi B*. **2005**, *242*(3), 710–720.
- [6] Dong, L.; Lakes, R. Advanced damper with high stiffness and high hysteresis damping based on negative structural stiffness. *Int. J. Solids Struct.* **2013**, *50*, 2416–2423.
- [7] Spitas, V.; Spitas, C.; Michelis, P. Modeling of the elastic damping response of a carbon nanotube–polymer nanocomposite in the stress–strain domain using an elastic energy release approach based on stick–slip. *Mech. Adv. Mater. Struct.* **2013**, *20*, 791–800.
- [8] Chronopoulos, D.; Antoniadis, I.; Collet, M.; Ichchou, M. Enhancement of wave damping within metamaterials having embedded negative stiffness inclusions. *Wave Motion*. **2015**, *58*, 165–179.
- [9] Waitukaitis, S.; Menaut, R.; Chen, B. G-g.; van Hecke, M. Origami multistability: From single vertices to metasheets. *Phys. Rev. Lett.* **2015**, *114*, 055503.
- [10] Hanna, B. H.; Lund, J. M.; Lang, R. J.; Magleby, S. P.; Howell, L. L. Waterbomb base: A symmetric single-vertex bistable origami mechanism. *Smart Mater. Struct.* **2014**, *23*, 094009.
- [11] Silverberg, J. L. et al. Origami structures with a critical transition to bistability arising from hidden degrees of freedom. *Nature Mater.* **2015**, *14*, 389–393.
- [12] Nicolaou, Z. G.; Motter, A. E. Mechanical metamaterials with negative compressibility transitions. *Nature Mater.* **2012**, *11*, 608.
- [13] Nicolaou, Z. G.; Motter, A. E. Longitudinal inverted compressibility in super-strained metamaterials. *J. Stat. Phys.* **2013**, *151*, 1162.
- [14] Chen, M. L.; Karpov, E. G. Bistability and thermal coupling in elastic metamaterials with negative compressibility. *Phys. Rev. E*. **2014**, *90*, 033201.
- [15] Imre, A.R.; Metamaterials with negative compressibility – a novel concept with a long history. *Materials Science-Poland*. **2014**, *32*, 126–129.
- [16] Milton, G. W.; Cherkaev, A. V. Which Elasticity Tensors are Realizable? *Journal of Engineering Materials and Technology*. **1995**, *117* (4), 483.
- [17] Kadic, M.; Bückmann, T.; Stenger, N.; Thiel, M.; Wegener, M. On the practicability of pentamode mechanical metamaterials. *Appl. Phys. Lett.* **2012**, *100*(19), 191901.
- [18] Fraternali, F.; Amendola, A. Mechanical modeling of innovative metamaterials alternating pentamode lattices and confinement plates. *J. Mech. Phys. Solids*. **2017**, *99*, 259
- [19] Kane, C. L.; Lubensky, T. C. Topological boundary modes in isostatic lattices. *Nat. Phys.* **2014**, *10*, 39–45.
- [20] Rocklin, D. Z.; Zhou, S.; Sun, K.; Mao, X. Transformable topological mechanical metamaterials. *Nature Comm.* **2017**, *8*, p.14201.

- [21] Bertoldi, K.; Vitelli, V.; Christensen, J.; van Hecke, M. Flexible mechanical metamaterials. *Nature Reviews Materials*. **2017**, 2 (17066), pp. 1-11.
- [22] Donev, A.; Torquato, S. Energy-efficient actuation in infinite lattice structures. *J Mech Phys Solids*. **2003**, 51(8), 1459.
- [23] Karpov, E.G. Structural metamaterials with Saint-Venant edge reversal, *Acta Materialia*. **2017**, 123, 245-254.
- [24] Eringen, A.C. Nonlocal Continuum Field Theories. *Springer-Verlag*, **2002**.
- [25] Rade, L.; Westergren, B. Mathematics Handbook for Science and Engineering. *5th ed, Springer*. **2004**.
- [26] Gradshteyn, I. S.; Ryzhik, I. M. Tables of Integrals, Series and Products, *6th ed, Academic Press*. **2000**.
- [27] Tolstov, G. P. Fourier Series. *Prentice-Hall, Inc*. **1962**.
- [28] Shannon, C. E. A mathematical theory of communication. *Bell System Technical Journal*. **1948**, 27, 379-423.
- [29] Hankerson, D. R.; Harris, G. A. Johnson PD. Introduction to Information Theory and Data Compression. **2003**, *2nd edition, CRC Press*.
- [30] Vajapeyam, S. Understanding Shannon's Entropy metric for Information. *arXiv preprint arXiv*. **2014**, 1405.2061.
- [31] Robinson, D. W. Entropy and uncertainty. *Entropy*, **2008**, 10(4), 493–506
- [32] Dean, D.L. Discrete field analysis of structural systems. *New York: Springer*. **1976**.
- [33] Dean, D.L.; Tauber, S. Solutions for one-dimensional structural lattices. *Journal of the Engineering Mechanics Division, ASCE*. **1959**, 85, 31-41.
- [34] Avent, R. R.; Issa, R. R. A.; Chow, M. L. Discrete field stability analysis of planar trusses. *Journal of Structural Engineering, ASCE*. **1991**, 117 (2), 423–439.
- [35] Karpov, E.G.; Stephen, N.G.; Dorofeev, D.L. On static analysis of finite repetitive structures by discrete Fourier transform. *Int. J. Solids Struct.* 2002, 39 (16), 4291-4310.
- [36] Nilsson, J.; Castro Neto, A. H.; Guinea, F.; Peres, N. M. R. Electronic properties of bilayer and multilayer graphene, *Phys. Rev. B*. **2008**, 78, 045405.
- [37] Karpov, E.G.; Wagner, G. J.; Liu, W. K. A Green's function approach to deriving non-reflecting boundary conditions in molecular dynamics simulations. *Int. J. Numer. Methods Eng.* **2005**, 62 (9), 1250-1262.
- [38] Medyanik, S. N.; Karpov, E. G.; Liu, W. K. Domain reduction approach to molecular mechanics simulations of carbon nanostructures. *J. Comput. Phys.* **2006**, 218 (2), 836-859.

- [39] Qian, D.; Phadke, M.; Karpov, E. G. A domain-reduction approach to bridging scale simulation of one-dimensional nanostructures, *Comput. Mech.* **2011**, *47* (1), 31-47.
- [40] Zok, F. N.; Latture, R. M.; Begley, M. R. Periodic truss structures. *Journal of the Mechanics and Physics of Solids.* **2016**, *96*, 184-203.
- [41] Norris, A. N. Mechanics of elastic networks. *Proceeding of the Royal Society A.* **2014**, *470*, 20140522.
- [42] Cabras, L.; Brun, M. A Class of Auxetic three-dimensional lattices. *Journal of the Mechanics and Physics of Solids.* **2016**, *91*, 56-72.
- [43] Karpov, E. G.; Dorofev, D. L.; Stephen, N. G. Characteristic solutions for the statics of repetitive beam-like trusses. *Int. J. Mech. Sci.* **2002**, *44* (7), 1363-1379.
- [44] Pease, M. C. Methods of matrix algebra. *New York: Academic Press.* **1965**.
- [45] Meyer, K. R.; Hall, G. R. 1991 Introduction to Hamiltonian dynamic systems and the N-body problem. Applied Mathematical Sciences, Berlin: Springer. **1991**, vol. 90.
- [46] Stephen, N.G. Transfer matrix analysis of the elastostatics of one-dimensional repetitive, structures. *Proc. R. Soc. A.* **2006**, *462*, 2245–2270.

CHAPTER 5 APPENDIX

Finding eigenvectors of the transfer matrix $\mathbf{H}(q)$ of 2DoF x-braced lattice:

$$\mathbf{H}(q) = \begin{bmatrix} 0 & 0 & 1 & 0 \\ 0 & 0 & 0 & 1 \\ \beta_1 & \beta_3 i & \beta_4 & \beta_6 i \\ \beta_2 i & \beta_1 & \beta_5 i & \beta_7 \end{bmatrix} \quad (5-A1)$$

$$\beta_1 = -\frac{(\sqrt{2} \cos q + k \cos 2q)}{k + \sqrt{2} \cos q}, \quad \beta_2 = \frac{2(\sqrt{2} + k \cos q) \sin q}{k + \sqrt{2} \cos q}, \quad \beta_3 = \frac{k \sin q}{k + \sqrt{2} \cos q}, \quad \beta_4 = \frac{2(\sqrt{2} + k) \cos q}{k + \sqrt{2} \cos q}$$

$$\beta_5 = -\frac{2(\sqrt{2} + k) \sin q}{k + \sqrt{2} \cos q},$$

$$\beta_6 = -\frac{2(k - \sqrt{2}(k \cos q - 1)) \sin q}{k + \sqrt{2} \cos q}, \quad \beta_7 = \frac{(2 + k\sqrt{2} - 2 \cos q)(2 + \sqrt{2} k \cos q)}{k + \sqrt{2} \cos q}$$

To find eigenvectors $\begin{Bmatrix} \mathbf{h}(q) \\ \lambda \mathbf{h}(q) \end{Bmatrix} = \begin{Bmatrix} x \\ y \\ w \\ z \end{Bmatrix}$ of $\mathbf{H}(q)$ we use the *row reduction echelon method* to solve

$(\mathbf{H}(q) - \mathbf{I}\lambda)\mathbf{h}(q) = \mathbf{0}$ and get the equation

$$\begin{bmatrix} 1 & 0 & \frac{1}{-\lambda} & 0 \\ 0 & 1 & 0 & \frac{1}{-\lambda} \\ 0 & 0 & 1 & \frac{\beta_6 i + \beta_3 i \frac{1}{\lambda}}{(\beta_4 - \lambda) + \beta_1 \frac{1}{\lambda}} \\ 0 & 0 & 0 & \left(\beta_7 + \beta_1 \frac{1}{\lambda} \right) - \left(\beta_5 i + \beta_2 i \frac{1}{\lambda} \right) \frac{\beta_6 i + \beta_3 i \frac{1}{\lambda}}{(\beta_4 - \lambda) + \beta_1 \frac{1}{\lambda}} \end{bmatrix} \begin{Bmatrix} x \\ y \\ w \\ z \end{Bmatrix} = \begin{Bmatrix} 0 \\ 0 \\ 0 \\ 0 \end{Bmatrix} \quad (5-A2)$$

Writing down equations, z is 0 which makes the eigenvector zero but since an eigenvector cannot be zero we take z as any real or complex number. However, taking z = 1 and solving for (x, y, w, z) we get

$$\begin{Bmatrix} \mathbf{h}(q) \\ \lambda(q)\mathbf{h}(q) \end{Bmatrix} = C \begin{Bmatrix} \frac{i(\beta_3 + \beta_6 \lambda)}{\lambda(\lambda^2 - \beta_4 \lambda - \beta_1)} \\ \frac{1}{\lambda} \\ \frac{i(\beta_3 + \beta_6 \lambda)}{\lambda^2 - \beta_4 \lambda - \beta_1} \\ 1 \end{Bmatrix} \quad (5-A3)$$

The above expression can be rewritten as

$$\begin{Bmatrix} \mathbf{h}(q) \\ \lambda(q)\mathbf{h}(q) \end{Bmatrix} = C \begin{Bmatrix} i(\beta_3 + \beta_6 \lambda) \\ \lambda^2 - \beta_4 \lambda - \beta_1 \\ i \lambda(\beta_3 + \beta_6 \lambda) \\ \lambda(\lambda^2 - \beta_4 \lambda - \beta_1) \end{Bmatrix} \quad (5-A4)$$

Constructing real-valued cyclic Raleigh wave solutions:

Complex Eigenvalues:

$$\mathbf{h}(q) = \begin{Bmatrix} a \pm ib \\ -c + id \end{Bmatrix};$$

$$\mathbf{d}_{nm}^{(1)} = C_1 \rho^n(q) \left\{ \begin{Bmatrix} a \cos(\theta n + qm) - b \sin(\theta n + qm) \\ c \cos(\theta n + qm) - d \sin(\theta n + qm) \end{Bmatrix} + i \begin{Bmatrix} a \sin(\theta n + qm) + b \cos(\theta n + qm) \\ c \sin(\theta n + qm) + d \cos(\theta n + qm) \end{Bmatrix} \right\} \quad (5-A5)$$

$$\mathbf{d}_{nm}^{(2)} = C_1 \rho^n(q) \left\{ \begin{Bmatrix} a \cos(-\theta n + qm) + b \sin(-\theta n + qm) \\ -c \cos(-\theta n + qm) - d \sin(-\theta n + qm) \end{Bmatrix} + i \begin{Bmatrix} a \sin(-\theta n + qm) - b \cos(-\theta n + qm) \\ -c \sin(-\theta n + qm) + d \cos(-\theta n + qm) \end{Bmatrix} \right\} \quad (5-A6)$$

Possible cyclic harmonic solutions are obtained by summing and subtracting the corresponding real and imaginary parts of the above equations as shown below:

$$\mathbf{d}_{nm} = \text{Re } \mathbf{d}_{nm}^{(1)} + \text{Re } \mathbf{d}_{nm}^{(2)} = C \rho^n(q) \begin{Bmatrix} a \cos qm \\ -d \sin qm \end{Bmatrix} \quad (5-A7)$$

$$\mathbf{d}_{nm} = \text{Im } \mathbf{d}_{nm}^{(1)} - \text{Im } \mathbf{d}_{nm}^{(2)} = C \rho^n(q) \begin{Bmatrix} b \cos qm \\ c \sin qm \end{Bmatrix} \quad (5-A8)$$

Real Eigenvalues:

$$\text{Case 1: } \mathbf{h}(q) = \begin{Bmatrix} ib \\ c \end{Bmatrix}$$

$$\mathbf{d}_{nm} = C_2 \lambda^n(q) \left\{ \begin{array}{l} -b \sin qm \\ c \cos qm \end{array} \right\} + i \left\{ \begin{array}{l} b \cos qm \\ c \sin qm \end{array} \right\} \quad (5-A9)$$

The real-cyclic solution is the imaginary part of the solution above:

$$\mathbf{d}_{nm} = C_2 \lambda^n(q) \left\{ \begin{array}{l} b \cos qm \\ c \sin qm \end{array} \right\} \quad (5-A10)$$

Case 2: $\mathbf{h}(q) = \begin{Bmatrix} b \\ ic \end{Bmatrix}$:

$$\mathbf{d}_{nm} = C_2 \lambda^n \left\{ \begin{array}{l} b \cos qm \\ -c \sin qm \end{array} \right\} + i \left\{ \begin{array}{l} b \sin qm \\ c \cos qm \end{array} \right\} \quad (5-A11)$$

The real-cyclic solution is the real part of the solution above

$$\mathbf{d}_{nm} = C_2 \lambda^n(q) \left\{ \begin{array}{l} b \cos qm \\ -c \sin qm \end{array} \right\} \quad (5-A12)$$

Finding the zero-eigenvalue relationship for a 2DoF x-braced lattice:

$$\det \mathbf{H}(q) = \prod_{i=1}^n \lambda_i(q) = \frac{k(k+\sqrt{2} \cos q)^2}{k(k+\sqrt{2} \cos q)^2} \quad (5-A13)$$

Since $\lambda(q) = 0$ when $\det \mathbf{H}(q) = 0$, we write the zero-eigenvalue relationship as

$$k + \sqrt{2} \cos q = 0 \quad (5-A14)$$

The transfer matrix $\mathbf{H}(q)$ when we introduce aspect ratio α :

$$\mathbf{H}(q) = \begin{bmatrix} 0 & 0 & 1 & 0 \\ 0 & 0 & 0 & 1 \\ \gamma_1 & \gamma_3 i & \gamma_4 & \gamma_6 i \\ \gamma_2 i & \gamma_1 & \gamma_5 i & \gamma_7 \end{bmatrix} \quad (5-A15)$$

$$\gamma_1 = -\frac{(1+\alpha^2)^2 \cos q + 2k\alpha^3 \sqrt{1+\alpha^2} \cos 2q}{2k\alpha^3 \sqrt{1+\alpha^2} + (1+\alpha^2)^2 \cos q}, \quad \gamma_2 = \frac{2\alpha((1+\alpha^2)^2 + 2k\alpha^3 \sqrt{1+\alpha^2} \cos q) \sin q}{2k\alpha^3 \sqrt{1+\alpha^2} + (1+\alpha^2)^2 \cos q}$$

$$\gamma_3 = \frac{4k\alpha^2 \sqrt{1+\alpha^2} \cos q \sin q}{2k\alpha^3 \sqrt{1+\alpha^2} + (1+\alpha^2)^2 \cos q}, \quad \gamma_4 = \frac{2(1+\alpha^2(2+\alpha^2+2k\alpha\sqrt{1+\alpha^2})) \cos q}{2k\alpha^3 \sqrt{1+\alpha^2} + (1+\alpha^2)^2 \cos q}$$

$$\gamma_5 = -\frac{2\alpha(1+\alpha^2(2+\alpha^2+2k\alpha\sqrt{1+\alpha^2})) \sin q}{2k\alpha^3 \sqrt{1+\alpha^2} + (1+\alpha^2)^2 \cos q}, \quad \gamma_6 = \frac{2\alpha^2(-2k\sqrt{1+\alpha^2} - (1+\alpha^2)^2 + (1+\alpha^2)^2 \cos q) \sin q}{2k\alpha^3 \sqrt{1+\alpha^2} + (1+\alpha^2)^2 \cos q}$$

$$\gamma_7 = -\frac{\sqrt{1+\alpha^2}((1+\alpha^2)^{3/2} + 2k\alpha^3 \cos q)(-2k - (1+\alpha^2)^{3/2} + (1+\alpha^2)^{3/2} \cos q)}{k(2k\alpha^3 \sqrt{1+\alpha^2} + (1+\alpha^2)^2 \cos q)}$$

6 CONCLUSIONS AND FUTURE WORK

Mechanical metamaterials are materials with preconceived elastic properties like negative Poisson's ratio, negative compressibility, negative stiffness, etc. that cannot be achieved by natural materials. In recent times, this class of metamaterials have garnered significant research interest due to the enormous functionalities and applications attainable when such materials are used in composites, intelligent structures and resilient systems. The unusual elastic properties of these artificial materials mean their deformation mechanisms could be programmed to possess functionalities such as stress and strain alleviation, vibration control, strain energy storage that are far reaching in natural materials.

The aim of the thesis was to understand the deformation and strain energy anomalies in bistable and nonlocal mechanical metamaterials. Bistable structures and materials are those that possess multiple states of stability where there exist two states of stable equilibrium and a single unstable equilibrium state. During loading and unloading cycles, at certain critical loads a bistable structure or material transitions from one stable state to another. The unstable state features a negative stiffness which can only be harnessed under a displacement-controlled scheme. Even though several authors have studied the topic, a fully analytical procedure for designing bistability behavior in elastic structures was presented in Chapter 2 by employing stability and phase diagrams that serve as great stability predicting tools. For the analyzed truss, the stability and phase diagrams gave all the regions of the possible states of stability namely monostability, superelasticity and superplasticity based on only truss system design parameters. The present study could lead to efficient designs of advanced space truss structures used in the civil and aerospace industry where structures still maintain stability by adapting to critical forces. The concept of autonomous systems that base structure's response on natural external actuation or stimulation of active materials could depend on this approach of designing bistable actuators to maximize structure's response to the required limit.

The property where a structure contracts or pulls back under a tensile load in the direction of the load is termed negative extensibility. The already available study on the subject of linear negative compressibility does not address the negative behavior in the direction aligned to the direction of the applied load but a result of a

hydrostatic pressure which was aim of this chapter. This mechanical behavior is analogous to negative compressibility which is a bulk material property. Since negative compressibility studies have shown bistable systems with multiple degrees of freedom and at least a single internal degree of freedom to have such a potential, this chapter was directed to study a truss structure having similar features with the aim of achieving a longitudinal negative extensibility behavior. We showed with the help of stability and phase diagrams studied in Chapter 2 that negative extensibility is typical of a system that undergoes two forward transitions and two reverse transitions and so the unique characteristic of a beak-shaped bifurcation set or a double cusp. The phase diagram for a negative extensible truss showed five regions of interest namely monostability, superelasticity, superplasticity, negative extensibility superelasticity and negative extensibility superplasticity. The negative extensibility has been shown to be attainable in simple structural systems and that is an encouraging attribute for future studies into vibration control mechanisms and super-dampers.

To aid in the identification and analysis of anomalous strain energy distribution in periodic lattice materials, this chapter is used to present an efficient numerical method of strain energy analysis by developing an analogy to the Parseval's theorem in digital analysis for continuum applications. In so doing, the spectral strain energy density (SESD) term was derived with an equal quantitative measure to the usual spatial or volumetric strain energy density but possesses rich qualitative difference due its description of harmonic presence and contribution to the continuum strain energy behavior. The strain energy spectral density (SESD) became an important parameter for quantifying the strain energy spectral entropy (SESE) of elastic deformation, a concept from Shannon's entropy of information studies which measures the amount of disorder or disruption as in a thermodynamic system. The spectral entropy (SESE) study was convincingly used to explain the transformation of strain energy in a plane solid continuum material and as such was seen as a powerful numerical tool capable of addressing issues of high stress and strain localization and non-uniform strain energy distribution that could be present in periodic lattice mechanical metamaterials.

Analogous to how in acoustic mechanics, sound waves could be blocked by tuning bandgap characteristics of a material's dispersion curves, static Raleigh deformation can be blocked when there exist bandgaps in the deformation decay spectrum of a lattice by tuning system design parameters. The existence of bandgaps

however reverses the rate of Raleigh mode decay such that Raleigh modes corresponding to lower wave numbers (coarse) decay faster compared to that of higher wave number (even). This chapter was used to develop the studies to cover multiple degrees of freedom systems as well as solution to arbitrary (Gaussian, impact e.t.c) non-Raleigh mode natural boundary conditions. 2D periodic nonlocal lattice structures provide an incentive of repeated eigenvalues ($\lambda_1 \& \lambda_2 \rightarrow 0$), a study of this feature was shown to classify those special nonlocal lattice polarizing structures. The chapter also looked at strain energy distribution in periodic lattices using the spectral strain energy density and strain energy spectral entropy concepts seen in Chapter 4, as there exist potential for anomalous strain energy storage in these periodic nonlocal lattices. The 45^o maximal strain energy rerouting and the channeling of low energy pockets in the 2D periodic nonlocal x-braced lattice material were identified as anomalous strain energy behaviors far from a continuum behavior. Strain energy spectral entropy also showed that lattice materials could showcase a non-monotonic behavior explaining complexities in their spectral energy distributions. The tools presented in this chapter could be expanded to the study of other unit-cell geometries and other periodic lattice systems that have been studied to have metamaterial behaviors like negative Possion's ratio and negative compressibility. Future studies could also be directed in the area designing composite materials which will depend on anomalous deformation and strain energy behaviors of an RSV lattice material to build high resilience lattice material.

CITED LITERATURE

- Ai, L.; Gao, X.L. Metamaterials with negative Poisson's ratio and non-positive thermal expansion. *Compos. Struct.* **2017**, *162*, 70–84.
- Alabuzhev, P.; Rivin, E.I. *Vibration Protection and Measuring Systems with Quasi-zero Stiffness*. CRC Press. **1989**.
- Avent, R. R.; Issa, R. R. A.; Chow, M. L. Discrete field stability analysis of planar trusses. *Journal of Structural Engineering, ASCE*. **1991**, *117* (2), 423–439.
- Ayatollahi, M. R.; Mirsayar, M. M.; Dehghany, M. Experimental determination of stress field parameters in bi-material notches using photoelasticity. *Materials & Design*. **2011**, *32*, 4901–4908.
- Barnes, D. L.; Miller, W.; Evans, K. E.; Marmier, A. S. H. Modelling negative linear compressibility in tetragonal beam structures. *Mech. Mater.* **2012**, *46*, 123–8
- Baughman, R. H.; Stafstram, S.; Cui, C.; Dantas, S. O. Materials with negative compressibilities in one or more dimensions. *Science* **1998**, *279*(5356), 1522–4.
- Bertoldi, K.; Vitelli, V.; Christensen, J.; van Hecke, M. Flexible mechanical metamaterials. *Nature Review Materials*. **2017**, *2* (17066), pp. 1-11.
- Bigoni, D.; Noselli, G. Localized stress percolation through dry masonry walls. *Part I - Experiments Eur. J of Mechanics & Solids*. **2010**, *29*, 291-298
- Cai, J. G.; Xu, Y. X.; Feng, J.; Zhang, J. 2011. Mechanical Behavior of Bistable Struts. *J. Mechanical Engineering Science Proc. IMech*. **2011**, *226* Part C.
- Cairns, A. B.; Catafesta, J.; Levelut, C.; Rouquette, J.; van der Lee, A.; Peters, L.; Thompson, A. L.; Dmitriev, V.; Haines, J.; Goodwin, A. L. Giant negative linear compressibility in zinc dicyanoaurate. *Nat. Mater.* **2013**, *12*, 212–6
- Chen, M. L.; Karpov E. G. Bistability and thermal coupling in elastic metamaterials with negative compressibility, *Phys.Rev. E*. **2014**, *90*, 033201.
- Chen, T.; Shea, K. An Autonomous Programmable Actuator and Shape Reconfigurable Structures using Bistability and Shape Memory Polymers. *Cornell University Library*. Nov **2017**.
- Chronopoulos, D.; Antoniadis, I.; Collet, M.; Ichchou, M. Enhancement of wave damping within metamaterials having embedded negative stiffness inclusions. *Wave Motion*. **2015**, *58*, 165–179.
- Coullais, C.; Sounas, D.; Alu, A. Static non-reciprocity in mechanical metamaterials. *Nature*. **2017**, *542*, 461-464.
- Cummer, S.A.; Christensen, J.; Alu, A. Controlling sound with acoustic metamaterials. *Nat. Rev. Mater.* **2016** *1*, 16001.
- Dean, D.L. Discrete field analysis of structural systems. *New York: Springer*. **1976**.

- Dean, D.L.; Tauber, S. Solutions for one-dimensional structural lattices. *Journal of the Engineering Mechanics Division, ASCE*. **1959**, *85*, 31-41.
- Donev, A.; Torquato, S. Energy-efficient actuation in infinite lattice structures. *J. Mech. Phys. Solids*. **2003**, *51*(8), 1459-1475.
- Dong, L.; Lakes, R. Advanced damper with high stiffness and high hysteresis damping based on negative structural stiffness. *Int. J. Solids Struct.* **2013**, *50*, 2416–2423.
- Dudek, K. K.; Attard, D.; Caruana-Gauci, R.; Wojciechowski, K.W.; Grima, J.N. Unimode metamaterials exhibiting negative linear compressibility and negative thermal expansion. *Smart Mater. Struct.* **2016**, *25*, 025009.
- Ekštejn, K.; Pavelka, T. 2004. Entropy and Entropy-based Features In Signal Processing. *In Proceedings of PhD Workshop Systems & Control, Balatonfüred*. **2004**.
- Erigen, A.C. Nonlocal Continuum Field Theories. *Springer-Verlag*, **2002**.
- Fraternali, F.; Amendola, A. 2017 Mechanical modeling of innovative metamaterials alternating pentamode lattices and confinement plates. *J. Mech. Phys. Solids*. **2017**, *99*, 259-271.
- Frocht, M. M.; Photoelasticity. *J. Wiley and Sons, London*. **1965**.
- Gradshteyn, I. S.; Ryzhik, I. M. Tables of Integrals, Series and Products, *6th ed, Academic Press*. **2000**.
- Grima, J. N.; Caruana-Gauci, R. 2012 Mechanical metamaterials: materials that push back. *Nat. Mater.* **2012**, *11*, 565–6.
- Grima, J. N.; Caruana-Gauci, R.; Attard, D.; Gatt, R. Three-dimensional cellular structures with negative Poisson's ratio and negative compressibility properties. *Proc R Soc A: Mathe, Phys Eng Sci*. **2012**, *468*, 3121–38.
- Grima, J. N.; Farrugia, P. S.; Gatt, R.; Zammit, V. A system with adjustable positive or negative thermal expansion. *Proc. R. Soc. A*. **2007**, *463*, 1585–1596.
- Grima, J.N.; Attard, D.; Gatt, R. Truss-type systems exhibiting negative compressibility. *Phys. Status Solidi B*. **2008**, *245*, 2405–2414.
- Grima, J.N.; Caruana-Gauci, R.; Wojciechowski, K.W.; Evans, K.E. Smart hexagonal truss systems exhibiting negative compressibility through constrained angle stretching. *Smart Mater. Struct.* **2013**, *22*, 084015.
- Guariglia, E. Entropy and Fractal Antennas. *Entropy* **2016**, *18*, 84.
- Hankerson, D. R.; Harris, G. A. Johnson PD. Introduction to Information Theory and Data Compression. **2003**, *2nd edition, CRC Press*.
- Hankerson, D. R.; Harris, G. A.; Johnson, P. D. Introduction to Information Theory and Data Compression. *2nd edition, CRC Press*. **2003**.
- Hanna, B. H.; Lund, J. M.; Lang, R. J.; Magleby, S. P.; Howell, L. L. Waterbomb base: A symmetric single-vertex bistable origami mechanism. *Smart Mater. Struct.* **2014**, *23*, 094009.

- Herrmann, H. J. Introduction to Modern Ideas on Fracture Patterns. *Random Fluctuations and Pattern Growth: Experiments and Models*, H. E. Stanley and N. Ostrowsky, eds., Kluwer Academic, Dordrecht, The Netherlands. **1988**, pp. 149–160.
- Hrennikoff, A. Solution of Problems of Elasticity by the Framework Method. *ASME J. Appl. Mech.* **1941**, *12*, pp. 169–175.
- Hu, N.; Burgueno, R. Buckling-induced smart applications: recent advances and trends. *Smart Materials and Structures*. **2015**, *24*: 063001.
- Hussein, M.I.; Leamy, M.J.; Ruzzene, M. Dynamics of phononic materials and structures: Historical origins, recent progress, and future outlook. *Appl. Mech. Rev.* **2014**, *66*, 040802.
- Imre, A. R. Metamaterials with negative compressibility – a novel concept with a long history. *Materials Science-Poland*. **2014**, *32*, 126–129.
- Jiang, J. W.; Park, H. S. Negative Poisson's ratio in single-layer black phosphorus. *Nature Communications*. **2014**, *5*, 4727.
- Kadic, M.; Bückmann, T.; Stenger, N.; Thiel, M.; Wegener, M. On the practicability of pentamode mechanical metamaterials. *Appl. Phys. Lett.* **2012**, *100*, 191901.
- Kaminakis, N. T.; Stavroulakis, G. E. Topology optimization for compliant mechanisms, using evolutionary-hybrid algorithms and application to the design of auxetic materials. *Composites Part B: Engineering*. **2012**, *43* (6): 2655–2668.
- Kane, C. L.; Lubensky, T. C. Topological boundary modes in isostatic lattices. *Nat. Phys.* **2014**, *10*, 39–45.
- Karpov, E. G. Structural metamaterials with Saint-Venant edge effect reversal. *Acta Materialia*. **2017**, *123*, 245-254.
- Karpov, E. G.; Danso, L. A.; Klein, J. T. Negative extensibility metamaterials: Occurrence and design space topology. *Physical Review E*. **2017**, *96*, 023002.
- Karpov, E. G.; Stephen, N. G.; Dorofeev, D. L. On static analysis of finite repetitive structures by discrete Fourier Transform. *International Journal of Solids and Structures*. **2002**, *39*, 4291-4310.
- Karpov, E.G.; Wagner, G. J.; Liu, W. K. A Green's function approach to deriving non-reflecting boundary conditions in molecular dynamics simulations. *Int. J. Numer. Methods Eng.* **2005**, *62* (9), 1250-1262.
- Kinoshita, T.; Oshaki, M. Synthesis of Bistable Compliant Structures from Truss Mechanisms. *Journal of Computational Science and Technology*. **2009**, *3*(2).
- Klein, J. T.; Karpov, E. G. Negative extensibility metamaterials: Phase diagram calculation. *Computational Mechanics*. **2018**, *62*(4), p.669.
- Kolpakov A.G. On the determination of the averaged moduli of elastic gridworks. *Prikl. Mat. Mekh.* **1985** *59*, 969–977.
- Kubo, R.; Thermodynamics. (*North-Holland Publ. Company, Amsterdam*). **1968**, pp. 140–147.

- Lakes, R. Foam Structures with a negative Poisson's ratio. *Science*. 1987, 235, 1038-1040.
- Lakes, R.; Wojciechowski, K. W. Negative compressibility, negative Poisson's ratio, and stability. *Phys. Stat. Sol. B*. **2008**, 245, 545-551.
- Lakes, R.S. Foam structures with a negative Poisson's ratio. *Science*. **1987**, 235, 1038–1040.
- Lakes, R.S. Negative Poisson's ratio materials. *Science*. **1987**, 238, 551.
- Lui, Z.; Zhang, X.; Mao, Y.; Zhu, Y.; Yang, Z.; Chan, C.; Sheng, P. Locally resonant sonic materials. *Science* **2000**, 289, 1734–1736.
- Medyanik, S. N.; Karpov, E. G.; Liu, W. K. Domain reduction approach to molecular mechanics simulations of carbon nanostructures. *J. Comput. Phys.* **2006**, 218 (2), 836-859.
- Milton, G. W.; Cherkaev, A. V. Which Elasticity Tensors are Realizable? *Journal of Engineering Materials and Technology*. **1995**, 117 (4): 483.
- Miyamaru, F.; Saito, Y.; Takeda, M.W.; Hou, B.; Liu, L.; Wen, W.; Sheng, P. Terahertz electric response of fractal metamaterial structures. *Phys. Rev. Lett. B* **2008**, 77, 045124.
- Molyneaux, W. Supports for Vibration Isolation. *Aeronautical Research Council, Great Britain*. **1957**. ARC/CP-322.
- Munster, A. Statistical Thermodynamics. 1st Engl. ed. (Springer-Verlag, Berlin). **1969**, Vol. 1, sect. 4.2, pp. 212, 217, 218, 226; sect. 4.5, p. 261.
- Nicolaou, Z. G.; Motter, A. E. Longitudinal inverted compressibility in super-strained metamaterials. *J. Stat. Phys.* **2013**, 151, 1162.
- Nicolaou, Z. G.; Motter, A. E. Mechanical metamaterials with negative compressibility transitions. *Nature Materials*. **2012**, 11, 608–613.
- Nilsson, J.; Castro Neto, A. H.; Guinea, F.; Peres, N. M. R. Electronic properties of bilayer and multilayer graphene, *Phys. Rev. B*. **2008**, 78, 045405.
- Pendry, J.B. Negative refraction makes a perfect lens. *Phys. Rev. Lett.* **2000**, 85, 3966–3969.
- Pendry, J.B.; Holden, A.J.; Robbins, D.J.; Stewart, W.J. Magnetism from conductors and enhanced nonlinear phenomena. *IEEE Trans. Microw. Theory Tech.* **1999**, 47, 2075–2084.
- Pendry, J.B.; Holden, A.J.; Stewart, W.J.; Youngs, I. Extremely low frequency plasmons in metallic mesostructures. *Phys. Rev. Lett.* **1996**, 76, 4773–4776.
- Plante, J.S.; Santer, M. Compliant Bistable Dielectric Elastomer Actuators for Binary Mechatronic Systems. *Proceedings Of IDECT/CIE 2005 ASME Mechanism and Robotics Conference, Long Beach, California, USA*, **2005**, 24-28.
- Post, D. Photoelasticity, *Exp. Mechanics*. **1979**, 19 (5), 176-192
- Rade, L.; Westergren, B. Mathematics Handbook for Science and Engineering. 5th ed, Springer. **2004**.

- Rafsanjani, A.; Akbarzadeh, A.; Pasini, D. Snapping Mechanical Metamaterials under Tension. *Advanced Materials*. **2015**, *27*, 5931–5935.
- Robinson, D. W. Entropy and uncertainty. *Entropy*, **2008**, *10*(4), 493–506.
- Rocklin, D. Z.; Zhou, S.; Sun, K.; Mao, X. Transformable topological mechanical metamaterials. *Nature Comm.* **2017**, *8*, p.14201.
- Sadd, M. H. Elasticity: Theory, Applications and Numerics. *Elsevier*, **2005**.
- Schenk, M.; Guest, S. D. Geometry of Miura-Folded Metamaterials. *PNAS*. **2013**, *110*, 3276–3281.
- Schlangen, E.; van Mier, J. G. M. 1992, Experimental and Numerical Analysis of Micromechanisms of Fracture of Cement-Based Composites. *Cem. Concr. Compos.* **1992**, *14*(2), pp. 105–118.
- Shan, S.; Kang, S.; Raney, J. R.; Wang, P.; Fang, L.; Candido, F.; Lewis, J. A.; Bertoldi, K. Multistable architected materials for trapping elastic strain energy. *Advanced Materials*. **2015**, *27*, 4296–4301.
- Shannon, C. E. A mathematical theory of communication. *Bell System Technical Journal*. **1948**, *27*, 379–423.
- Shon, S.; Lee, S.; Ha, J.; Cho, C. 2015. Semi- Analytic Solution and Stability of Space Truss Using a Higher-Order Taylor Series. *Materials*. **2015**, *8*, 2400–2414.
- Silverberg, J. L. et al. Origami structures with a critical transition to bistability arising from hidden degrees of freedom. *Nature Mater.* **2015**, *14*, 389–393.
- Smith, D.R.; Padilla, W.J.; Vier, D.C.; Nemat-Nasser, S.C.; Schultz, S. Composite medium with simultaneously negative permeability and permittivity. *Phys. Rev. Lett.* **2000**, *84*, 4184–4187.
- Soukoulis, C.;Wegener, M. Past achievements and future challenges in the development of three-dimensional photonic metamaterials. *Nat. Photonics* **2011**, *5*, 523–530.
- Spitas, V.; Spitas, C.; Michelis, P. Modeling of the elastic damping response of a carbon nanotube–polymer nanocomposite in the stress–strain domain using an elastic energy release approach based on stick–slip. *Mech. Adv. Mater. Struct.* **2013**, *20*, 791–800.
- Stavroulakis, G.E. Auxetic behaviour: Appearance and engineering applications. *Physica Status Solidi B*. **2005**, *242* (3): 710–720.
- Sutton, M. A.; Orteu, J. J.; Schreier, H. W. Image Correlation for Shape, Motion and Deformation Measurements: Basic Concepts, Theory and Applications. (*Springer*), **2009**, p. 322
- Tankasala, H.C.; Deshpande, V.S.; Fleck, N.A., Koiter medal paper: crack-tip fields and toughness of two-dimensional elastoplastic lattices. *J. Appl. Mech.* **2015**, *82*(9), p.091004.
- Timoshenko, S. P.; Goodier, J. N. Theory of Elasticity. *3rd ed. (McGraw-Hill)*. **1970**
- Tolstov, G. P. Fourier Series, *Prentice-Hall, Inc.* **1962**.
- Vajapeyam, S. Understanding Shannon’s Entropy metric for Information. *arXiv preprint arXiv*. **2014**, 1405.2061.

- Veselago, V.G. The electrodynamics of substances with simultaneously negative values of permittivity and permeability. *Sov. Phys. Uspekhi* **1968**, *10*, 509–514.
- Waitukaitis, S.; Menaut, R.; Chen, B. G-g; van Hecke, M. Origami multistability: From single vertices to metasheets. *Phys. Rev. Lett.* **2015**, *114*, 055503.
- Wallace, D. C. Thermodynamics of crystals. (*John Wiley & Sons, New York*). **1972**.
- Wang, Y.Z.; Li, F.M.; Huang, W.-H.; Jiang, X.; Wang, Y.-S.; Kishimoto, K. Wave band gaps in two-dimensional piezoelectric/piezomagnetic phononic crystals. *Int. J. Solids Struct.* **2008**, *45*, 4203–4210.
- Weng, C. N.; Wang, K. T.; Chen, T. Design of microstructures and structures with negative linear compressibility in certain directions. *Adv. Mater. Res.* **2008**, *33(37)*, 807–14
- Xu, H.; Pasini, D. Structurally efficient three-dimensional metamaterials with controllable thermal expansion. *Sci Rep*, **2016**, *6*, 34924–1~8.
- Yu, X.L.; Zhou, J.; Liang H.Y.; Jiang, Z.Y., Wu, L.L. Mechanical metamaterials associated with stiffness, rigidity and compressibility: A brief review. *Prog. Mater. Sci.* **2018**, *94*, 114–173.
- Zhou, J.; Koschny, T.; Kafesaki, M.; Economou, E.N.; Pendry, J.B.; Soukoulis, C.M. Saturation of magnetic response of split-ring resonators at optical frequencies. *Phys. Rev. Lett.* **2005**, *95*, 223902.

APPENDIX

6/28/2019

RightsLink Printable License

SPRINGER NATURE LICENSE TERMS AND CONDITIONS	
Jun 28, 2019	
<p>This Agreement between Larry Appiah Danso ("You") and Springer Nature ("Springer Nature") consists of your license details and the terms and conditions provided by Springer Nature and Copyright Clearance Center.</p>	
License Number	4617811300700
License date	Jun 28, 2019
Licensed Content Publisher	Springer Nature
Licensed Content Publication	Nature Reviews Materials
Licensed Content Title	Flexible mechanical metamaterials
Licensed Content Author	Katia Bertoldi, Vincenzo Vitelli, Johan Christensen, Martin van Hecke
Licensed Content Date	Oct 17, 2017
Licensed Content Volume	2
Licensed Content Issue	11
Type of Use	Thesis/Dissertation
Requestor type	academic/university or research institute
Format	print and electronic
Portion	figures/tables/illustrations
Number of figures/tables/illustrations	2
High-res required	no
Will you be translating?	no
Circulation/distribution	>50,000
Author of this Springer Nature content	no
Title	Deformation and Strain Energy Anomalies in Bistable and Nonlocal Mechanical Metamaterials
Institution name	University of Illinois at Chicago
Expected presentation date	Jun 2019
Portions	Box 1
Requestor Location	Larry Appiah Danso 663 W Grace St. Unit 103 CHICAGO, IL 60613 United States Attn: Larry Appiah Danso
Total	0.00 USD
Terms and Conditions	

<https://s100.copyright.com/AppDispatchServlet>

Springer Nature Customer Service Centre GmbH Terms and Conditions

This agreement sets out the terms and conditions of the licence (the **Licence**) between you and **Springer Nature Customer Service Centre GmbH** (the **Licensor**). By clicking 'accept' and completing the transaction for the material (**Licensed Material**), you also confirm your acceptance of these terms and conditions.

1. Grant of License

- 1. 1.** The Licensor grants you a personal, non-exclusive, non-transferable, world-wide licence to reproduce the Licensed Material for the purpose specified in your order only. Licences are granted for the specific use requested in the order and for no other use, subject to the conditions below.
- 1. 2.** The Licensor warrants that it has, to the best of its knowledge, the rights to license reuse of the Licensed Material. However, you should ensure that the material you are requesting is original to the Licensor and does not carry the copyright of another entity (as credited in the published version).
- 1. 3.** If the credit line on any part of the material you have requested indicates that it was reprinted or adapted with permission from another source, then you should also seek permission from that source to reuse the material.

2. Scope of Licence

- 2. 1.** You may only use the Licensed Content in the manner and to the extent permitted by these Ts&Cs and any applicable laws.
- 2. 2.** A separate licence may be required for any additional use of the Licensed Material, e.g. where a licence has been purchased for print only use, separate permission must be obtained for electronic re-use. Similarly, a licence is only valid in the language selected and does not apply for editions in other languages unless additional translation rights have been granted separately in the licence. Any content owned by third parties are expressly excluded from the licence.
- 2. 3.** Similarly, rights for additional components such as custom editions and derivatives require additional permission and may be subject to an additional fee. Please apply to Journalpermissions@springernature.com/bookpermissions@springernature.com for these rights.
- 2. 4.** Where permission has been granted **free of charge** for material in print, permission may also be granted for any electronic version of that work, provided that the material is incidental to your work as a whole and that the electronic version is essentially equivalent to, or substitutes for, the print version.
- 2. 5.** An alternative scope of licence may apply to signatories of the [STM Permissions Guidelines](#), as amended from time to time.

3. Duration of Licence

- 3. 1.** A licence for is valid from the date of purchase ('Licence Date') at the end of the relevant period in the below table:

Scope of Licence	Duration of Licence
Post on a website	12 months
Presentations	12 months
Books and	Lifetime of the edition in the language

<https://s100.copyright.com/AppDispatchServlet>

||journals ||purchased

4. Acknowledgement

4. 1. The Licensor's permission must be acknowledged next to the Licenced Material in print. In electronic form, this acknowledgement must be visible at the same time as the figures/tables/illustrations or abstract, and must be hyperlinked to the journal/book's homepage. Our required acknowledgement format is in the Appendix below.

5. Restrictions on use

5. 1. Use of the Licensed Material may be permitted for incidental promotional use and minor editing privileges e.g. minor adaptations of single figures, changes of format, colour and/or style where the adaptation is credited as set out in Appendix 1 below. Any other changes including but not limited to, cropping, adapting, omitting material that affect the meaning, intention or moral rights of the author are strictly prohibited.

5. 2. You must not use any Licensed Material as part of any design or trademark.

5. 3. Licensed Material may be used in Open Access Publications (OAP) before publication by Springer Nature, but any Licensed Material must be removed from OAP sites prior to final publication.

6. Ownership of Rights

6. 1. Licensed Material remains the property of either Licensor or the relevant third party and any rights not explicitly granted herein are expressly reserved.

7. Warranty

IN NO EVENT SHALL LICENSOR BE LIABLE TO YOU OR ANY OTHER PARTY OR ANY OTHER PERSON OR FOR ANY SPECIAL, CONSEQUENTIAL, INCIDENTAL OR INDIRECT DAMAGES, HOWEVER CAUSED, ARISING OUT OF OR IN CONNECTION WITH THE DOWNLOADING, VIEWING OR USE OF THE MATERIALS REGARDLESS OF THE FORM OF ACTION, WHETHER FOR BREACH OF CONTRACT, BREACH OF WARRANTY, TORT, NEGLIGENCE, INFRINGEMENT OR OTHERWISE (INCLUDING, WITHOUT LIMITATION, DAMAGES BASED ON LOSS OF PROFITS, DATA, FILES, USE, BUSINESS OPPORTUNITY OR CLAIMS OF THIRD PARTIES), AND WHETHER OR NOT THE PARTY HAS BEEN ADVISED OF THE POSSIBILITY OF SUCH DAMAGES. THIS LIMITATION SHALL APPLY NOTWITHSTANDING ANY FAILURE OF ESSENTIAL PURPOSE OF ANY LIMITED REMEDY PROVIDED HEREIN.

8. Limitations

8. 1. BOOKS ONLY:Where 'reuse in a dissertation/thesis' has been selected the following terms apply: Print rights of the final author's accepted manuscript (for clarity, NOT the published version) for up to 100 copies, electronic rights for use only on a personal website or institutional repository as defined by the Sherpa guideline (www.sherpa.ac.uk/romeo/).

9. Termination and Cancellation

- 9. 1.** Licences will expire after the period shown in Clause 3 (above).
- 9. 2.** Licensee reserves the right to terminate the Licence in the event that payment is not received in full or if there has been a breach of this agreement by you.

Appendix 1 — Acknowledgements:**For Journal Content:**

Reprinted by permission from [**the Licensor**]: [**Journal Publisher** (e.g. Nature/Springer/Palgrave)] [**JOURNAL NAME**] [**REFERENCE CITATION** (Article name, Author(s) Name), [**COPYRIGHT**] (year of publication)

For Advance Online Publication papers:

Reprinted by permission from [**the Licensor**]: [**Journal Publisher** (e.g. Nature/Springer/Palgrave)] [**JOURNAL NAME**] [**REFERENCE CITATION** (Article name, Author(s) Name), [**COPYRIGHT**] (year of publication), advance online publication, day month year (doi: 10.1038/sj.[**JOURNAL ACRONYM**].)

For Adaptations/Translations:

Adapted/Translated by permission from [**the Licensor**]: [**Journal Publisher** (e.g. Nature/Springer/Palgrave)] [**JOURNAL NAME**] [**REFERENCE CITATION** (Article name, Author(s) Name), [**COPYRIGHT**] (year of publication)

Note: For any republication from the British Journal of Cancer, the following credit line style applies:

Reprinted/adapted/translated by permission from [**the Licensor**]: on behalf of Cancer Research UK: : [**Journal Publisher** (e.g. Nature/Springer/Palgrave)] [**JOURNAL NAME**] [**REFERENCE CITATION** (Article name, Author(s) Name), [**COPYRIGHT**] (year of publication)

For Advance Online Publication papers:

Reprinted by permission from The [**the Licensor**]: on behalf of Cancer Research UK: [**Journal Publisher** (e.g. Nature/Springer/Palgrave)] [**JOURNAL NAME**] [**REFERENCE CITATION** (Article name, Author(s) Name), [**COPYRIGHT**] (year of publication), advance online publication, day month year (doi: 10.1038/sj.[**JOURNAL ACRONYM**])

For Book content:

Reprinted/adapted by permission from [**the Licensor**]: [**Book Publisher** (e.g. Palgrave Macmillan, Springer etc) [**Book Title**] by [**Book author(s)**] [**COPYRIGHT**] (year of publication)

Other Conditions:

Version 1.2

Questions? customercare@copyright.com or +1-855-239-3415 (toll free in the US) or +1-978-646-2777.



Note: Copyright.com supplies permissions but not the copyrighted content itself.

1
PAYMENT

2
REVIEW

3
CONFIRMATION

Step 3: Order Confirmation

Thank you for your order! A confirmation for your order will be sent to your account email address. If you have questions about your order, you can call us 24 hrs/day, M-F at +1.855.239.3415 Toll Free, or write to us at info@copyright.com. This is not an invoice.

Confirmation Number: 11827775
Order Date: 06/28/2019

If you paid by credit card, your order will be finalized and your card will be charged within 24 hours. If you choose to be invoiced, you can change or cancel your order until the invoice is generated.

Payment Information

Larry Danso
lappia2@uic.edu
+1 (773) 495-4225
Payment Method: n/a

Order Details

Smart Materials and Structures

Order detail ID: 71934197
Order License Id: 4617810334793
ISSN: 0964-1726
Publication Type: Journal
Volume:
Issue:
Start page:
Publisher: IOP Publishing
Society of Photo-optical
Instrumentation Engineers ; American
Institute of Physics ; Institute of
Physics (Great Britain)
Author/Editor:

Permission Status: **Granted**

Permission type: Republish or display content
Type of use: Thesis/Dissertation

Requestor type: Academic institution

Format: Print, Electronic

Portion: chart/graph/table/figure

Number of charts/graphs/tables/figures: 1

The requesting person/organization: Larry Appiah Danso/
University of Illinois at
Chicago

Title or numeric reference of the portion(s): Figure 2

Title of the article or chapter the portion is from: Waterbomb base: A
symmetric single-vertex
bistable origami
mechanism.

Editor of portion(s)	N/A
Author of portion(s)	Brandon H Hanna
Volume of serial or monograph	N/A
Page range of portion	2
Publication date of portion	2014
Rights for	Main product
Duration of use	Life of current and all future editions
Creation of copies for the disabled	no
With minor editing privileges	no
For distribution to	Worldwide
In the following language(s)	Original language of publication
With incidental promotional use	no
Lifetime unit quantity of new product	More than 2,000,000
Title	Deformation and Strain Energy Anomalies in Bistable and Nonlocal Mechanical Metamaterials
Institution name	University of Illinois at Chicago
Expected presentation date	Jun 2019

Note: This item will be invoiced or charged separately through CCC's [RightsLink](#) service. [More Info](#)

\$ 0.00

Total order items: 1

This is not an invoice.

Order Total: 0.00 USD

Confirmation Number: 11827775

Special Rightsholder Terms & Conditions

The following terms & conditions apply to the specific publication under which they are listed

Smart Materials and Structures

Permission type: Republish or display content

Type of use: Thesis/Dissertation

TERMS AND CONDITIONS

The following terms are individual to this publisher:

These special terms and conditions are in addition to the standard terms and conditions for CCC's Republication Service and, together with those standard terms and conditions, govern the use of the Works.

As the "User" you will make all reasonable efforts to contact the author(s) of the article which the Work is to be reused from, to seek consent for your intended use. Contacting one author who is acting expressly as authorised agent for their co-author(s) is acceptable.

User will reproduce the following wording prominently alongside the Work:

- the source of the Work, including author, article title, title of journal, volume number, issue number (if relevant), page range (or first page if this is the only information available) and date of first publication. This information can be contained in a footnote or reference note; and
- a link back to the article (via DOI); and
- If practicable, and IN ALL CASES for new works published under any of the Creative Commons licences, the words "© IOP Publishing. Reproduced with permission. All rights reserved"

Without the express permission of the author(s) and the Rightsholder of the article from which the Work is to be reused, User shall not use it in any way which, in the opinion of the Rightsholder, could: (i) distort or alter the author(s)' original intention(s) and meaning; (ii) be prejudicial to the honour or reputation of the author(s); and/or (iii) imply endorsement by the author(s) and/or the Rightsholder.

This licence does not apply to any article which is credited to another source and which does not have the copyright line '© IOP Publishing Ltd'. User must check the copyright line of the article from which the Work is to be reused to check that IOP Publishing Ltd has all the necessary rights to be able to grant permission. User is solely responsible for identifying and obtaining separate licences and permissions from the copyright owner for reuse of any such third party material/figures which the Rightsholder is not the copyright owner of. The Rightsholder shall not reimburse any fees which User pays for a republication licence for such third party content.

This licence does not apply to any material/figure which is credited to another source in the Rightsholder's publication or has been obtained from a third party. User must check the Version of Record of the article from which the Work is to be reused, to check whether any of the material in the Work is third party material. Third party citations and/or copyright notices and/or permissions statements may not be included in any other version of the article from which the Work is to be reused and so cannot be relied upon by the User. User is solely responsible for identifying and obtaining separate licences and permissions from the copyright owner for reuse of any such third party material/figures where the Rightsholder is not the copyright owner. The Rightsholder shall not reimburse any fees which User pays for a republication licence for such third party content.

User and CCC acknowledge that the Rightsholder may, from time to time, make changes or additions to these special terms and conditions without express notification, provided that these shall not apply to permissions already secured and paid for by User prior to such change or addition.

User acknowledges that the Rightsholder (which includes companies within its group and third parties for whom it publishes its titles) may make use of personal data collected through the service in the course of their business.

If User is the author of the Work, User may automatically have the right to reuse it under the rights granted back when User transferred the copyright in the article to the Rightsholder. User should check the copyright form and the relevant author rights policy to check whether permission is required. If User is the author of the Work and does require permission for proposed reuse of the Work, User should select 'Author of requested content' as the Requestor Type. The Rightsholder shall not reimburse any fees which User pays for a republication licence.

If User is the author of the article which User wishes to reuse in User's thesis or dissertation, the republication licence covers the right to include the Accepted Manuscript version (not the Version of Record) of the article. User must include citation details and, for online use, a link to the Version of Record of the article on the Rightsholder's website. User may need to obtain separate permission for any third party content included within the article. User must check this with the copyright owner of such third party content. User may not include the article in a thesis or dissertation which is published by ProQuest. Any other commercial use of User's thesis or dissertation containing the article would also need to be expressly notified in writing to the Rightsholder at the time of request and would require separate written permission from the Rightsholder.

User does not need to request permission for Work which has been published under a CC BY licence. User must check the Version of Record of the CC BY article from which the Work is to be reused, to check whether any of the material in the Work is third party material and so not published under the CC BY licence. User is solely responsible for identifying and obtaining separate licences and permissions from the copyright owner for reuse of any such third party material/figures. The Rightsholder shall not reimburse any fees which User pays for such licences and permissions.

As well as CCC, the Rightsholder shall have the right to bring any legal action that it deems necessary to enforce its rights should it consider that the Work infringes those rights in any way.

For STM Signatories ONLY (as agreed as part of the STM Guidelines)

Any licence granted for a particular edition of a Work will apply also to subsequent editions of it and for editions in other languages, provided such editions are for the Work as a whole in situ and do not involve the separate exploitation of the permitted illustrations or excerpts.

Other Terms and Conditions:

STANDARD TERMS AND CONDITIONS

1. Description of Service; Defined Terms. This Republication License enables the User to obtain licenses for republication of one or more copyrighted works as described in detail on the relevant Order Confirmation (the "Work(s)"). Copyright Clearance Center, Inc. ("CCC") grants licenses through the Service on behalf of the rightsholder identified on the Order Confirmation (the "Rightsholder"). "Republication", as used herein, generally means the inclusion of a Work, in whole or in part, in a new work or works, also as described on the Order Confirmation. "User", as used herein, means the person or entity making such republication.

2. The terms set forth in the relevant Order Confirmation, and any terms set by the Rightsholder with respect to a particular Work, govern the terms of use of Works in connection with the Service. By using the Service, the person transacting for a republication license on behalf of the User represents and warrants that he/she/it (a) has been duly authorized by the User to accept, and hereby does accept, all such terms and conditions on behalf of User, and (b) shall inform User of all such terms and conditions. In the event such person is a "freelancer" or other third party independent of User and CCC, such party shall be deemed jointly a "User" for purposes of these terms and conditions. In any event, User shall be deemed to have accepted and agreed to all such terms and conditions if User republishes the Work in any fashion.

3. Scope of License; Limitations and Obligations.

3.1 All Works and all rights therein, including copyright rights, remain the sole and exclusive property of the Rightsholder. The license created by the exchange of an Order Confirmation (and/or any invoice) and payment by User of the full amount set forth on that document includes only those rights expressly set forth in the Order Confirmation and in these terms and conditions, and conveys no other rights in the Work(s) to User. All rights not expressly granted are hereby reserved.

3.2 General Payment Terms: You may pay by credit card or through an account with us payable at the end of the month. If you and we agree that you may establish a standing account with CCC, then the following terms apply: Remit Payment to: Copyright Clearance Center, 29118 Network Place, Chicago, IL 60673-1291. Payments Due: Invoices are payable upon their delivery to you (or upon our notice to you that they are available to you for downloading). After 30 days, outstanding amounts will be subject to a service charge of 1-1/2% per month or, if less, the maximum rate allowed by applicable law. Unless otherwise specifically set forth in the Order Confirmation or in a separate written agreement signed by CCC, invoices are due and payable on "net 30" terms. While User may exercise the rights licensed immediately upon issuance of the Order Confirmation, the license is automatically revoked and is null and void, as if it had never been issued, if complete payment for the license is not received on a timely basis either from User directly or through a payment agent, such as a credit card company.

3.3 Unless otherwise provided in the Order Confirmation, any grant of rights to User (i) is "one-time" (including the editions and product family specified in the license), (ii) is non-exclusive and non-transferable and (iii) is subject to any and all limitations and restrictions (such as, but not limited to, limitations on duration of use or circulation) included in the Order Confirmation or invoice and/or in these terms and conditions. Upon completion of the licensed use, User shall either secure a new permission for further use of the Work(s) or immediately cease any new use of the Work(s) and shall render inaccessible (such as by deleting or by removing or severing links or other locators) any further copies of the Work (except for copies printed on paper in accordance with this license and still in User's stock at the end of such period).

3.4 In the event that the material for which a republication license is sought includes third party materials (such as photographs, illustrations, graphs, inserts and similar materials) which are identified in such material as having been used by permission, User is responsible for identifying, and seeking separate licenses (under this Service or otherwise) for, any of such third party materials; without a separate license, such third party materials may not be used.

3.5 Use of proper copyright notice for a Work is required as a condition of any license granted under the Service. Unless otherwise provided in the Order Confirmation, a proper copyright notice will read substantially as follows: "Republished with permission of [Rightsholder's name], from [Work's title, author, volume, edition number and year of copyright]; permission conveyed through Copyright Clearance Center, Inc." Such notice must be provided in a reasonably legible font size and must be placed either immediately adjacent to the Work as used (for example, as part of a by-line or footnote but not as a separate electronic link) or in the place where substantially all other credits or notices for the new work containing the republished Work are located. Failure to include the required notice results in loss to the Rightsholder and CCC, and the User shall be liable to pay liquidated damages for each such failure equal to twice the use fee specified in the Order Confirmation, in addition to the use fee itself and any other fees and charges specified.

3.6 User may only make alterations to the Work if and as expressly set forth in the Order Confirmation. No Work may be used in any way that is defamatory, violates the rights of third parties (including such third parties' rights of copyright, privacy, publicity, or other tangible or intangible property), or is otherwise illegal, sexually explicit or obscene. In addition, User may not conjoin a Work with any other material that may result in damage to the reputation of the Rightsholder. User agrees to inform CCC if it becomes aware of any infringement of any rights in a Work and to cooperate with any reasonable request of CCC or the Rightsholder in connection therewith.

4. Indemnity. User hereby indemnifies and agrees to defend the Rightsholder and CCC, and their respective employees and directors, against all claims, liability, damages, costs and expenses, including legal fees and expenses, arising out of any use of a Work beyond the scope of the rights granted herein, or any use of a Work which has been altered in any unauthorized way by User, including claims of defamation or infringement of rights of copyright, publicity, privacy or other tangible or intangible property.

5. Limitation of Liability. UNDER NO CIRCUMSTANCES WILL CCC OR THE RIGHTSHOLDER BE LIABLE FOR ANY DIRECT, INDIRECT, CONSEQUENTIAL OR INCIDENTAL DAMAGES (INCLUDING WITHOUT LIMITATION DAMAGES FOR LOSS OF BUSINESS PROFITS OR INFORMATION, OR FOR BUSINESS INTERRUPTION) ARISING OUT OF THE USE OR INABILITY TO USE A WORK, EVEN IF ONE OF THEM HAS BEEN ADVISED OF THE POSSIBILITY OF SUCH DAMAGES. In any event, the total liability of the Rightsholder and CCC (including their respective employees and directors) shall not exceed the total amount actually paid by User for this license. User assumes full liability for the actions and omissions of its principals, employees, agents, affiliates, successors and assigns.

6. Limited Warranties. THE WORK(S) AND RIGHT(S) ARE PROVIDED "AS IS". CCC HAS THE RIGHT TO GRANT TO USER THE RIGHTS GRANTED IN THE ORDER CONFIRMATION DOCUMENT. CCC AND THE RIGHTSHOLDER DISCLAIM ALL OTHER WARRANTIES RELATING TO THE WORK(S) AND RIGHT(S), EITHER EXPRESS OR IMPLIED, INCLUDING WITHOUT LIMITATION IMPLIED WARRANTIES OF MERCHANTABILITY OR FITNESS FOR A PARTICULAR PURPOSE. ADDITIONAL RIGHTS MAY BE REQUIRED TO USE ILLUSTRATIONS, GRAPHS, PHOTOGRAPHS, ABSTRACTS, INSERTS OR OTHER PORTIONS OF THE WORK (AS OPPOSED TO THE ENTIRE WORK) IN A MANNER CONTEMPLATED BY USER; USER UNDERSTANDS AND AGREES THAT NEITHER CCC NOR THE RIGHTSHOLDER MAY HAVE SUCH ADDITIONAL RIGHTS TO GRANT.

7. Effect of Breach. Any failure by User to pay any amount when due, or any use by User of a Work beyond the scope of the license set forth in the Order Confirmation and/or these terms and conditions, shall be a material breach of the license created by the Order Confirmation and these terms and conditions. Any breach not cured within 30 days of written notice thereof shall result in immediate termination of such license without further notice. Any unauthorized (but licensable) use of a Work that is terminated immediately upon notice thereof may be liquidated by payment of the Rightsholder's ordinary license price therefore; any unauthorized (and unlicensable) use that is not terminated immediately for any reason (including, for example, because materials containing the Work cannot reasonably be recalled) will be subject to all remedies available at law or in equity, but in no event to a payment of less than three times the Rightsholder's ordinary license price for the most closely analogous licensable use plus Rightsholder's and/or CCC's costs and expenses incurred in collecting such payment.

8. Miscellaneous.

8.1 User acknowledges that CCC may, from time to time, make changes or additions to the Service or to these terms and conditions, and CCC reserves the right to send notice to the User by electronic mail or otherwise for the purposes of notifying User of such changes or additions; provided that any such changes or additions shall not apply to permissions already secured and paid for.

8.2 Use of User-related information collected through the Service is governed by CCC's privacy policy, available online here: <http://www.copyright.com/content/cc3/en/tools/footer/privacypolicy.html>.

8.3 The licensing transaction described in the Order Confirmation is personal to User. Therefore, User may not assign or transfer to any other person (whether a natural person or an organization of any kind) the license created by the Order Confirmation and these terms and conditions or any rights granted hereunder; provided, however, that User may assign such license in its entirety on written notice to CCC in the event of a transfer of all or substantially all of User's rights in the new material which includes the Work(s) licensed under this Service.

8.4 No amendment or waiver of any terms is binding unless set forth in writing and signed by the parties. The Rightsholder and CCC hereby object to any terms contained in any writing prepared by the User or its principals, employees, agents or affiliates and purporting to govern or otherwise relate to the licensing transaction described in the Order Confirmation, which terms are in any way inconsistent with any terms set forth in the Order Confirmation and/or in these terms and conditions or CCC's standard operating procedures, whether such writing is prepared prior to, simultaneously with or subsequent to the Order Confirmation, and whether such writing appears on a copy of the Order Confirmation or in a separate instrument.

8.5 The licensing transaction described in the Order Confirmation document shall be governed by and construed under the law of the State of New York, USA, without regard to the principles thereof of conflicts of law. Any case, controversy, suit, action, or proceeding arising out of, in connection with, or related to such licensing transaction shall be brought, at CCC's sole discretion, in any federal or state court located in the County of New York, State of New York, USA, or in any federal or state court whose geographical jurisdiction covers the location of the Rightsholder set forth in the Order Confirmation. The parties expressly submit to the personal jurisdiction and venue of each such federal or state court. If you have any comments or questions about the Service or Copyright Clearance Center, please contact us at 978-750-8400 or send an e-mail to info@copyright.com.

v 1.1

Close

Confirmation Number: 11827775

Citation Information

Order Detail ID: 71934197

Smart Materials and Structures by Society of Photo-optical Instrumentation Engineers ; American Institute of Physics ; Institute of Physics (Great Britain) Reproduced with permission of IOP Publishing in the format Thesis/Dissertation via Copyright Clearance Center.

Close

SPRINGER NATURE LICENSE TERMS AND CONDITIONS	
Jun 28, 2019	
This Agreement between Larry Appiah Danso ("You") and Springer Nature ("Springer Nature") consists of your license details and the terms and conditions provided by Springer Nature and Copyright Clearance Center.	
License Number	4617820126726
License date	Jun 28, 2019
Licensed Content Publisher	Springer Nature
Licensed Content Publication	Nature Materials
Licensed Content Title	Mechanical metamaterials with negative compressibility transitions
Licensed Content Author	Zachary G. Nicolaou, Adilson E. Motter
Licensed Content Date	May 20, 2012
Licensed Content Volume	11
Licensed Content Issue	7
Type of Use	Thesis/Dissertation
Requestor type	academic/university or research institute
Format	print and electronic
Portion	figures/tables/illustrations
Number of figures/tables/illustrations	1
High-res required	no
Will you be translating?	no
Circulation/distribution	>50,000
Author of this Springer Nature content	no
Title	Deformation and Strain Energy Anomalies in Bistable and Nonlocal Mechanical Metamaterials
Institution name	University of Illinois at Chicago
Expected presentation date	Jun 2019
Portions	Figure 2
Requestor Location	Larry Appiah Danso 663 W Grace St. Unit 103 CHICAGO, IL 60613 United States Attn: Larry Appiah Danso
Total	0.00 USD
Terms and Conditions	

<https://s100.copyright.com/AppDispatchServlet>

Springer Nature Customer Service Centre GmbH Terms and Conditions

This agreement sets out the terms and conditions of the licence (the **Licence**) between you and **Springer Nature Customer Service Centre GmbH** (the **Licensor**). By clicking 'accept' and completing the transaction for the material (**Licensed Material**), you also confirm your acceptance of these terms and conditions.

1. Grant of Licence

- 1. 1.** The Licensor grants you a personal, non-exclusive, non-transferable, world-wide licence to reproduce the Licensed Material for the purpose specified in your order only. Licences are granted for the specific use requested in the order and for no other use, subject to the conditions below.
- 1. 2.** The Licensor warrants that it has, to the best of its knowledge, the rights to license reuse of the Licensed Material. However, you should ensure that the material you are requesting is original to the Licensor and does not carry the copyright of another entity (as credited in the published version).
- 1. 3.** If the credit line on any part of the material you have requested indicates that it was reprinted or adapted with permission from another source, then you should also seek permission from that source to reuse the material.

2. Scope of Licence

- 2. 1.** You may only use the Licensed Content in the manner and to the extent permitted by these Ts&Cs and any applicable laws.
- 2. 2.** A separate licence may be required for any additional use of the Licensed Material, e.g. where a licence has been purchased for print only use, separate permission must be obtained for electronic re-use. Similarly, a licence is only valid in the language selected and does not apply for editions in other languages unless additional translation rights have been granted separately in the licence. Any content owned by third parties are expressly excluded from the licence.
- 2. 3.** Similarly, rights for additional components such as custom editions and derivatives require additional permission and may be subject to an additional fee. Please apply to Journalpermissions@springernature.com/bookpermissions@springernature.com for these rights.
- 2. 4.** Where permission has been granted **free of charge** for material in print, permission may also be granted for any electronic version of that work, provided that the material is incidental to your work as a whole and that the electronic version is essentially equivalent to, or substitutes for, the print version.
- 2. 5.** An alternative scope of licence may apply to signatories of the [STM Permissions Guidelines](#), as amended from time to time.

3. Duration of Licence

- 3. 1.** A licence for is valid from the date of purchase ('Licence Date') at the end of the relevant period in the below table:

Scope of Licence	Duration of Licence
Post on a website	12 months
Presentations	12 months
Books and journals	Lifetime of the edition in the language purchased

<https://s100.copyright.com/AppDispatchServlet>

4. Acknowledgement

4. 1. The Licensor's permission must be acknowledged next to the Licenced Material in print. In electronic form, this acknowledgement must be visible at the same time as the figures/tables/illustrations or abstract, and must be hyperlinked to the journal/book's homepage. Our required acknowledgement format is in the Appendix below.

5. Restrictions on use

5. 1. Use of the Licensed Material may be permitted for incidental promotional use and minor editing privileges e.g. minor adaptations of single figures, changes of format, colour and/or style where the adaptation is credited as set out in Appendix 1 below. Any other changes including but not limited to, cropping, adapting, omitting material that affect the meaning, intention or moral rights of the author are strictly prohibited.

5. 2. You must not use any Licensed Material as part of any design or trademark.

5. 3. Licensed Material may be used in Open Access Publications (OAP) before publication by Springer Nature, but any Licensed Material must be removed from OAP sites prior to final publication.

6. Ownership of Rights

6. 1. Licensed Material remains the property of either Licensor or the relevant third party and any rights not explicitly granted herein are expressly reserved.

7. Warranty

IN NO EVENT SHALL LICENSOR BE LIABLE TO YOU OR ANY OTHER PARTY OR ANY OTHER PERSON OR FOR ANY SPECIAL, CONSEQUENTIAL, INCIDENTAL OR INDIRECT DAMAGES, HOWEVER CAUSED, ARISING OUT OF OR IN CONNECTION WITH THE DOWNLOADING, VIEWING OR USE OF THE MATERIALS REGARDLESS OF THE FORM OF ACTION, WHETHER FOR BREACH OF CONTRACT, BREACH OF WARRANTY, TORT, NEGLIGENCE, INFRINGEMENT OR OTHERWISE (INCLUDING, WITHOUT LIMITATION, DAMAGES BASED ON LOSS OF PROFITS, DATA, FILES, USE, BUSINESS OPPORTUNITY OR CLAIMS OF THIRD PARTIES), AND WHETHER OR NOT THE PARTY HAS BEEN ADVISED OF THE POSSIBILITY OF SUCH DAMAGES. THIS LIMITATION SHALL APPLY NOTWITHSTANDING ANY FAILURE OF ESSENTIAL PURPOSE OF ANY LIMITED REMEDY PROVIDED HEREIN.

8. Limitations

8. 1. BOOKS ONLY:Where '**reuse in a dissertation/thesis**' has been selected the following terms apply: Print rights of the final author's accepted manuscript (for clarity, NOT the published version) for up to 100 copies, electronic rights for use only on a personal website or institutional repository as defined by the Sherpa guideline (www.sherpa.ac.uk/romeo/).

9. Termination and Cancellation

- 9. 1.** Licences will expire after the period shown in Clause 3 (above).
- 9. 2.** Licensee reserves the right to terminate the Licence in the event that payment is not received in full or if there has been a breach of this agreement by you.

Appendix 1 — Acknowledgements:

For Journal Content:

Reprinted by permission from [the Licensor]: [Journal Publisher (e.g. Nature/Springer/Palgrave)] [JOURNAL NAME] [REFERENCE CITATION (Article name, Author(s) Name), [COPYRIGHT] (year of publication)

For Advance Online Publication papers:

Reprinted by permission from [the Licensor]: [Journal Publisher (e.g. Nature/Springer/Palgrave)] [JOURNAL NAME] [REFERENCE CITATION (Article name, Author(s) Name), [COPYRIGHT] (year of publication), advance online publication, day month year (doi: 10.1038/sj.[JOURNAL ACRONYM].)

For Adaptations/Translations:

Adapted/Translated by permission from [the Licensor]: [Journal Publisher (e.g. Nature/Springer/Palgrave)] [JOURNAL NAME] [REFERENCE CITATION (Article name, Author(s) Name), [COPYRIGHT] (year of publication)

Note: For any republication from the British Journal of Cancer, the following credit line style applies:

Reprinted/adapted/translated by permission from [the Licensor]: on behalf of Cancer Research UK: : [Journal Publisher (e.g. Nature/Springer/Palgrave)] [JOURNAL NAME] [REFERENCE CITATION (Article name, Author(s) Name), [COPYRIGHT] (year of publication)

For Advance Online Publication papers:

Reprinted by permission from The [the Licensor]: on behalf of Cancer Research UK: [Journal Publisher (e.g. Nature/Springer/Palgrave)] [JOURNAL NAME] [REFERENCE CITATION (Article name, Author(s) Name), [COPYRIGHT] (year of publication), advance online publication, day month year (doi: 10.1038/sj.[JOURNAL ACRONYM].)

For Book content:

Reprinted/adapted by permission from [the Licensor]: [Book Publisher (e.g. Palgrave Macmillan, Springer etc) [Book Title] by [Book author(s)] [COPYRIGHT] (year of publication)

Other Conditions:

Version 1.2

Questions? customercare@copyright.com or +1-855-239-3415 (toll free in the US) or +1-978-646-2777.

<https://s100.copyright.com/AppDispatchServlet>

SPRINGER NATURE LICENSE TERMS AND CONDITIONS	
Jun 28, 2019	
<p>This Agreement between Larry Appiah Danso ("You") and Springer Nature ("Springer Nature") consists of your license details and the terms and conditions provided by Springer Nature and Copyright Clearance Center.</p>	
License Number	4617830237252
License date	Jun 28, 2019
Licensed Content Publisher	Springer Nature
Licensed Content Publication	Nature Materials
Licensed Content Title	Mechanical metamaterials: Materials that push back
Licensed Content Author	Joseph N. Grima, Roberto Caruana-Gauci
Licensed Content Date	Jun 21, 2012
Licensed Content Volume	11
Licensed Content Issue	7
Type of Use	Thesis/Dissertation
Requestor type	academic/university or research institute
Format	print and electronic
Portion	figures/tables/illustrations
Number of figures/tables/illustrations	1
High-res required	no
Will you be translating?	no
Circulation/distribution	>50,000
Author of this Springer Nature content	no
Title	Deformation and Strain Energy Anomalies in Bistable and Nonlocal Mechanical Metamaterials
Institution name	University of Illinois at Chicago
Expected presentation date	Jun 2019
Portions	Figure 1
Requestor Location	Larry Appiah Danso 663 W Grace St. Unit 103 CHICAGO, IL 60613 United States Attn: Larry Appiah Danso
Total	0.00 USD
Terms and Conditions	

<https://s100.copyright.com/AppDispatchServlet>

Springer Nature Customer Service Centre GmbH Terms and Conditions

This agreement sets out the terms and conditions of the licence (the **Licence**) between you and **Springer Nature Customer Service Centre GmbH** (the **Licensor**). By clicking 'accept' and completing the transaction for the material (**Licensed Material**), you also confirm your acceptance of these terms and conditions.

1. Grant of Licence

- 1. 1.** The Licensor grants you a personal, non-exclusive, non-transferable, world-wide licence to reproduce the Licensed Material for the purpose specified in your order only. Licences are granted for the specific use requested in the order and for no other use, subject to the conditions below.
- 1. 2.** The Licensor warrants that it has, to the best of its knowledge, the rights to license reuse of the Licensed Material. However, you should ensure that the material you are requesting is original to the Licensor and does not carry the copyright of another entity (as credited in the published version).
- 1. 3.** If the credit line on any part of the material you have requested indicates that it was reprinted or adapted with permission from another source, then you should also seek permission from that source to reuse the material.

2. Scope of Licence

- 2. 1.** You may only use the Licensed Content in the manner and to the extent permitted by these Ts&Cs and any applicable laws.
- 2. 2.** A separate licence may be required for any additional use of the Licensed Material, e.g. where a licence has been purchased for print only use, separate permission must be obtained for electronic re-use. Similarly, a licence is only valid in the language selected and does not apply for editions in other languages unless additional translation rights have been granted separately in the licence. Any content owned by third parties are expressly excluded from the licence.
- 2. 3.** Similarly, rights for additional components such as custom editions and derivatives require additional permission and may be subject to an additional fee. Please apply to Journalpermissions@springernature.com/bookpermissions@springernature.com for these rights.
- 2. 4.** Where permission has been granted **free of charge** for material in print, permission may also be granted for any electronic version of that work, provided that the material is incidental to your work as a whole and that the electronic version is essentially equivalent to, or substitutes for, the print version.
- 2. 5.** An alternative scope of licence may apply to signatories of the [STM Permissions Guidelines](#), as amended from time to time.

3. Duration of Licence

- 3. 1.** A licence for is valid from the date of purchase ('Licence Date') at the end of the relevant period in the below table:

Scope of Licence	Duration of Licence
Post on a website	12 months
Presentations	12 months
Books and journals	Lifetime of the edition in the language purchased

<https://s100.copyright.com/AppDispatchServlet>

4. Acknowledgement

4. 1. The Licensor's permission must be acknowledged next to the Licenced Material in print. In electronic form, this acknowledgement must be visible at the same time as the figures/tables/illustrations or abstract, and must be hyperlinked to the journal/book's homepage. Our required acknowledgement format is in the Appendix below.

5. Restrictions on use

5. 1. Use of the Licensed Material may be permitted for incidental promotional use and minor editing privileges e.g. minor adaptations of single figures, changes of format, colour and/or style where the adaptation is credited as set out in Appendix 1 below. Any other changes including but not limited to, cropping, adapting, omitting material that affect the meaning, intention or moral rights of the author are strictly prohibited.

5. 2. You must not use any Licensed Material as part of any design or trademark.

5. 3. Licensed Material may be used in Open Access Publications (OAP) before publication by Springer Nature, but any Licensed Material must be removed from OAP sites prior to final publication.

6. Ownership of Rights

6. 1. Licensed Material remains the property of either Licensor or the relevant third party and any rights not explicitly granted herein are expressly reserved.

7. Warranty

IN NO EVENT SHALL LICENSOR BE LIABLE TO YOU OR ANY OTHER PARTY OR ANY OTHER PERSON OR FOR ANY SPECIAL, CONSEQUENTIAL, INCIDENTAL OR INDIRECT DAMAGES, HOWEVER CAUSED, ARISING OUT OF OR IN CONNECTION WITH THE DOWNLOADING, VIEWING OR USE OF THE MATERIALS REGARDLESS OF THE FORM OF ACTION, WHETHER FOR BREACH OF CONTRACT, BREACH OF WARRANTY, TORT, NEGLIGENCE, INFRINGEMENT OR OTHERWISE (INCLUDING, WITHOUT LIMITATION, DAMAGES BASED ON LOSS OF PROFITS, DATA, FILES, USE, BUSINESS OPPORTUNITY OR CLAIMS OF THIRD PARTIES), AND WHETHER OR NOT THE PARTY HAS BEEN ADVISED OF THE POSSIBILITY OF SUCH DAMAGES. THIS LIMITATION SHALL APPLY NOTWITHSTANDING ANY FAILURE OF ESSENTIAL PURPOSE OF ANY LIMITED REMEDY PROVIDED HEREIN.

8. Limitations

8. 1. BOOKS ONLY:Where 'reuse in a dissertation/thesis' has been selected the following terms apply: Print rights of the final author's accepted manuscript (for clarity, NOT the published version) for up to 100 copies, electronic rights for use only on a personal website or institutional repository as defined by the Sherpa guideline (www.sherpa.ac.uk/romeo/).

9. Termination and Cancellation

- 9. 1.** Licences will expire after the period shown in Clause 3 (above).
- 9. 2.** Licensee reserves the right to terminate the Licence in the event that payment is not received in full or if there has been a breach of this agreement by you.

Appendix 1 — Acknowledgements:

For Journal Content:

Reprinted by permission from [the Licensor]: [Journal Publisher (e.g. Nature/Springer/Palgrave)] [JOURNAL NAME] [REFERENCE CITATION (Article name, Author(s) Name), [COPYRIGHT] (year of publication)]

For Advance Online Publication papers:

Reprinted by permission from [the Licensor]: [Journal Publisher (e.g. Nature/Springer/Palgrave)] [JOURNAL NAME] [REFERENCE CITATION (Article name, Author(s) Name), [COPYRIGHT] (year of publication), advance online publication, day month year (doi: 10.1038/sj.[JOURNAL ACRONYM].)]

For Adaptations/Translations:

Adapted/Translated by permission from [the Licensor]: [Journal Publisher (e.g. Nature/Springer/Palgrave)] [JOURNAL NAME] [REFERENCE CITATION (Article name, Author(s) Name), [COPYRIGHT] (year of publication)]

Note: For any republication from the British Journal of Cancer, the following credit line style applies:

Reprinted/adapted/translated by permission from [the Licensor]: on behalf of Cancer Research UK: : [Journal Publisher (e.g. Nature/Springer/Palgrave)] [JOURNAL NAME] [REFERENCE CITATION (Article name, Author(s) Name), [COPYRIGHT] (year of publication)]

For Advance Online Publication papers:

Reprinted by permission from The [the Licensor]: on behalf of Cancer Research UK: [Journal Publisher (e.g. Nature/Springer/Palgrave)] [JOURNAL NAME] [REFERENCE CITATION (Article name, Author(s) Name), [COPYRIGHT] (year of publication), advance online publication, day month year (doi: 10.1038/sj.[JOURNAL ACRONYM])]

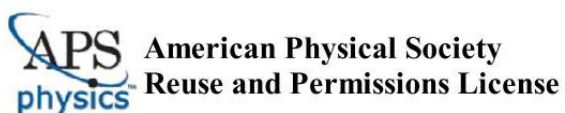
For Book content:

Reprinted/adapted by permission from [the Licensor]: [Book Publisher (e.g. Palgrave Macmillan, Springer etc)] [Book Title] by [Book author(s)] [COPYRIGHT] (year of publication)

Other Conditions:

Version 1.2

Questions? customercare@copyright.com or +1-855-239-3415 (toll free in the US) or +1-978-646-2777.



28-Jun-2019

This license agreement between the American Physical Society ("APS") and Larry Danso ("You") consists of your license details and the terms and conditions provided by the American Physical Society and SciPris.

Licensed Content Information

License Number: RNP/19/JUN/016167
License date: 28-Jun-2019
DOI: 10.1103/PhysRevE.96.023002
Title: Negative extensibility metamaterials: Occurrence and design-space topology
Author: Eduard G. Karpov, Larry A. Danso, and John T. Klein
Publication: Physical Review E
Publisher: American Physical Society
Cost: USD \$ 0.00

Request Details

Does your reuse require significant modifications: No
Specify intended distribution locations: Worldwide
Reuse Category: Reuse in a thesis/dissertation
Requestor Type: Author of requested content
Items for Reuse: Whole Article
Format for Reuse: Electronic and Print
Total number of print copies: More Than 10000

Information about New Publication:

University/Publisher: UNIVERSITY OF ILLINOIS
Title of dissertation/thesis: Deformation and Strain Energy Anomalies in Bistable and Nonlocal Mechanical Metamaterials.
Author(s): Larry Appiah Danso
Expected completion date: Aug. 2019

License Requestor Information

Name: Larry Danso
Affiliation: Individual
Email Id: lappia2@uic.edu
Country: United States

TERMS AND CONDITIONS

The American Physical Society (APS) is pleased to grant the Requestor of this license a non-exclusive, non-transferable permission, limited to Electronic and Print format, provided all criteria outlined below are followed.

1. You must also obtain permission from at least one of the lead authors for each separate work, if you haven't done so already. The author's name and affiliation can be found on the first page of the published Article.
2. For electronic format permissions, Requestor agrees to provide a hyperlink from the reprinted APS material using the source material's DOI on the web page where the work appears. The hyperlink should use the standard DOI resolution URL, <http://dx.doi.org/{DOI}>. The hyperlink may be embedded in the copyright credit line.
3. For print format permissions, Requestor agrees to print the required copyright credit line on the first page where the material appears: "Reprinted (abstract/excerpt/figure) with permission from [(FULL REFERENCE CITATION) as follows: Author's Names, APS Journal Title, Volume Number, Page Number and Year of Publication.] Copyright (YEAR) by the American Physical Society."
4. Permission granted in this license is for a one-time use and does not include permission for any future editions, updates, databases, formats or other matters. Permission must be sought for any additional use.
5. Use of the material does not and must not imply any endorsement by APS.
6. APS does not imply, purport or intend to grant permission to reuse materials to which it does not hold copyright. It is the requestor's sole responsibility to ensure the licensed material is original to APS and does not contain the copyright of another entity, and that the copyright notice of the figure, photograph, cover or table does not indicate it was reprinted by APS with permission from another source.
7. The permission granted herein is personal to the Requestor for the use specified and is not transferable or assignable without express written permission of APS. This license may not be amended except in writing by APS.
8. You may not alter, edit or modify the material in any manner.
9. You may translate the materials only when translation rights have been granted.
10. APS is not responsible for any errors or omissions due to translation.
11. You may not use the material for promotional, sales, advertising or marketing purposes.
12. The foregoing license shall not take effect unless and until APS or its agent, Aptara, receives payment in full in accordance with Aptara Billing and Payment Terms and Conditions, which are incorporated herein by reference.
13. Should the terms of this license be violated at any time, APS or Aptara may revoke the license with no refund to you and seek relief to the fullest extent of the laws of the USA. Official written notice will be made using the contact information provided with the permission request. Failure to receive such notice will not nullify revocation of the permission.
14. APS reserves all rights not specifically granted herein.
15. This document, including the Aptara Billing and Payment Terms and Conditions, shall be the entire agreement between the parties relating to the subject matter hereof.

VITA

NAME

Larry Appiah Danso

EDUCATION

University of Illinois at Chicago

PhD Civil Engineering

Expected Summer 2019

Dissertation: "Deformation and Strain Energy Anomalies in Bistable and Nonlocal Mechanical Metamaterials"

Advisor – Dr. Eduard Karpov

University of Illinois at Chicago

MS Civil Engineering

Aug. 2014 - May. 2016

Area of Concentration: Structural Engineering

Specialization Courses: Finite Element Analysis, Structural Analysis and Design of Tall Buildings, Structural Dynamics, Bridge Design, Sustainability Engineering, Design of Concrete Plate and Shell Structures, Structural Load Determination, Failure and Fracture Analysis, Nondestructive Testing

Kwame Nkrumah University of Science and Technology, Ghana

BSc. Civil Engineering

Aug. 2005 - May. 2009

Area of Concentration: Structural Engineering

Thesis: "Flexural Behavior of Reinforced Concrete Beams Using Phyllite As Coarse Aggregate"

Advisor – Dr. Mark Adom-Asamoah

Specialization Courses: Elementary structures, Theory of Structures, Computer Aided design, Structural Analysis, Reinforced Concrete Design, Steel and Timber Design, Foundation Engineering, Civil Engineering Quantities, Structural Engineering, Civil Engineering Design, Structural Dynamics, Construction Management, Ground Engineering

AWARDS

Univerlecco Gold Scholarship - Politecnico di Milano

Mar. 2014 - Aug. 2014

Graduate Assistantship – University of Illinois at Chica

Aug. 2014 – Present

RESEARCH EXPERIENCE

Department of Civil and Materials Engineering, University of Illinois at Chicago

Research Assistant (Advisor – Dr. Eduard Karpov)

Jan. 2015 – Present

- Modelled structures and materials having potential for bistability and ultimately a negative extensibility mechanical metamaterial behavior
- Undertook research under the NSF Grant # 1634577: Structural Metamaterials with Saint-Vent Edge Effect Reversal for Load Pattern Modification and Recognition
- Undertaking research under Gas Technology Institute (GTI) project: Metamaterials for Gas-Fired Equipment

JOURNAL PUBLICATIONS

1. Karpov, E. G.; Danso, L. A., Klein, J. T. Anomalous Strain Energy Transformation Pathways in Mechanical Metamaterials. *Proceedings of the Royal Society A*. **2019**, 2019004.
2. Danso, L. A.; Karpov, E.G. Reprogramming Static Deformation Patterns in Mechanical Metamaterials. *Materials*. **2018**, 11, 2050.
3. Karpov, E. G.; Danso, L. A. Strain Energy Spectral Density and Information Content of Materials Deformation. *International Journal of Mechanical Sciences*. **2018**, 148, 676-683.
4. Karpov, E. G.; Danso, L. A.; Klein, J. T. Negative Extensibility Metamaterials: Occurrence and Design Space Topology. *Physical Review E*. **2017**, 96(2), [023002].
5. Danso, L. A.; Karpov, E.G. Cusp Singularity-Based Bistability Criterion for Geometrically Nonlinear Structures. *Extreme Mechanics Letters*. **2016**, 13, 135-140.

CONFERENCE PRESENTATIONS

1. Karpov, E. G.; Klein, J. T.; Danso, L. A. Recent Findings and Perspectives in "Zero-Frequency" Phononics, *Proceedings of Phononics 2019: 5th International Conference on Phononic Crystals, Metamaterials, Phonon Transport and Topological Phononics* (Tucson, AZ, June 3-7, **2019**), paper #2019-0080
2. Karpov, E. G.; Danso, L. A.; Klein, J. T. Strain Energy Transformation Pathways in Highly Nonlocal Mechanical Metamaterials, *ASME International Mechanical Engineering Congress & Exposition*, Pittsburgh PA, Nov 9-15, **2018**
3. Karpov, E. G.; Danso, L. A.; Klein, J. T. Mechanical Metamaterials: Recent Advances and Opportunities for NDE and Nonlinear Acoustics, *SPIE Nanoscience+Engineering*, San Diego CA, Aug 19-23, **2018**
4. Danso, L. A.; Karpov, E.G. Strain Energy Spectral Density Behavior in Nonlocal Metamaterials. *U.S. National Congress of Theoretical and Applied Mechanics*, Rosemont, IL, June 4-9, **2018**

5. Karpov, E. G.; Danso, L. A.; Klein, J. T. Multistability, Polymorphism & Symmetry Breaking in Mechanical Metamaterials. *U.S. National Congress of Theoretical and Applied Mechanics*, Rosemont, IL, June 4-9, **2018**
6. Karpov, E. G.; Danso, L. A. Recent Advances and Opportunities of Mechanical Metamaterials. 2017 International Congress on Ultrasonics, Honolulu, HI, December 18-20, **2017**
7. Karpov, E. G.; Danso, L. A. Saint-Venant Edge Effect Reversal in Highly Nonlocal Mechanical Metamaterials, *ASME International Mechanical Engineering Congress & Exposition*, Tampa FL, Nov 3-9, **2017**
8. Karpov, E. G.; Danso, L. A.; Klein, J. T. Cusp Singularity-Enabled Criterion of Structural Bistability and Polymorphism. *ASME International Mechanical Engineering Congress & Exposition*, Tampa FL, Nov 3-9, **2017**
9. Danso, L. A.; Karpov, E.G. Structural metamaterials with Saint-Venant edge effect reversal. *SPIE Nanoscience+Engineering*, San Diego CA, Aug 6-10, **2017**
10. Karpov, E. G.; Danso, L. A. Mechanical Metamaterials - Recent Advances and Applications. *Engineering Mechanics Institute Conference*, San Diego CA, June 4-7, **2017**

TEACHING EXPERIENCE

Department of Civil and Materials Engineering, University of Illinois at Chicago
Teaching Assistant **Jan. 2019 – May. 2019**
 CME 434: Finite Element Analysis

Department of Civil and Materials Engineering, University of Illinois at Chicago
Teaching Assistant **Aug. 2018 – Dec. 2018**
 CME 260: Properties of Materials

Department of Civil and Materials Engineering, University of Illinois at Chicago
Teaching Assistant **Jan. 2018 – May. 2018**
 CME 434: Finite Element Analysis 1

Department of Civil and Materials Engineering, University of Illinois at Chicago
Teaching Assistant **Aug. 2017 – Dec. 2017**
 CME 260: Properties of Materials

Department of Civil and Materials Engineering, University of Illinois at Chicago
Teaching Assistant **Jan. 2017 – May. 2017**
 CME 434: Finite Element Analysis 1

Department of Civil and Materials Engineering, University of Illinois at Chicago
Teaching Assistant **Aug. 2016 – Dec. 2016**
 CME 201: Statics

Department of Civil and Materials Engineering, University of Illinois at Chicago
Teaching Assistant **Jan. 2016 – May. 2016**
 CME 434: Finite Element Analysis 1

Department of Civil and Materials Engineering, University of Illinois at Chicago
Teaching Assistant Aug. 2015 – Dec. 2015
CME 201: Statics

Department of Civil and Materials Engineering, University of Illinois at Chicago
Teaching Assistant Jan. 2015 – May. 2015
CME 203: Strength of Materials & CME 260: Properties of Materials

Department of Civil and Materials Engineering, University of Illinois at Chicago
Teaching Assistant Aug. 2014 – Dec. 2014
CME 201: Statics

Department of Civil Engineering, Kwame Nkrumah University of Science and Technology, Ghana
Teaching Assistant Aug. 2009 – Dec. 2010
CE 355: Hydrology & CE 356: Hydraulic Engineering

PROFESSIONAL AND RELATED EXPERIENCE

African American Academic Network, University of Illinois at Chicago
Peer Tutor Aug. 2015 – May. 2016
Assisted students to develop skills for effective studies and success in STEM (Physics, Mathematics, Statistics) related coursework

Ballast Nedam Ghana BV, Ghana
Assistant Quantity Surveyor Mar. 2012 – Feb. 2014
Performed contract administrative duties related involving pricing, feasibility studies and monitoring of \$ 10 -50 million water supply projects in Ghana.

Taivani Consult, Ghana
Assistant Civil/Geotechnical Engineer Nov. 2011 – Feb. 2012
Prepared AutoCAD drawings and reports on geotechnical investigations

KOCKS Consult GmbH, Ghana
Earthworks Supervisor Nov. 2010 – Oct. 2011
Collaborated with site engineer and surveyor in implementing feeder roadway earthworks designs for a \$ 70 million road project under the Millennium Challenge Corporation grant to Ghana

LANGUAGES

English– native language
Twi– speak, read, and write with basic competence

TECHNICAL SKILLS

Programming languages and mathematical packages: Mathematica, Matlab, Visual basic
Computer aided design / engineering: AutoCAD, SolidWorks, ANSYS, SAP2000, ETABS
Other: SPSS, Simapro8, Windows OS, Mac OS